SECOND EDITION

Interventions in Structural, Valvular, and Congenital Heart Disease

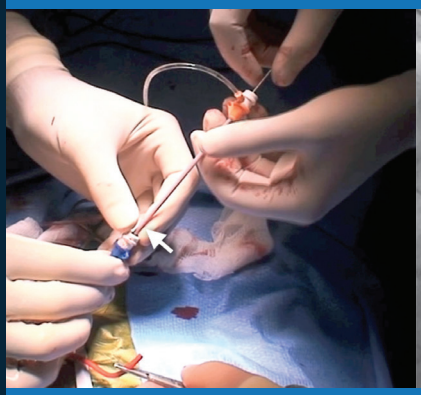
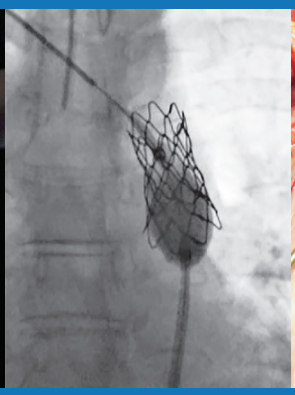
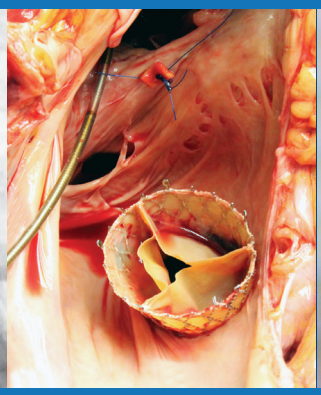
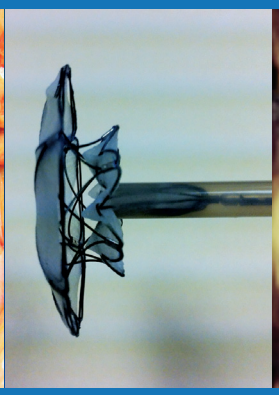
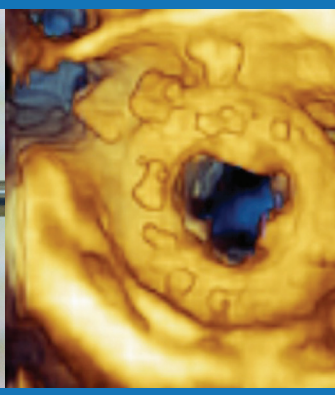

EDITED BY

Horst Sievert • Shakeel A. Qureshi
Neil Wilson • Ziyad M. Hijazi

ASSOCIATE EDITORS

Jennifer Franke • Stefan Bertog • Sameer Gafoor

CRC Press
Taylor & Francis Group

SECOND EDITION

Interventions in Structural, Valvular, and Congenital Heart Disease

SECOND EDITION

Interventions in Structural, Valvular, and Congenital Heart Disease

EDITED BY

Horst Sievert, MD
CardioVascular Center Frankfurt;
Sankt Katharinen Hospital
Frankfurt, Germany

Shakeel A. Qureshi, FRCP
Evelina London Children's Hospital
Guy's & St Thomas Trust
London, United Kingdom

Neil Wilson, FRCP
Department of Paediatric Cardiology
John Radcliffe Hospital
Oxford, United Kingdom

Ziyad M. Hijazi, MD MPH FACC MSCAI
Rush Center for Congenital & Structural Heart Disease
Rush University Medical Center
Chicago, IL, United States

ASSOCIATE EDITORS

Jennifer Franke, MD
CardioVascular Center Frankfurt
Frankfurt, Germany;
University of Heidelberg
Heidelberg, Germany

Stefan Bertog, MD
CardioVascular Center Frankfurt
Frankfurt, Germany

Sameer Gafoor, MD
CardioVascular Center Frankfurt;
Sankt Katharinen Hospital
Frankfurt, Germany

CRC Press
Taylor & Francis Group
Boca Raton London New York

CRC Press is an imprint of the
Taylor & Francis Group, an **informa** business

CRC Press
Taylor & Francis Group
6000 Broken Sound Parkway NW, Suite 300
Boca Raton, FL 33487-2742

Version Date: 20141017

International Standard Book Number-13: 978-1-4822-1564-9 (eBook - PDF)

Contents

Section 4 Valves

Preface to the Second Edition

This book is intended as a practical guide for the interventional treatment of congenital, valvular, and structural heart disease for invasive cardiologists in the pediatric and adult fields. You will appreciate that this second edition gives us the opportunity to report consolidated results and increase the bibliography of established interventional procedures. In keeping with the explosion of structural interventions in adults and the huge increase in transcatheter aortic valve replacement we have recruited many new authors who are pioneers and leaders in those fields. We have also encouraged younger interventionists who we feel write well and who will become leaders in the future. We have also expanded the concept of the importance of imaging alongside the technical details of equipment and its safe and effective delivery.

Where possible we have tried to emphasize practical aspects of the procedures, including the important issues of indications and patient selection, potential pitfalls, and complications. Greater understanding, technical know-how, and wider availability of catheters, balloons, delivery systems, and devices have spread intervention into the realm of acquired valve disease, degenerative disease of the aorta, paravalve leakage, postinfarction ventricular septal defects, and closure of the left atrial appendage.

Some of the procedures covered in the book, such as fetal interventions, hybrid procedures, mitral valve repair, are emerging techniques representing the forefront of interventional treatment today, and will not be practiced in every catheter laboratory. We have collated contributions from a team of expert interventionists throughout the world in an effort to draw together, via the common link of catheter technology, an approach to congenital and structural heart disease that results in a new emerging specialist, the cardiovascular interventionist.

We hope this edition will go a little further than the first to provide guidance and in-depth education to personnel of all levels and disciplines involved in interventional cardiac catheterization. We see it as a tool of reference for all. Our aim is to see a well-thumbed copy in catheter lab viewing rooms and coffee rooms throughout the world. Please do send feedback to us if you perceive shortcomings or have interests and techniques that you feel should be included in future editions.

Horst Sievert
Shakeel A Qureshi
Neil Wilson
Ziyad M Hijazi

Foreword by Dr. Michael Tynan

This is the second edition of the book *Percutaneous Interventions for Congenital Heart Disease*, now with "Structural Heart Disease" preceding "Congenital Heart Disease." Thus, it encompasses almost everything that is not atherosclerotic, inflammatory, or metabolic. The new edition is considerably larger, with an additional 300 pages, which includes 41 chapters. The contributors come from all over the world representing rising talent as well as the "Old Guard." However, it still retains the essential "how to" philosophy of the first edition and of the annual Frankfurt CSI course, which gave birth to the book. The expansion is not just in pages but in concepts, such as the online video resources that are incorporated.

Having lived through this era of less invasive treatment for heart disease, from the introduction of balloon atrial septostomy by Bill Rashkind in 1966, perhaps I should not be astonished at the rapidity with which it has blossomed, but I am astonished. The slow start in the 1960s has given way to ever-increasing momentum. In the 1980s and 1990s, the ideas and practice of peripheral vascular interventionists were incorporated into pediatric cardiology and so balloon dilation of valves and vessels became routine. Stents and implantable occlusion devices were explored. Devices have come and gone with technology improvements so that defect closure is now effective and safe. Over these early years of the twenty-first century the rate of innovation appears almost exponential. What would the pioneers such as Rashkind, Gianturco, and Gruentzig make of the possibilities today? They would love it.

This rapid development has been made possible by the close cooperation between physicians and industry. It would be hard to overstate the importance of the contribution of our colleagues in industry. But the number and complexity of the procedures dealt with in this book pose problems for trainers and trainees alike. It is in this area that the book will be invaluable.

Michael Tynan, MD, FRCP
Emeritus Professor of Paediatric Cardiology
King's College
London

Foreword by Dr. Martin Leon

Most knowledgeable interventional historians would argue that the era of less-invasive nonsurgical cardiovascular therapy mushroomed when Andreas Gruentzig performed the first successful coronary angioplasty in 1977, fulfilling his dream to accomplish catheter-based percutaneous treatment of vascular disease in alert, awake patients. Undoubtedly, Andreas would have delighted in the astounding developments of the ensuing decades, as disciples of his "simple" procedure applied creativity, technical acumen, and scientific rigor to sculpt the burgeoning multidisciplinary subspecialty of interventional cardiovascular therapeutics.

Thus, a heritage has emerged within the interventional cardiovascular community. We believe that "less invasive" is preferred, certainly by patients and also by the healthcare system in general; and less-invasive means catheter-based, nonsurgical, whenever possible. We are technology addicts, especially new gizmos which can shorten procedures, improve outcomes, and expand treatment indications. We are passionate about experimental and clinical research and evidence-based medicine, which is fundamental to every important therapy change and to the interventional device development process. We rely heavily on adjunctive imaging—this is a visual subspecialty …echo/IVUS/OCT, MR/CT, "fusion" imaging, and other new invasive imaging modalities. We are passionate about the interface of clinical medicine and the rapid communication of ideas, including educational meetings and physician training initiatives. We have a vibrant entrepreneurial spirit, are risk-takers, and rapidly embrace new therapies. We strongly support and promote global and multidisciplinary collaborations. *In short, we have a cultural identity … innovation, strong industry partnerships, impatience leading to evolution and forward motion; we have a need to stimulate change and to continually reinvent ourselves, in pace with advances in biomedical science and technology!*

This second edition of *Interventions in Structural, Valvular, and Congenital Heart Disease* is the embodiment of our rapidly expanding subspecialty and now represents the definitive textbook covering all forms of nonvascular interventional therapies. The wastebasket term "structural" heart disease refers to the newest and most diverse branch of the interventional tree, embracing a potpourri of congenital, valvular, and acquired cardiovascular disorders, previously left untreated or relegated to surgical therapy alternatives. This newcomer on the interventional horizon is unique for several reasons. First, the diversity and complexity of interventional skills required to safely and successfully treat both neonates and octogenarians with advanced cardiac lesions is unprecedented. Second, the intersecting physician groups are far-reaching, spanning pediatric and adult interventional cardiology, imaging specialists (not just angiography, but also echocardiography, MR imaging, and CT angiography), and hybrid surgical therapists. Finally, since many of the cardiac anomalies targeted for catheter-based treatment occur rarely, the focused interventionalists working in this rarified zone have clustered into a small, well-bonded fraternity. The purpose of this textbook is to highlight the practical teaching experiences of this congenital, valvular, and structural interventional fraternity.

This textbook serves as a comprehensive syllabus including a virtual "who's who" author list, representing the thought leaders from all allied fields under the umbrella of congenital, valvular, and structural heart disease. The organizational structure is both authoritative and intuitive with easy-to-navigate sections beginning with the catheterization laboratory environment, new imaging modalities for diagnosis and procedural guidance, vascular access, fetal and infant interventions, valvular interventions, and marching through an orderly progression of every conceivable congenital and structural lesion category, which has been managed using existing or proposed interventional therapies. Every section has been expanded and enhanced since the first edition with new contributors and topics, representing the absolute latest in new devices, interventional techniques, and clinical data descriptions. Clearly, the greatest area of expansion is in the breakthrough area of interventional valve therapies, especially transcatheter aortic valve implantation and new mitral regurgitation therapies. The textbook has a familiar stylistic consistency emphasizing clinical treatment indications and practical operator technique issues with helpful procedural "tips and tricks" and careful descriptions of potential complications. The breadth of this textbook is impressive extending from commonly recognized conditions (such as an expanded section on left atrial appendage closure methodologies for atrial fibrillation), to less well-established domains, including innovations in interventional heart failure diagnosis and therapy.

Lest one thinks that this textbook is merely a compendium of obscure interventional oddities, this segment of

the subspecialty is exploding and the topics in this textbook represent the greatest potential growth area in all of interventional cardiovascular medicine. In 5 to 10 years it is entirely conceivable that this small fraternity of interventionalists focused on congenital, valvular, and structural therapies will multiply into an army of catheter-based therapists with specialized operator skills, an advanced appreciation of cardiac imaging modalities, and a thorough clinical understanding of multivaried cardiac disease states. This dramatically improved second edition of *Interventions in Structural, Valvular, and Congenital Heart Disease* fills a medical literature void and should be heartily embraced by all cardiovascular healthcare professionals, from the curious to the diehard interventional practitioner. I expect as this field continues to transform in the future that subsequent editions of this textbook will help to define the unpredictable progress of this unique subspecialty.

Martin B. Leon, MD
Professor of Medicine,
Columbia University Medical Center
Director, Center for Interventional Vascular Therapy
Chairman Emeritus, Cardiovascular Research Foundation
New York City

Video Contents

For users of the VitalSource® eBook:
The accompanying video files as indicated by the throughout the text can be accessed via links in the eBook. Please see the front page of this text for login instructions. Alternately, you can use the URLs provided here.

No.	Description	URL
Video 5.1	3D Jet.	http://goo.gl/3Xifcl
Video 7.1	Great vessel axial plane.	http://goo.gl/YXAgna
Video 7.2	Guide wire crossing the interatrial septum.	http://goo.gl/r4qnXR
Video 7.3	Parasagittal long axis four-chamber plane.	http://goo.gl/7CW38U
Video 7.4	Profile of Amplatzer septal occluder implanted.	http://goo.gl/gJRdXm
Video 13.1	The needle is directed medially, superiorly and posteriorly while small amount of dilute contrast is injected to outline the hepatic vein.	http://goo.gl/pQEwlw
Video 13.2	Contrast is injected outlining the hepatic vein.	http://goo.gl/DjDivW
Video 13.3	Hand injection outlines portal vein rather than the hepatic vein.	http://goo.gl/gIVGxu
Video 13.4	The needle is guided toward the hepatic vein while contrast is being injected.	http://goo.gl/85B9g9
Video 13.5	Hand injection demonstrates thrombosis of the inferior baffle of Fontan patient. Thus the hepatic route could not be used.	http://goo.gl/pgiclw
Video 13.6	The wire is manipulated along the hepatic vein to the heart.	http://goo.gl/I8CsxT
Video 13.7	Sheath advancement is facilitated by the straight wire course. The dilator may need to be separated from the sheath while advancing the sheath in small infants to avoid trauma to the heart.	http://goo.gl/3aSuf1
Video 13.8	Transhepatic stenting of stenosed RV to PA conduit.	http://goo.gl/cduQNG
Video 13.9	Balloon atrial septostomy is being performed in a 2-day-old newborn using the transhepatic approach.	http://goo.gl/BAxryP
Video 13.10	A pulmonary vein wedge angiogram using the transhepatic approach outlines the stenoses of Sano anastomosis in a patient with hypoplastic left heart syndrome.	http://goo.gl/zT62zR
Video 13.11	A pulmonary vein wedge angiogram using the transhepatic approach outlines the stenoses of Sano anastomosis in a patient with hypoplastic left heart syndrome.	http://goo.gl/mgd0Cx
Video 13.12	Dilated hepatic veins in a patient with single ventricle.	http://goo.gl/8Yf9xK
Video 13.13	The transhepatic approach allowed the use of a relatively larger sheath for balloon angioplasty of coarctation in a patient with single ventricle post-stage 1 palliation preserving the femoral artery.	http://goo.gl/hPMq8Q
Video 13.14	Transhepatic stenting of LPA in a Fontan patient with complex congenital heart disease consisting of heterotaxy syndrome, interrupted IVC, and left SVC with no right SVC.	http://goo.gl/mhguiO

(*continued*)

(continued)

No.	Description	URL
Video 25.1	Two-step XT deployment.	http://goo.gl/vfBMWF
Video 25.2	Catheter delivery.	http://goo.gl/T9Lehk
Video 25.3	Crossing AO valve.	http://goo.gl/klT622
Video 25.4	Mattos rotational aortography.	http://goo.gl/80tKx2
Video 48.1	Intraprocedural transoesophageal echocardiography in long-axis view showing perforated aneurysm of right coronary sinus draining into the RVOT with turbulent color flow across. Typical windsock is seen in the RVOT. There is trivial AR.	http://goo.gl/giCtK6
Video 48.2	Following catheter closure with Amplatzer duct occluder there is a complete closure with no color flow across. There is no AR seen.	http://goo.gl/gpmP1B
Video 48.3	The delivery sheath can be seen crossing the defect from the RVOT into the ascending aorta.	http://goo.gl/8Y6eeb
Video 48.4	The aortic disk, with its attached delivery cable passing through the sheath, being pulled to block the aortic end of the defect.	http://goo.gl/1OhRVV
Video 48.5	Postdeployment transesophageal 3D acquisition showing the ADO device *en face*, in its profile, and in rotation.	http://goo.gl/0aTq6T
Video 48.6	Postdeployment transesophageal 3D acquisition showing the ADO device *en face*, in its profile, and in rotation.	http://goo.gl/CLroxo
Video 48.7	Postdeployment transesophageal 3D acquisition showing the ADO device *en face*, in its profile, and in rotation.	http://goo.gl/uRd6x7
Video 53.1	Configuration sequence of Pfm NitOcclud ASD-R device where the "reverse" configuration of left atrial disk can be seen and the polyester membrane that closes the left atrial side of the device.	http://goo.gl/u2lCJO
Video 53.2	Left atrial disk is deployed in left upper pulmonary vein reaching a complete final reconfiguration once the device is pulled into the left atrial body.	http://goo.gl/gZkyW5
Video 53.3	Locking wire is retracted and device is released.	http://goo.gl/TnEn28
Video 53.4	To obtain the lowest profile it is important to finish a gentle "pull and push" maneuver ("Minnesota wiggle") pushing the right disk until it adopts a "concave shape," usually accompanied by a "click" sensation on the operator's hand.	http://goo.gl/IzEhsz
Video 75.1	Angiogram of the PDA obtained through a hand injection of contrast into the side arm of the long sheath in the lateral view. This usually allows excellent definition of the duct ampulla and measurement of duct diameter at pulmonary insertion. Frozen frames of the same angiogram are shown in Figure 75.5.	http://goo.gl/HNErV9
Video 75.2	Angiogram of the PDA obtained through a hand injection of contrast into the side arm of the long sheath in 45° right anterior oblique view. This is particularly useful when the duct arises from the leftward aspect of the aorta.	http://goo.gl/GGgwSd
Video 75.3	The first video of the coil-delivery sequence. Three coils are simultaneously delivered with bioptome assistance through the long sheath. They are seen emerging from the distal end of the sheath placed in the descending aorta across the PDA.	http://goo.gl/btlLVf
Video 75.4	The second video of the coil-delivery sequence. Most of the coil turns are extruded and are seen to oscillate with the aortic flows.	http://goo.gl/8KM3bP

(*continued*)

(continued)

No.	Description	URL
Video 75.5	The third video of the coil-delivery sequence. The coil turns are seen to compact in the ampulla, aided by the retrograde flow in the proximal descending thoracic aorta.	http://goo.gl/UMIVSf
Video 75.6	The final video of the coil-delivery sequence. Once the coils are compacted in the ampulla, they stop oscillating altogether. The bioptome and the distal sheath tip are now in the MPA and this is reflected in the sudden fall in pressures recorded via the side arm of the long sheath. At this time some resistance is encountered. The coil is given a gentle tug and the jaws of the bioptome are opened to release the coil.	http://goo.gl/6cLpha
Video 75.7	The first video of the sequence for coil occlusion of the patent ductus arteriosus in a preterm infant. This video shows how the duct is crossed with a 0.025 inch J-tipped Terumo wire passed through a 4 F right coronary catheter placed at the junction of the inferior vena cava with right atrium. This allows minimal manipulation of catheter in the heart of the preterm infant.	http://goo.gl/LZ1xRE
Video 75.8	Coil occlusion of the patent duct in a preterm infant. An angiogram is obtained in the lateral view via the side arm of a 4 F long sheath placed in the duct ampulla. This angiogram serves as a landmark to guide coil placement.	http://goo.gl/VK8PVO
Video 75.9	Coil occlusion of the patent duct in a preterm infant; first video of the coil-delivery sequence. Two 0.038-inch-thick coils are simultaneously delivered into the ampulla using a 3 F bioptome.	http://goo.gl/ZQpjI2
Video 75.10	Coil occlusion of the patent duct in a preterm infant; second video of the coil-delivery sequence. A hand injection via the side arm of the sheath demonstrates the coil position. The coils are situated in the ampulla but need to be pulled in toward the pulmonary artery end.	http://goo.gl/j6YGJU
Video 75.11	Coil occlusion of the patent duct in a preterm infant; third video of the coil-delivery sequence. The coils have been pulled in toward the pulmonary artery end. The branch pulmonary arteries are seen filling well.	http://goo.gl/CCugRr
Video 75.12	Coil occlusion of the patent duct in a preterm infant; fourth video of the coil-delivery sequence. The jaws of the bioptome are opened to release the coils.	http://goo.gl/j9qOdg
Video 75.13	Coil occlusion of the patent duct in a preterm infant; final video of the coil-delivery sequence. A vigorous hand injection through the femoral artery cannula of diluted contrast allows opacification of the descending aorta and demonstrates the position of the coils in the ampulla and occlusion of the duct.	http://goo.gl/Xew8G6
Video 82.1	Cranial angulation fails to demonstrate the proximal left pulmonary artery stenosis because of opacification of the dilated main pulmonary artery on this pulmonary arteriogram.	http://goo.gl/SiYSMf
Video 82.2	Caudal and slightly LAO angulation demonstrates the proximal left pulmonary artery stenosis much better.	http://goo.gl/HLYfIS
Video 95.1	Loading the device.	http://goo.gl/jXZaru

Contributors

Tommaso Acquaviva
Department of Emergency and Organs Transplantation
University of Bari
Bari, Italy

Hitesh Agrawal
Department of Pediatrics
John H. Stroger Jr. Hospital of Cook County
Chicago, Illinois

Zaheer Ahmad
King Abdulaziz Cardiac Center
King Abdulaziz Medical City
National Guard Health Affairs
Riyadh, Saudi Arabia

Lishan Aklog
Pavilion Holdings Group
and
PAXmed Inc.
New York, New York

Mustafa Al-Qbandi
Department of Pediatric Cardiology
Chest Diseases Hospital
Kuwait City, Kuwait

Mazeni Alwi
Paediatric and Congenital Heart Centre
Institut Jantung Negara (National Heart Institute)
Kuala Lumpur, Malaysia

Rui Anjos
Department of Pediatric Cardiology
Hospital de Santa Cruz
Lisbon, Portugal

R. Arora
New Delhi, India

Jeremy Asnes
Pediatric Cardiology
Yale School of Medicine
New Haven, Connecticut

Nitish Badhwar
Department of Medicine
University of California–San Francisco
San Francisco, California

Jesus Damsky Barbosa
Catheterization Laboratory for Congenital Heart Disease
Hospital de Niños Pedro de Elizalde
Buenos Aires, Argentina

Krzysztof Bartus
Department of Cardiovascular Surgery and Transplantology
Jagiellonian University
John Paul II Hospital
Krakow, Poland

John L. Bass
University of Minnesota
Amplatz Children's Hospital
Minneapolis, Minnesota

Lee Benson
Department of Pediatrics
Hospital for Sick Children
University of Toronto School of Medicine
Toronto, Ontario, Canada

Jamie Bentham
Department of Paediatric Cardiology
John Radcliffe Hospital
Oxford, United Kingdom

Stefan Bertog
CardioVascular Center Frankfurt
Frankfurt, Germany

Peter C. Block
Emory University School of Medicine
Emory University Hospital
Atlanta, Georgia

Philipp Bonhoeffer
Department of Cardiology
Fondazione G. Monasterio
Pisa, Italy

Alessandro Santo Bortone
Department of Emergency and Organs Transplantation
University of Bari
Bari, Italy

I. Bozdag-Turan
Department of Cardiology
University Hospital Rostock
Rostock, Germany

Andras Bratincsak
Department of Pediatrics
University of Hawaii
Honolulu, Hawaii

Annkathrin Braut
CardioVascular Center Frankfurt
Frankfurt, Germany

Grazyna Brzezinska-Rajszys
The Heart Catheterization Laboratory
Department of Pediatric Cardiology
Children's Memorial Health Institute
Warsaw, Poland

Lutz Buellesfeld
Department of Cardiology
Bern University Hospital
Bern, Switzerland

Franziska Buescheck
CardioVascular Center Frankfurt
Frankfurt, Germany

Haran Burri
Department of Medical Specialties
University Hospital of Geneva
Geneva, Switzerland

Carla Canniffe
Mater Misericordiae Hospital
Dublin, Ireland

Qi-Ling Cao
Rush Center for Congenital and Structural Heart Disease
Rush University Medical Center
Chicago, Illinois

Massimo Caputo
University of Bristol
Bristol, United Kingdom

Francesco Casilli
Emodinamica e Radiologia Cardiovascolare
Policlinico San Donato IRCCS
Milan, Italy

John P. Cheatham
Nationwide Children's Hospital
and
Cardiology Division
The Ohio State University
Columbus, Ohio

Jonathan M. Chen
Seattle Children's Hospital
and
University of Washington School of Medicine
Seattle, Washington

Albert K. Chin
Pavilion Medical Innovations
Norwell, Massachusetts

Antonio Colombo
San Raffaele Scientific Institute
and
EMO-GVM Centro Cuore Columbus
Milan, Italy

Rodrigo N. Costa
Catheterization Laboratory for Congenital Heart Disease
Instituto Dante Pazzanese de Cardiologia and Hospital do Coração
São Paulo, Brazil

Matt Daniels
Radcliffe Department of Medicine
John Radcliffe Hospital
Oxford, United Kingdom

Ryan R. Davies
Nemours Cardiac Center
Alfred I. DuPont Hospital for Children
Wilmington, Delaware

Emanuela de Cillis
Institute of Cardiac Surgery
Department of Emergency and Organs Transplantation
University of Bari
Bari, Italy

Joseph DeGiovanni
Birmingham Children's and Queen Elizabeth Hospitals
Birmingham, United Kingdom

Brian J. deGuzman
Pavilion Holdings Group
and
Kaleidoscope Medical LLC
Paradise Valley, Arizona

Mirko Doss
Department of Thoracic and Cardiovascular Surgery
Kerckhoff Clinic
Bad Nauheim, Germany

Makram R. Ebeid
University of Mississippi Medical Center
Jackson, Mississippi

Tina Edwards-Lehr
CardioVascular Center Frankfurt
Sankt Katharinen Hospital
Frankfurt, Germany

Neal Eigler
Heart Institute
Cedars-Sinai Medical Center
Los Angeles, California

Howaida El Said
Department of Pediatrics
Rady Children's Hospital
University of California San Diego
San Diego, California

Ted Feldman
Cardiology Division
Evanston Hospital
NorthShore University Health System
Evanston, Illinois

Hans Reiner Figulla
Department of Internal Medicine I
(Cardiology, Angiology, Pneumology and Intensive Care Medicine)
University Hospital Jena
Friedrich-Schiller University
Jena, Germany

Jennifer Franke
CardioVascular Center Frankfurt
Frankfurt, Germany

and

Department of Cardiology
University Hospital Heidelberg
Heidelberg, Germany

Christian Frerker
Division of Cardiology
Asklepios Klinik St. Georg
Hamburg, Germany

Sameer Gafoor
CardioVascular Center Frankfurt
and
Sankt Katharinen Hospital
Frankfurt, Germany

Mark Galantowicz
Department of Cardiothoracic Surgery
The Heart Center
Nationwide Children's Hospital
Columbus, Ohio

Wei Gao
Department of Cardiology
Shanghai Jiaotong University School of Medicine
Shanghai, People's Republic of China

Marc Gewillig
Pediatric Cardiology
University Hospital Gasthuisberg
Leuven, Belgium

Alexander Ghanem
Department of Cardiology
Asklepios Klinik St. Georg
Hamburg, Germany

Sebastian Goreczny
Evelina London Children's Hospital
London, United Kingdom

Miguel A. Granja
Catheterization Laboratory for Congenital Heart Disease
Hospital Italiano de Buenos Aires
Buenos Aires, Argentina

David Gregg
Division of Cardiology
Medical University of South Carolina
Charleston, South Carolina

Eberhard Grube
Department of Medicine/Cardiology
University Hospital Bonn
Bonn, Germany

Alexandra Heath
Pediatric Cardiology Section
Kardiocentrum
La Paz, Bolivia

William E. Hellenbrand
Pediatric Cardiology Department
Yale University Medical Center
New Haven, Connecticut

Ziyad M. Hijazi
Department of Pediatrics
Sidra Medical and Research Center
Doha, Qatar

and

Pediatrics and Internal Medicine
James A.Hunter, MD, University
Rush University Medical Center
Chicago, Illinois

Ilona Hofmann
Cardiovascular Center Frankfurt
Frankfurt, Germany

Noa Holoshitz
Rush Center for Congenital and Structural Heart Disease
Rush University Medical Center
Chicago, Illinois

H. Ince
Department of Cardiology
Vivantes Klinikum Am Urban und im Friedrichshain
Berlin, Germany

Frank F. Ing
Children's Hospital–Los Angeles
and
University of Southern California
Los Angeles, California

Vladimir Jelnin
Lenox Hill Heart and Vascular Institute
North Shore/LIJ Health System
New York, New York

Saibal Kar
Heart Institute
Cedars-Sinai Medical Center
Los Angeles, California

Damien Kenny
Rush Center for Congenital and Structural Heart Disease
Rush University Medical Center
Chicago, Illinois

Prafulla Kerkar
Department of Cardiology
King Edward VII Memorial Hospital
Mumbai, India

Sachin Khambadkone
Paediatric and Adolescent Cardiology
Great Ormond Street Hospital
London, United Kingdom

S. Kische
Department of Cardiology
Vivantes Klinikum Am Urban und im Friedrichshain
Berlin, Germany

Chad Kliger
Lenox Hill Heart and Vascular Institute
North Shore/LIJ Health System
New York, New York

Miltiadis Krokidis
Department of Radiology
Addenbrooke's University Hospital
Cambridge, United Kingdom

Karl-Heinz Kuck
Division of Cardiology
Asklepios Klinik St. Georg
Hamburg, Germany

R. Krishna Kumar
Amrita Institute of Medical Sciences and Research Centre
Kerala, India

Robert Kumar
Lenox Hill Heart and Vascular Institute
North Shore/LIJ Health System
New York, New York

Simon Lam
Cardiovascular Center Frankfurt
Frankfurt, Germany

Azeem Latib
San Raffaele Scientific Institute
and
EMO-GVM Centro Cuore Columbus
Milan, Italy

Larry Latson
Pediatric and Adult Congenital Cardiology
Joe DiMaggio Children's Hospital
Memorial Healthcare System
Hollywood, Florida

Alexander Lauten
Department of Internal Medicine I
(Cardiology, Angiology, Pneumology and Intensive Care Medicine)
University Hospital Jena
Friedrich-Schiller University
Jena, Germany

Trong-Phi Le
Department of Structural and Congenital Heart Disease
Klinikum Links der Weser
Bremen, Germany

Randall J. Lee
Department of Medicine
University of California–San Francisco
San Francisco, California

Ting-Liang Liu
Department of Cardiology
Shanghai Children's Medical Center
Shanghai, People's Republic of China

Kiran K. Mallula
Rush Center for Congenital and Structural Heart Disease
Rush University Medical Center
Chicago, Illinois

Katharina Malsch
Klinikum Hanau
Hanau, Germany

Takashi Matsumoto
Heart Institute
Cedars-Sinai Medical Center
Los Angeles, California

Bernhard Meier
Department of Cardiology
Bern University Hospital
Bern, Switzerland

Inês Carmo Mendes
Department of Pediatric Cardiology
Hospital de Santa Cruz
Lisbon, Portugal

Haverj Mikailian
Department of Pediatrics
The Hospital for Sick Children
The University of Toronto School of Medicine
Toronto, Ontario, Canada

Sa'ar Minha
MedStar Washington Hospital Center
Washington, DC

Marhisham Che Mood
Paediatric and Congenital Heart Centre
Institut Jantung Negara (National Heart Institute)
Kuala Lumpur, Malaysia

Jose Pablo Morales
Division of Cardiovascular Devices
U.S. Food and Drug Administration
Silver Spring, Maryland

Mamoo Nakamura
Heart Institute
Cedars-Sinai Medical Center
Los Angeles, California

Georg Nickenig
Department of Medicine II
University Hospital Bonn
Bonn, Germany

C. A. Nienaber
Department of Cardiology
University Hospital Rostock
Rostock, Germany

Fabian Nietlispach
University Heart Center
University Hospital Zurich
Zurich, Switzerland

Stéphane Noble
Department of Medical Specialties
University Hospital of Geneva
Geneva, Switzerland

Anthony Nobles
Westsachsen Hochschule
Zwickau, Germany

Eustaquio M. Onorato
Dipartimento Cardiovascolare
Humanitas Gavazzeni
Bergamo, Italy

Igor F. Palacios
Department of Medicine
Massachusetts General Hospital
Boston, Massachusetts

John L. Parks
Division of Cardiology
Medical University of South Carolina
Charleston, South Carolina

Carlos A. C. Pedra
Catheterization Laboratory for Congenital Heart Disease
Instituto Dante Pazzanese de Cardiologia
and
Hospital do Coração
São Paulo, Brazil

Simone R. F. Fontes Pedra
Echocardiography Laboratory for Congenital Heart Disease
Instituto Dante Pazzanese de Cardiologia
and
Hospital do Coração
São Paulo, Brazil

Alejandro Peirone
Pediatric Cardiology Section
Hospital Privado de Córdoba,
Córdoba, Argentina

C. Fábio A. Peralta
Hospital do Coração
and
Universidade de Campinas (UNICAMP)
São Paulo, Brazil

Augusto D. Pichard
MedStar Washington Hospital Center
Washington, DC

Fabien Praz
Department of Cardiology
Bern University Hospital
Bern, Switzerland

Worakan Promphan
Queen Sirikit National Institute of Child Health
Rangsit University
Bangkok, Thailand

Shakeel A. Qureshi
Department of Congenital Heart Disease
Evelina London Children's Hospital
London, United Kingdom

P. Syamasundar Rao
Department of Pediatrics and Medicine
The University of Texas/Houston Medical School
Memorial Hermann Children's Hospital
Houston, Texas

Oleg Reich
Children's Heart Center
University Hospital Motol
Prague, Czech Republic

John Reidy
Department of Radiology
Guy's Hospital
London, United Kingdom

Kristina Renkhoff
Cardiovascular Center Frankfurt
Sankt Katharinen Hospital
Frankfurt, Germany

Marcelo S. Ribeiro
Catheterization Laboratory for Congenital Heart Disease
Instituto Dante Pazzanese de Cardiologia
and
Hospital do Coração
São Paulo, Brazil

Phillip Roberts
The Heart Centre for Children
Childrens Hospital at Westmead
Westmead, Australia

Carlos E. Ruiz
Department of Cardiology in Pediatrics and Medicine
North Shore-LIJ School of Medicine
Hofstra University
New York, New York

Monique Sandhu
Division of Cardiology
Medical University of South Carolina
Charleston, South Carolina

Ulrich Schäfer
Division of Cardiology
Asklepios Klinik St. Georg
Hamburg, Germany

Martin B. E. Schneider
Department of Pediatric Cardiology
German Pediatric Heart Centre
Sankt Augustin, Germany

Gerhard C. Schuler
Department of Internal Medicine/Cardiology
University of Leipzig Heart Center
Leipzig, Germany

Peter Sick
Hopsital Barmherzige Brüder Regensburg
Regensburg, Germany

Horst Sievert
Cardiovascular Center Frankfurt
and
Sankt Katharinen Hospital
Frankfurt, Germany

Ulrich Sigwart
Department of Cardiology
University of Geneva
Geneva, Switzerland

Guilherme V. Silva
Texas Heart Institute
Houston, Texas

Jan-Malte Sinning
Department of Medicine II
University Hospital Bonn
Bonn, Germany

Daniel H. Steinberg
Division of Cardiology
Medical University of South Carolina
Charleston, South Carolina

Petr Tax
Children's Heart Center
University Hospital Motol
Prague, Czech Republic

Alejandro J. Torres
Pediatric Catheterization Laboratory
New York-Presbyterian Morgan Stanley Children's Hospital
New York, New York

Luis Trentacoste
Catheterization Laboratory for Congenital Heart Disease
Hospital de Niños Ricardo Gutiérrez
Buenos Aires, Argentina

R. Goekmen Turan
Department of Cardiology
University Hospital Rostock
Rostock, Germany

Laura Vaskelyte
Cardiovascular Center Frankfurt
Frankfurt, Germany

Joseph John Vettukattil
Congenital Cardiac Center
Helen DeVos Children's Hospital
Grand Rapids, Michigan

Ron Waksman
MedStar Washington Hospital Center
Washington, DC

Kevin P. Walsh
Mater Misericordiae Hospital
Dublin, Ireland

Nikos Werner
Department of Medicine II
University Hospital Bonn
Bonn, Germany

Brian Whisenant
Intermountain Heart Institute
Salt Lake City, Utah

Johannes Wilde
Department of Internal Medicine/Cardiology
University of Leipzig Heart Center
Leipzig, Germany

Neil Wilson
Department of Paediatric Cardiology
John Radcliffe Hospital
Oxford, United Kingdom

Stephan Windecker
Department of Cardiology
Bern University Hospital
Bern, Switzerland

Wen-Loong Yeow
Heart Institute
Cedars-Sinai Medical Center
Los Angeles, California

Evan M. Zahn
Congenital Heart Institute
Miami Children's Hospital
and
Arnold Palmer Women and Children's Hospital
Miami, Florida

Mario Zanchetta
Dipartimento Malattie Cardiovascolari
Azienda U.L.S.S.
Cittadella, Padova, Italy

1

How to design and operate a congenital-structural catheterization laboratory

John P. Cheatham

Introduction

What would Werner Forsmann say about what has happened since that fateful day, so long ago, when he performed the first cardiac catheterization on himself? Of course, he never actually reached his heart with the catheter the first time AND he was banished from his promising career as a young surgeon. However, his spirit exemplifies what has now become the modern-day interventional cardiologist. Since there is a distinction between the cardiologist trained to treat adults with predominant coronary artery and acquired cardiac disease and those cardiologists specially trained to manage congenital heart disease, the same can be said for the cardiac catheterization laboratories in which these patients are treated. For the purpose of this chapter, the design, equipment required, necessary inventory, and personnel requirements for the modern-day lab dedicated to advanced transcatheter therapy for the smallest newborn to the largest adult with complex congenital heart disease, will be discussed. The author readily acknowledges the biases instilled in him by his mentor and idol, Charles E. (Chuck) Mullins, MD, who has taught many of the congenital heart interventionalists across the globe (Figure 1.1a and b).

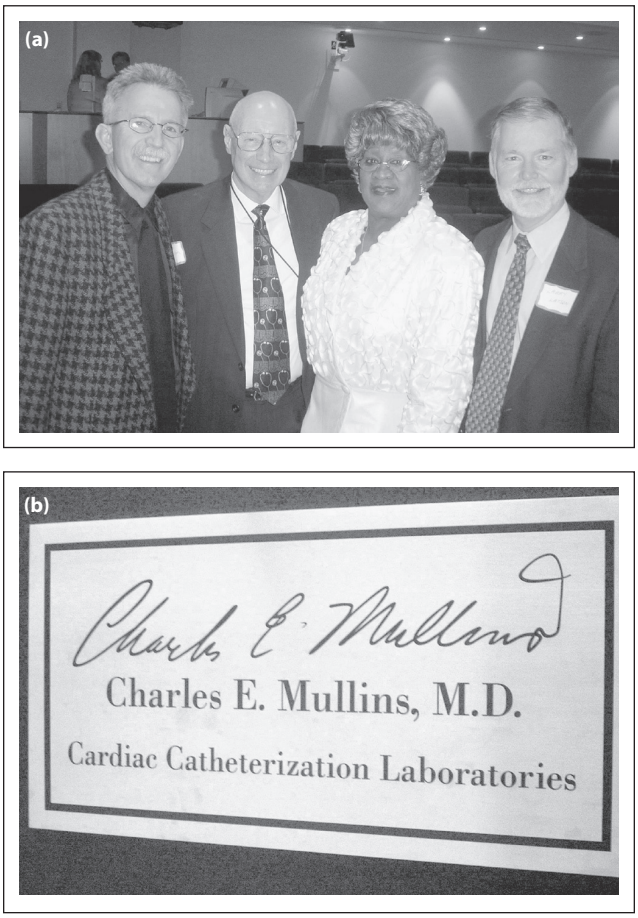

Figure 1.1 Charles E. (Chuck) Mullins, MD has taught and inspired many interventionalists specializing in congenital heart disease all over the world. (a) During the dedication ceremony at Texas Children's Hospital, Dr. Mullins gathers with some of his "aging" pupils and his longtime cath lab assistant. (b) The new cath labs were named in Chuck's honor … an honor well deserved.

A new era

Historically, cardiothoracic surgeons and interventional cardiologists have had a somewhat competitive relationship. This is especially true with physicians treating coronary and acquired cardiac disease in adults. However, a "team concept" has always been important when establishing a center of excellence for the treatment of complex congenital heart disease. The collaborative spirit between the cardiac surgeon and the entire cardiology team has advanced therapies offered to patients. More recently, the unique relationship between the interventionalist and

Figure 1.2 The unique and collegial relationship between the interventional cardiologist and cardiothoracic surgeon has fostered new Hybrid treatment strategies for complex congenital heart disease. However, sometimes the members of the team get confused and want each other's job!

surgeon has fostered combined transcatheter and surgical therapeutic options … so-called Hybrid treatment[1–3] (Figure 1.2). This innovative spirit mandates a fresh and open mind to create the "ideal" venue, or Hybrid Suite, to expand the capabilities of the traditional cath lab and operating room.[4] Now, our colleagues in structural heart disease (SHD) have also learned the value in collaborating with their cardiac surgeon colleagues. Transcatheter aortic valve replacement (TAVR) has been the "lightning rod" to encourage this teamwork, and new Hybrid Suites are being designed in this field as well.

Hybrid Suite design

In planning an ideal Hybrid Suite, there are five major considerations: (1) personnel who will be participating in the procedure, (2) adequate space for the equipment and personnel, (3) equipment that is necessary, (4) informational management and video display, and (5) necessary inventory and consideration of costs.

Personnel

Traditionally, the team responsible for performing both diagnostic and interventional cardiac catheterizations in children and adults with congenital heart disease consists of the interventional cardiologist, an assisting fellow or cath lab nurse, and technicians and nurses who are responsible for monitoring the physiologic recorder and the x-ray imaging equipment, and for "circulating" in the room to assist with the procedure. These team members were former ICU nurses, radiologic technicians, respiratory therapists, and paramedics who receive "on-the-job training." Specially trained registered cardiovascular invasive specialists (RCIS) are quite valuable in today's lab, as they are trained in all aspects of cath lab procedures and frequently have adult interventional experience. They are particularly helpful in treating adults with CHD and in the use of coronary stents, vascular closure devices, and small-diameter guidewires. All staff are "cross trained" to be able to run the imaging and hemodynamic equipment and rotate into any job necessary during the procedure. However, as the complexity of transcatheter procedures has evolved, many changes have been necessary to ensure safety and success.[5] A highly trained and competent assistant to the primary operator is imperative. A general pediatric cardiology fellow is usually inadequate to serve in this role today with the higher risk and complicated interventional procedures now performed. Therefore, it is becoming more common to have an advanced-level interventional cardiology fellow in the lab. However, many institutions do not have a general or advanced-level cardiology fellowship program, therefore, the role of a specially trained Interventional Nurse Practitioner has evolved and offers many advantages.

In addition to the team members mentioned above, dedicated cardiac anesthesia and cardiac ultrasound imaging is mandatory. This requires a staff anesthesiologist with assisting trainee or nurse anesthetist. A staff echocardiographer is also in attendance along with a fellow or technician. One gets the sense that the room is rapidly becoming crowded. By the way, dedicated anesthesia and echo equipment must find a home as well. With the new Hybrid procedures, the cardiothoracic surgeon and team will be present, which may include an assisting surgeon or resident, a scrub nurse, as well as the perfusionists and accompanying cardiopulmonary bypass machine. Now the suite really is shrinking! (Figure 1.3). The electrophysiologist and equipment when electrical therapy or a pacemaker is required can add up to 18 people, all with their specialized equipment, during a single Hybrid cardiac catheterization intervention for CHD!!! So, we have to design the suite to accommodate all of the personnel and the equipment.

Design: Space and ergonomics

The space required for a modern day Hybrid Cardiac Catheterization Suite is significantly more than a single-plane, adult coronary cath lab, or for that matter, the traditional biplane CHD cath lab built 10–20 years ago.[6–9] The suite design must account for the actual working space or procedure room, the control room, a computer "cold" room, an adjacent inventory supply room, and a new space very important to the modern suite … the induction room, where all of the "team" can assess the

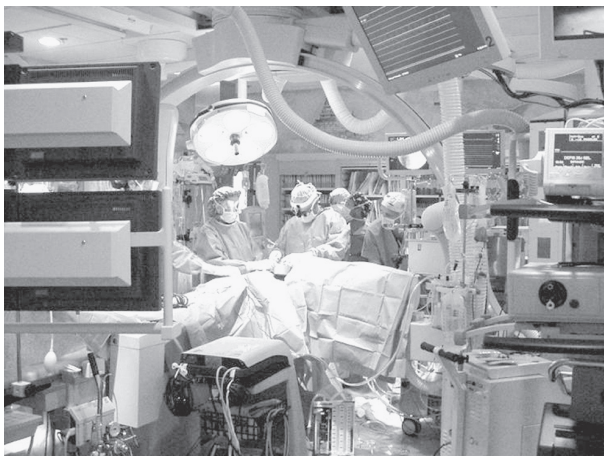

Figure 1.3 During a Hybrid cardiac procedure involving the surgical and interventional teams, as well as the perfusionist for cardiopulmonary bypass, the Hybrid Suite gets crowded very quickly. Space and proper ergonomics in design will overcome many obstacles in a traditional cath lab or operative suite.

patient and discuss the procedure, as well as administer sedative/anesthetic agents. With dedicated personnel now being assigned to the suites, it is desirable to also plan for administrative office space, personnel offices and workspace, a conference and editing room, a "break" area, and dressing rooms with bathroom and shower facilities. For the purpose of this chapter, we will confine our remarks to the essential space dedicated to the actual procedure being performed.

Ideally, the Hybrid Suite should be a minimum of 800 square feet (sq. ft), and preferably 900–1000 sq. ft (Figure 1.4). A square room, rather than the conventional rectangular suite, allows equal space around the catheterization table for complete patient accessibility … 30" × 30" or 33′ × 33′ would be "ideal." This is especially important when interventional procedures may be performed from either femoral, jugular, or subclavian sites, and let us also not forget about transhepatic access. In the majority of Hybrid procedures, access is required through a median sternotomy and personnel will be on both sides of the table. There must be room for the anesthesiology team and anesthesia equipment at the head of the patient and to either side, while space must also be available for the echocardiography personnel and echo machine at the head of the patient during transesophageal echo (TEE), and at the end of the table for intracardiac echo (ICE) or intravascular ultrasound (IVUS) (Figure 1.5a and b). The

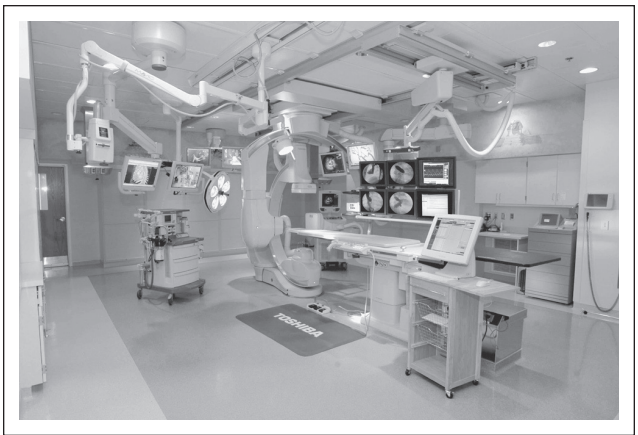

Figure 1.4 The appropriate space, design, and equipment are shown here in one of the Hybrid Suites at Columbus Children's Hospital. Note the flat-screen monitors, ceiling-mounted equipment, and video and equipment booms to allow easy access to the patient and informational imaging for all personnel.

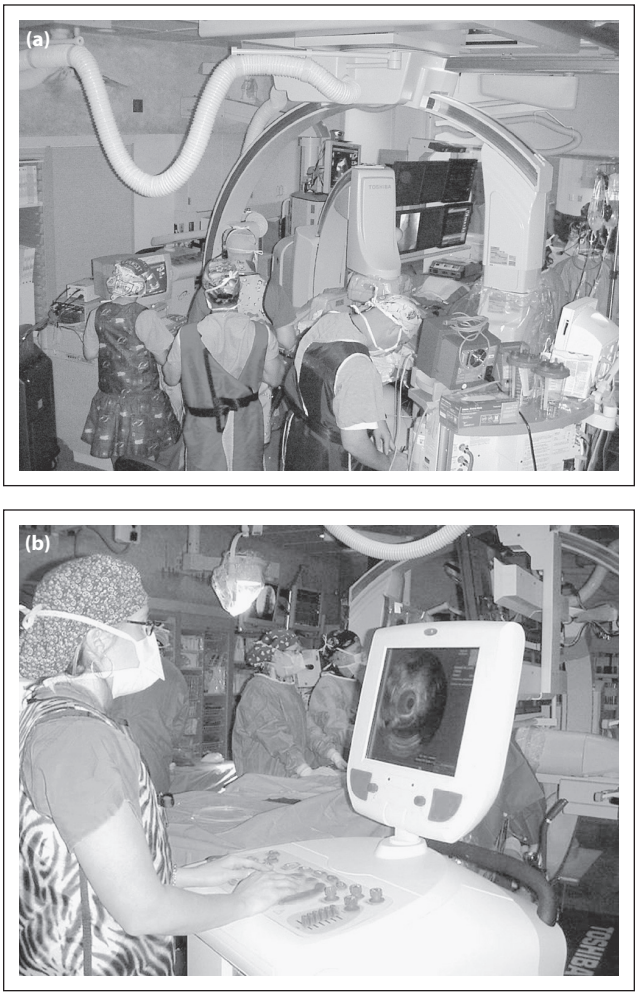

Figure 1.5 It is important to design appropriate space for the echo and anesthesia teams to be involved in transcatheter or Hybrid therapy for congenital heart disease. (a) The echo and anesthesia teams have a completely free space at the head of the table during TEE guidance of device closure. (b) In addition, during IVUS or ICE examination, the space at the foot of the table must also allow the team to do their job.

perfusionist and cardiopulmonary bypass machine will usually be positioned on the side opposite the surgeon and/or interventionalist, making the width of the room extremely important and different from a traditional cath lab … hence, a square room.

The control room should be as wide as the Hybrid Suite (25–33 ft) and approximately 10 ft in depth. This will allow all of the personnel, along with the physiologic and digital x-ray imaging equipment and monitors to be strategically placed. In addition, the digital review station and archiving system should be located in this room. In the combined interventional/electrophysiology suite, appropriate EP recording, pacing, radiofrequency ablation, and 3D mapping equipment must also be placed in the control room. This room should be designed in order for the personnel to view the procedure directly by looking down the table from the foot to the head of the patient (Figure 1.6). This ensures an unobstructed view of the procedure, regardless of the position of the biplane equipment or the team. Therefore, the patient table should be perpendicular to the control room. The adjacent computer or "cold room" size will be dependent on the manufacturer's specifications, but should allow easy access for maintenance or repair work to be performed. When building multiple suites, this room can be shared to conserve space.

The suite should also have an adjacent and ample supply room to store the extra inventory and consumable equipment that is not located in the cabinet storage within the procedure room. A blanket warmer is placed here, as well as other nonconsumable equipment. If possible, the adjacent supply room should be approximately 100–120 sq. ft and should be directly accessible from the procedure room for maximum efficiency. If there are multiple suites, then a larger central supply room could be used that is accessible to both suites.

A relatively new concept in both surgery and interventional cardiology is the use of an "induction room" adjacent to the Hybrid Suite (Figure 1.7). This room becomes very important, since it allows the interventional, anesthesia, and surgical teams direct access to the patient and family, while maintaining a quiet and comforting environment to explain the procedures, perform history and physical examinations, and administer sedation. By installing small, space-efficient anesthesia machines that can be mounted on the wall, induction can be performed here as needed. In addition, this room may serve as a separate TEE room while an interventional catheterization is being performed, allowing maximum efficiency of the anesthesiology team. Ideally, this room should be approximately 12 ft × 17 ft, which will allow the appropriate family members and personnel to interact in a comfortable environment.

Not mentioned is the mandatory soil or "dirty" room where reusable equipment is washed; this must be separate from the "clean" scrub room, as per OSCHA standards. Also, when building two Hybrid Suites, it becomes apparent that a centrally located scrub area with two separate sinks be located immediately outside the procedure rooms with open access from both control rooms, but appropriate barriers for infection control. This allows maximum efficiency and entry into both suites, while maintaining safety and a sterile environment.

Figure 1.6 The control room should be designed to allow personnel to view the catheterization procedure without obstruction. Note the clear line of view down the table during the final phase of Hybrid Suite construction.

Figure 1.7 A relatively new concept is the use of an "induction room," which allows access to the patient and family by all team members in a quiet environment. Wall-mounted anesthesia equipment conserves space and allows sedation or induction of anesthesia as needed. The room should be directly connected to the Hybrid Suite, as shown here.

Equipment

What used to be a pretty simple list of equipment needs 15 years ago, has mushroomed into a huge cloud of needs, wants, and money! Biplane x-ray imaging equipment and a physiologic monitoring system with recording and reporting capabilities occupied most of the capital expense requirements of the traditional lab. However, the new Hybrid Suite's capital equipment list has grown proportionally, incorporating many services within a Heart Center.

Beginning with x-ray equipment, we certainly live in a new age of imaging. While some might argue the merits of biplane versus single-plane fluoroscopic and angiographic units, no one would dispute the clear advantages of displaying complex spatial anatomy using biplane cameras. This is especially true when performing transcatheter procedures in the tiniest preterm neonate to the 200 kg adult with complex CHD. So in a perfect world and without consideration of costs or space requirements, a modern biplane, digital cath lab is mandatory to achieve optimal imaging for the complicated interventional procedures of today.

Today, no one would argue the merits of digital (film-free) radiographic systems. The obvious advantages of digital technology are real-time access and viewing; no deterioration of images; ease of storage, management, and retrieval of image data; and labor savings. The digital images are easily accessible both inside and outside the hospital using a web server, as well as by remote satellite transmission. Yet, just as the "digital age" in cardiac catheterization began over two decades ago, we now live in the world of PC-based digital platforms and flat-panel detectors (FPD). This began with General Electric Medical's introduction of a single-plane FPD, then the PC-based digital platform for hemodynamic monitoring systems arrived in 2004, and culminated with the introduction of biplane FPD technology in 2005 by Siemens Medical and Toshiba Medical Systems Corporation. The targeted specialties for this new equipment are centers specializing in CHD cardiac catheterizations, advanced electrophysiology laboratories, and neuroradiology treatment centers.

We must ask, what are the advantages of FPD technology?[10,11] The definition of FPD is a compressed or flat detector that uses semiconductors or thin-film transistors (TFT), converts x-ray energy into electrical signals, and creates x-ray images. Currently, indirect-conversion FPD technology is used for biplane systems. Eventually, direct conversion technology may be used, once the "blanking" and frame rate limitations are overcome in the biplane configuration. Direct conversion will improve resolution, as the image is never converted into light. The FPD will likely replace all existing x-ray detectors, such as image intensifier (I.I.)-TV cameras and spot film cameras, as well as film screen systems. For cardiovascular work, the small profile of the detector size will allow a more compact design and facilitate improved patient access. In addition, high image quality with improved blood vessel detectability by high modulation transfer function (MTF) and no distortion will be an advantage.

Finally, 3D digital tomography and interventions are now possible. A new imaging armamentarium that is proving extremely useful is 3D rotational angiography (3DRA). A single FPD is utilized and is rotated around the patient in ~4 s in a 200° arc while a continuous injection of contrast is being delivered. This image can be immediately displayed on the video monitor. More importantly, the data can be reconstructed by an image processor into a virtual 3D volume rendered image that can be viewed within 45–60 s. This 3D image has no limitations in demonstrating the complex anatomy in patients with CHD. One can view a structure from the patient's head, feet, back, front, and incorporating any angle of interrogation. One can also assess adjacent structures to evaluate their impact on the cardiac lesion. This greatly increases the interventionalists' understanding of spatial anatomy and defects … similar to a 3D CT scan. However, a great advantage is that transcatheter therapy can be performed with immediate 3DRA confirmation of the results (Figure 1.8). In the not too distant future 4DRA will become available. Some believe that the new technology of 3DRA and 4DRA may render biplane imaging equipment obsolete.

In the dedicated CHD Hybrid Suite, patient accessibility is equally important to high-quality imaging. Therefore, since the 3D gantry positioner was introduced by General Electric Medical nearly two decades ago, other companies now have realized the importance of patient access in a biplane lab. Since a three-dimensional gantry allows rotation of the C-arm in an X, Y, and Z axis, this allows additional space at the head of the table to accommodate the anesthesia and interventional teams. However, with the original design by GE and later Siemens Medical, the space was still crowded. The most recent and innovative design has come from Toshiba Medical Systems Corporation with a 5 axis C-arm positioner with biplane FPD (Infinix CF-i/BP), which allows movement in 5 axes around the patient, with rotation of the C-arm base to –135° or +135° which actually places the C-arm on the "foot" side of the lateral camera (Figure 1.9). This allows a completely "head-free zone" of 180° while in a biplane configuration, allowing easy access to the patient by the anesthesia, echo, and interventional teams (Figure 1.10). It is also highly beneficial to the electrophysiology service during complex studies with transvenous pacemaker implantation.

All teams must have not only free access to the patient, but also a clear line of sight to the image display monitors. Speaking of monitors, the days of the CRT monitors over. Flat-screen monitors have achieved comparable black-white, grayscale, and line resolution, and are ergonomically more versatile in a biplane laboratory. They take up less space, are lighter, and can be mounted on a

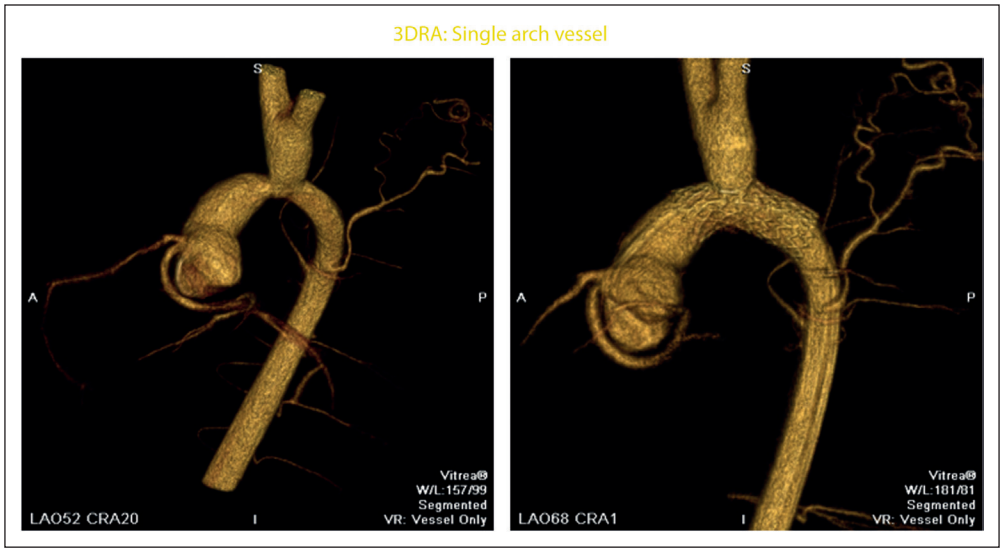

Figure 1.8 (**See color insert.**) A 3-dimensional rotational angiogram (3DRA) nicely demonstrates a complex postoperative aortic arch obstruction before and after stent therapy.

six-monitor gantry that can be strategically placed around the procedure table to allow optimal viewing by all personnel participating in the procedure, regardless of location (Figure 1.11). This gantry should be able to be placed on either side of the table, as well as over the table at the head or foot of the patient. Newer and larger, single multi-imaging monitors are becoming popular while allowing multiple sources of images to be displayed directly in front of the operator. In the Hybrid Suite, it is also important to install a surgical light mounted strategically on the ceiling. We also prefer to mount all other accessory equipment from the ceiling, that is, contrast injector with wall-mounted controls, local spotlight, and radiation shield.

The other components of x-ray imaging equipment found in the Hybrid Suite are fairly standard by today's standards. TV cameras using the charged-coupled device (CCD) technology, developed by Toshiba Medical Corporation, to improve brightness and resolution; x-ray tubes using spiral-grooved and liquid metal bearing technology, introduced by Phillips Medical to eliminate noise and reduce the delay in fluoro/digital acquisition; and high-frequency generators are now uniformly offered by all manufacturers. Furthermore, while using different technology, radiation dose management is a priority with all manufacturers to protect the patient and all those participating in the longer interventional catheterization procedures being performed today.[12] Advanced imaging processing (AIP) has been introduced by Toshiba Medical Systems to improve fluoroscopic images by reducing noise artifacts and eliminate frame averaging, which in turn allows "fluoro record" to be used instead of digital acquisition … significantly reducing x-ray exposure (Figure 1.12). New innovations,

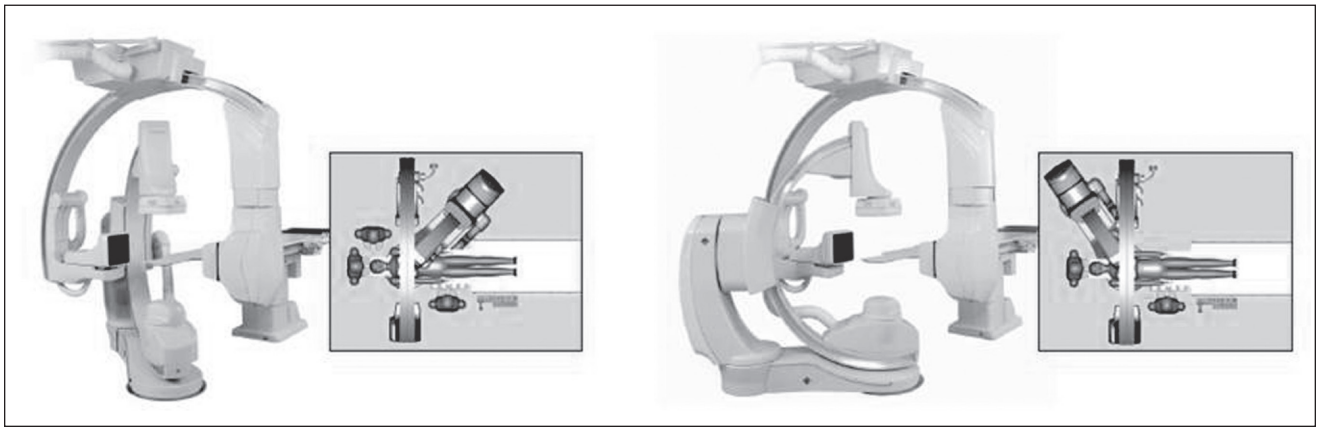

Figure 1.9 The new design of the Toshiba Infinix CF-i/BP positioners allows rotation of the C-arm base from –135° to +135°. This schematic drawing demonstrates the 180° of "head-free zone" afforded by this new design.

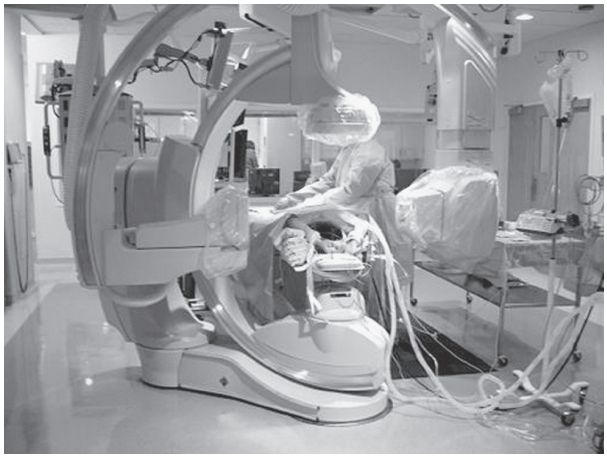

Figure 1.10 During a cardiac catheterization procedure, the open space at the head of the table is nicely demonstrated here. There is plenty of room for the interventional, echo, and anesthesia teams to perform their jobs.

such as "spot fluoroscopy" and "dose-tracking technology," are being introduced by the same manufacturer, which will further improve radiation safety for patients and personal in the Hybrid Suite.

An important, but forgotten, component of the new Hybrid Suite is the procedure table. Traditional cath lab tables have certain features that are well suited for x-ray imaging, patient positioning, quick and easy "free float" movement, and are electronically integrated into the manufacturer's x-ray imaging equipment. In addition, some tables have the ability to be placed in the Trendelenburg position. In comparison, the traditional operating room table is narrower, shorter, less "fluoro friendly," and does not provide "free float" capabilities. Additionally, the table has the very important feature of 15–30° lateral tilt, which provides the cardiothoracic surgeon with exposure to the desired operative field ergonomically, while the Trendelenburg position is also possible. So, currently, either the surgeon or the interventionalist must make sacrifices while performing Hybrid procedures in the traditional operative or catheterization suite. A new Hybrid table is essential to facilitate new Hybrid management strategies for complex CHD. The table must be manufactured by the x-ray equipment companies in order to provide "connectivity" to the imaging equipment and possess tableside controls. This table must possess all of the above-mentioned specifications, so will require input from both cardiothoracic surgeons and interventional cardiologists as they are designed. Phillips Medical initially designed the first integrated Hybrid table, then Toshiba Medical Systems (Figure 1.13). Stay tuned for more in the future!

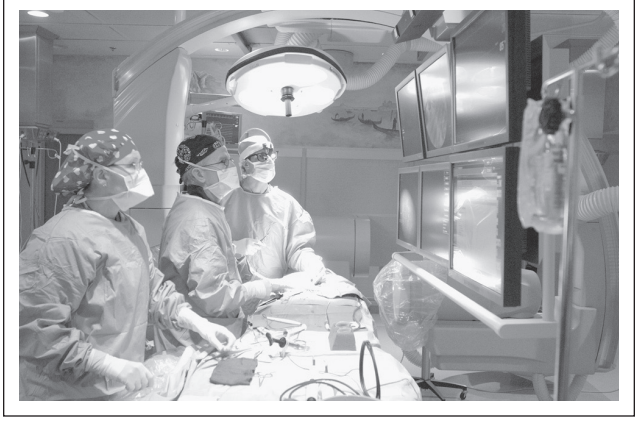

Figure 1.11 Flat-screen monitors have now approximated CRT monitors in terms of resolution. The lighter, more compact configuration of the flat-screen monitors allows a gantry holding six monitors to be easily positioned at any location for the Hybrid team to view the images, as depicted here during a Stage I Hybrid palliation for HLHS.

Informational management, video display, and transport

Staggering amounts of information are generated in today's healthcare environment and these data need to be readily available during the procedures. In our Heart Center, we attempted to provide access for angiography, echocardiography (including TTE, TEE, ICE, and IVUS), and the PACS system (CT, MRI, and chest x-ray) from any computer inside or outside the hospital with a dedicated web server and VPN access. This same information must be readily available in the new Hybrid Suites where complex procedures and decision making are being performed by the multidisciplinary team. The information needs to be accessible to all participants in the suite and must be specific to their assigned tasks. If the staff moves around the room, so must the displayed images. Furthermore, all of this information should be able to be transmitted to other sites within the hospital, that is, operative room, teleconference center, or research lab, as well as to sites anywhere in the world, that is, educational conferences, outside referring physicians for patient care, and teaching workshops. A dedicated and expansive archiving system is imperative for the digital technology of today. The data must be sent "seamlessly" between the archived source to the active procedure and/or educational site.

In an ideal world, money, space, and hospital administrative support would be unlimited. So, let us begin with the video display within the Hybrid Suite. Flat-screen monitors are strategically placed around the room, mounted to ceiling booms with a rotational axis that provides viewing from any location (Figure 1.14). We chose to enlist the expertise of Stryker Communications to fulfill these needs. Two monitors are mounted on three video booms, while one of the booms also serves as an equipment boom.

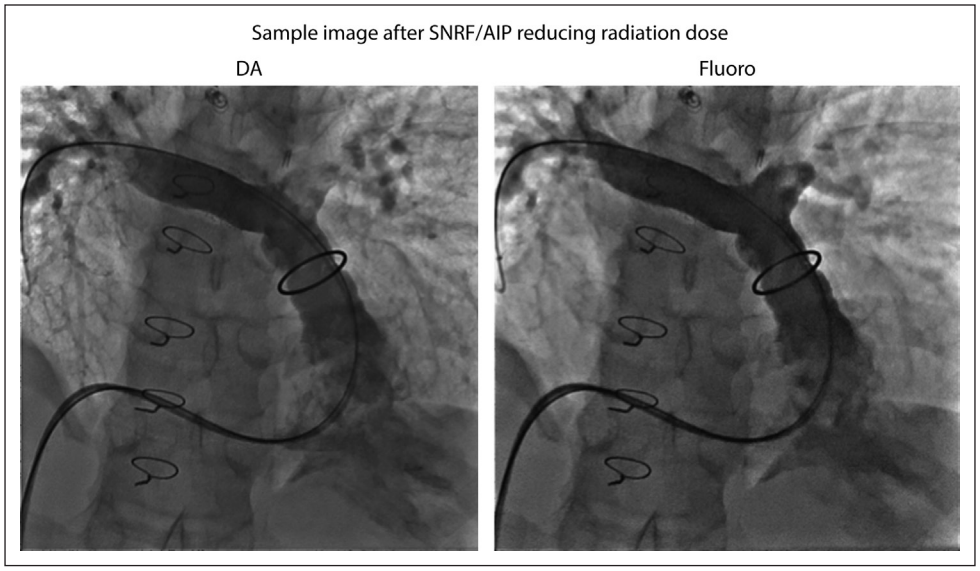

Figure 1.12 Advanced image processing (AIP) using signal noise reduction filter (SNRF) technology allows comparable diagnostic image quality compared with digital acquisition (DA) with significantly lower radiation dose, as seen in this patient before Melody TPV implant.

Mounted on the equipment boom is a defibrillator, fiber-optic surgeon's headlight, electrocautery, and a pan/tilt/zoom video camera. A second camera is mounted on the wall above the control room, providing expansive views of the suite and the procedures being performed. A video router is located within each suite and allows any image to be displayed on any video monitor, allowing each staff member optimal viewing of the information pertinent to their job. In turn, the video router in the Hybrid Suite is connected to a larger management and routing unit within the Teleconference Center, serving as the "mother ship" (Figure 1.15). All information can be transmitted anywhere in the world from this location. We believe this "video network topology" to be the framework of the future.

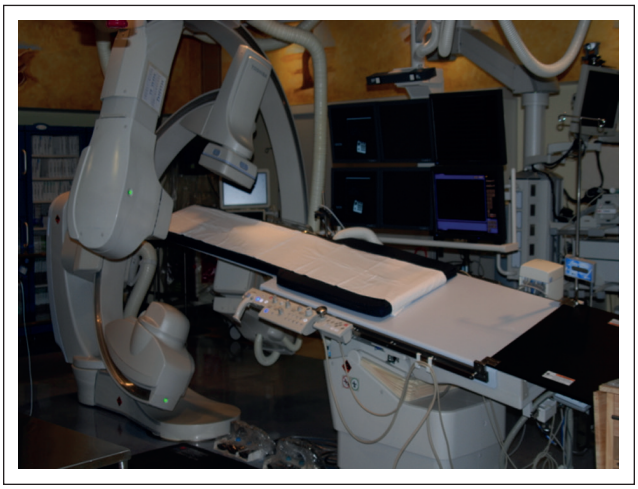

Figure 1.13 (**See color insert.**) An integrated table in the cardiac catheterization suite with x-ray equipment is mandatory. The ability of the table to "cradle or roll" and be placed in the Trendelenburg and reverse Trendelenburg positions is very important to the cardiac surgeon … as demonstrated in this photograph.

Inventory

Every cardiac catheterization procedure in patients with CHD requires a large inventory of "routine" consumable items. In addition, each interventional procedure requires an additional inventory of special and very expensive consumable materials. Words from my mentor, Dr. Mullins, are etched in my mind. "In a congenital heart laboratory, all consumable items must be available in a very wide range of sizes in order to accommodate every patient's size, from the tiniest premature neonate to the largest adult patient. A cardiac catheterization procedure NEVER should be compromised or terminated because of the lack of a necessary piece of consumable equipment." However, these special consumables will vary with the individual operator's experience and credentials, as well as with the availability of a particular device or material in any particular part of the world. Equally important in determining inventory is the individual hospital administrator's "budget" control. We are very fortunate to have tremendous hospital support, which seemingly allows unlimited access to all available consumables, that is, balloon catheters, devices, and delivery systems, stents, guidewires, RF perforating systems, all imaging

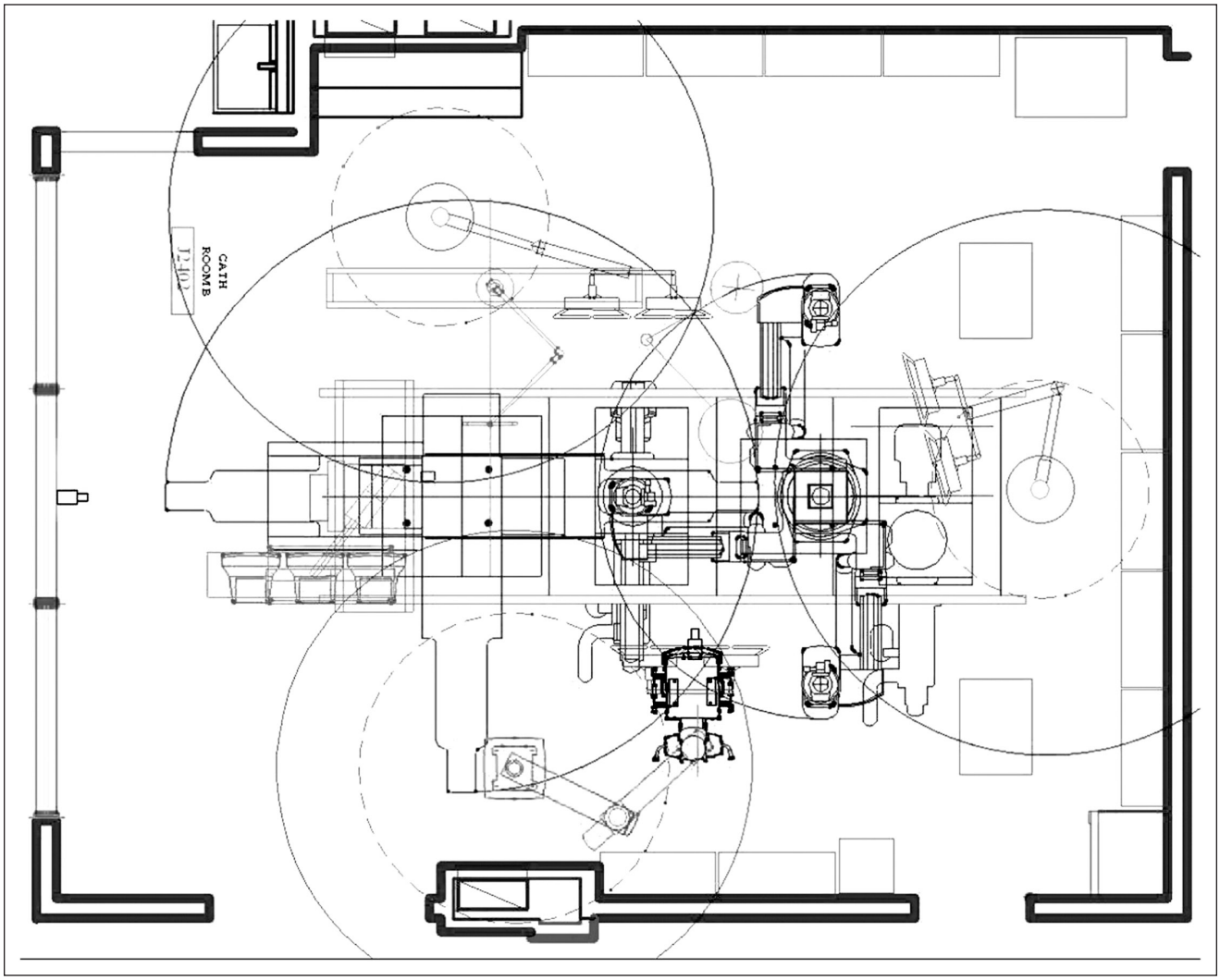

Figure 1.14 The schematic drawing of our Hybrid Suite demonstrates the importance of careful planning, input from multiple members of the Heart Center, and collaboration with several industry representatives. Note the video monitor and equipment boom design to ensure all personnel can view the appropriate images during the procedure, regardless of their location in the suite.

equipment (TTE, TEE, ICE, IVUS), and so on … which are justified and "reasonable." Now, we have to contend with stocking the extraordinarily expensive transcatheter heart valves! Accordingly, our inventory consumable costs are nearly US$2 million, so it is incumbent upon the cath lab manager and medical director to maintain strict inventory control and management. New "bar coders" can be used to scan all consumables used during the procedure to maintain an accurate accounting for billing purposes, as well as maintaining a computerized inventory and order management system. We have incorporated RFID technology (Mobile Aspects) in our suites that has proven to be extremely cost effective. The system tracts the inventory used for each patient, maintains par levels by reordering supplies, and bills the costs of the materials. Most new hemodynamic systems have an inventory management program that can be used for this purpose. Unfortunately, economics, rather than necessity, will continue to dictate the practice of medicine.

Hybrid Cardiac Operating Suite

As the Hybrid procedures may be heavily weighted to a surgical component, it became clear that we needed to also design a Hybrid Cardiac Operating Suite to meet these needs (Figure 1.16a). The room design and equipment needs are a bit different from the Hybrid Cath Suite. The room space is similar, but a single-plane, ceiling-mounted FPD is more desirable in order to maintain the ergonomics of the surgical, anesthesia, and perfusion teams. A floor-mounted imaging system would be in the way, while the

Figure 1.15 A large video router and informational management unit is located in our Teleconference Center and provides interconnectivity to the Hybrid Suites through the smaller video router and cameras within each suite. In turn, the operative suite and research laboratory can also be connected through the Teleconference Center, providing a "video network topology" for worldwide education and patient care.

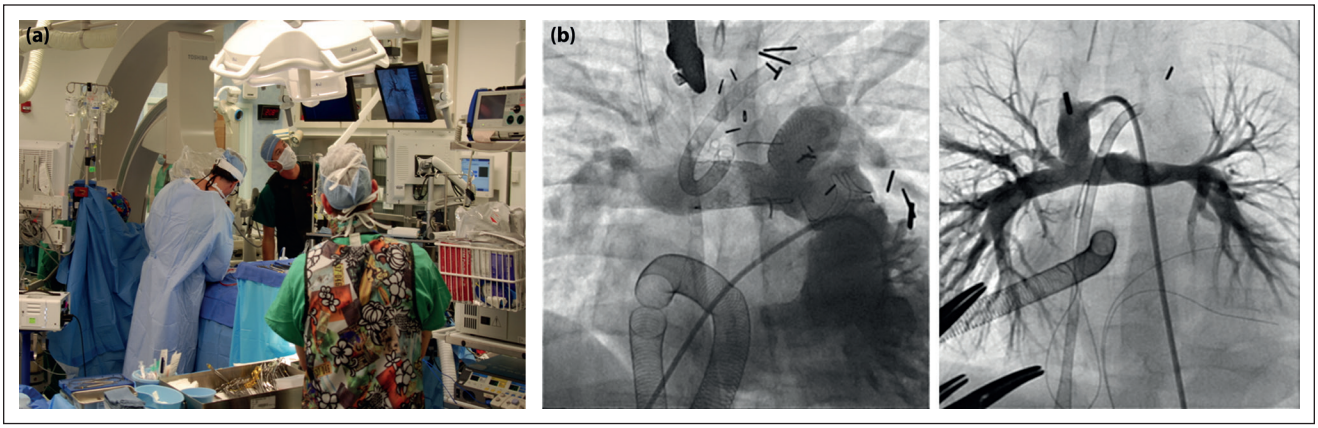

Figure 1.16 (**See color insert.**) The Hybrid Cardiac Operating Suite was the next evolution in Hybrid therapies and is used in both CHD and SHD. This will accommodate all members of the Hybrid team (a). Exit angiography can now be easily performed to assess the operative procedure before the patient returns to the ICU, as seen in these two patients: after pulmonary valve replacement and intraoperative stents and after Comprehensive Stage II repair for HLHS (b).

ceiling-mounted system can be parked and easily positioned at the table when needed. The video monitors and imaging equipment are similar to the Hybrid Cath Suite. The control and equipment rooms can be smaller.

We have introduced "exit angiography" in this suite to better understand the results of complex surgical treatment of CHD (Figure 1.16b). We may then elect to treat any residual anatomic abnormalities by either surgical or transcatheter techniques before the patient leaves the Operating Suite and minimize a "stormy" CTICU course. More recently, we have introduced 3DRA into the Hybrid Cardiac Operative Suite to allow a more comprehensive evaluation in a single-plane environment (Figure 1.17).

Summary

In conclusion, collaboration between the interventional cardiologist and cardiothoracic surgeon continues to increase as the Hybrid strategies for complex CHD evolve. Making informational resources available when and where they are needed can have a dramatic impact on patient care.

Figure 1.17 (**See color insert.**) The newest technology that has been added to the Hybrid Cardiac Operating Suite is 3DRA, as shown here in the meticulous setup in our suite.

The implementation of Hybrid Cardiac Catheterization and Operative Suites are a result of careful planning involving multiple disciplines, including Heart Center medical staff, equipment manufacturers, architects, contractors, and information technology specialists. Specially designed equipment and trained personnel are paramount to success. A huge inventory of consumables is required and must be judiciously managed. However, there is no substitute for a collegial and professional relationship and understanding among the Heart Center staff of the ultimate goals of success. Finally, it must be recognized that a progressive and forward-thinking hospital administrative staff is a prerequisite for the planning, building, and financial support necessary for the ideal Hybrid Cardiac Suites to become a reality.

References

1. Diab KA, Hijazi ZM, Cao QL, Bacha EA. A truly hybrid approach to perventricular closure of multiple muscular ventricular septal defects. *J Thorac Cardiovasc Surg* 2005;130(3):892–3.
2. Galantowicz M, Cheatham JP. Lessons learned from the development of a new hybrid strategy for the management of hypoplastic left heart syndrome. *Pediatr Cardiol* 2005;26(2):190–9.
3. Holzer R, Hijazi ZM. Interventional approach to congenital heart disease. *Curr Opin Cardiol* 2004;19(2):84–90.
4. Melvin DA, Chisolm JL, Lents JD, Chucta SD, Kish EC, Hardin J et al. A first generation hybrid catheterization laboratory: Ready for "prime time." *Catheter Cardiovasc Interv* 2004;63(1):123 (abst).
5. Mullins CE. History of pediatric interventional catheterization: Pediatric therapeutic cardiac catheterizations. *Pediatr Cardiol* 1998;19(1):3–7.
6. Mathewson JW. Building a pediatric cardiac catheterization laboratory and conference room: Design considerations and filmless imaging. *Pediatr Cardiol* 1996;17(5):279–94.
7. Verna E. Evolution of the catheterization laboratory: New instruments and imaging techniques. *Ital Heart J* 2001;2(2)116–7.
8. Section on Cardiology and Cardiac Surgery: American Academy of Pediatrics. Guidelines for pediatric cardiovascular centers. *Pediatrics* 2002; 109(3):544–9.
9. American College of Cardiology/Society for Cardiac Angiography and Interventions Clinical Expert Consensus Document on cardiac catheterization laboratory standards. A report of the American College of Cardiology Task Force on Clinical Expert Consensus Documents. *J Am Coll Cardiol* 2001;37(8):2170–214.
10. Holmes DR Jr, Laskey WK, Wondrow MA, Cusma JT. Flat-panel detectors in the cardiac catheterization laboratory: Revolution or evolution—What are the issues? *Catheter Cardiovasc Interv* 2004;63(3):324–30.
11. Chotas HG, Dobbins JT, Ravin CE. Principles of digital radiography with large-area, electronically readable detectors: A review of the basics. *Radiology* 1999;210:595–9.
12. Ross RD, Joshi V, Carravallah DJ, Morrow WR. Reduced radiation during cardiac catheterization of infants using acquisition zoom technology. *Am J Cardiol* 1997;79(5):691–3.

2

Operators' credentials and institutional requirements for congenital and structural heart disease

Ziyad M. Hijazi and Ted Feldman

Introduction

The category of congenital and structural (noncoronary) heart disease is large and growing. Congenital heart disease is the most common birth defect, with an incidence of approximately 1%. Most patients born with a cardiac defect live into adulthood. As of a few years ago in the United States, the number of adult patients with congenital cardiac defects (repaired, palliated, or unoperated) has exceeded those in the pediatric age group. Further, there are hundreds of thousands of patients who have valvular heart disease, including aortic valve stenosis, mitral regurgitation, and other valvular heart diseases. As the population ages, the number of patients with valvular heart disease is increasing.

The field of transcatheter treatment for congenital and structural/valvular heart disease has grown explosively over the past several years. Advances in new percutaneous devices and valves has enabled us to treat patients who only few years ago were thought to be either high-surgical-risk candidates or inoperable. The interest level in less invasive treatment options from patients and the medical community alike has increased significantly. Further, the recent regulatory approval of percutaneous valves and other devices to treat congenital and "structural" heart disease sparked the interest of many physicians and hospitals wanting to offer such treatment modalities to their patients.

While training program content, standards, credentialing, and board certifications for percutaneous coronary intervention have become well-developed, no such structure exists in the field of congenital, structural, or valvular heart disease therapies. In the absence of formalized criteria for training, some general principles are clear. Therefore, we believe that individuals and institutions that are interested in offering such therapies have to meet certain minimum criteria that will be discussed below.

Establishing a program in structural heart disease interventional therapies requires several key components (Table 2.1).

Operator knowledge base and training

Adequate knowledge in congenital and structural heart disease is essential for one individual to be able to care for and manage patients with various forms of congenital and structural heart disease. Currently, most interventional cardiovascular (CV) disease fellowship programs in the United States do not adequately train the individual to be able to perform or even care for such complex patients. We believe a minimum training of one year in a busy program that handles congenital and structural heart disease patients may be adequate to prepare such physicians on basic principles and to acquire core knowledge of the disease processes and treatment. The SCAI (Society for Cardiovascular Angiography and Interventions) has published a paper in which the core curriculum has been identified for pediatric invasive cardiologists who are to care for complex forms of congenital heart disease.[1] Also, the SCAI Structural Heart Disease Council has published

Table 2.1 Considerations for training

Knowledge base
Training
Simulation
Proctorship
Research trials
Multidisciplinary team
Institutional resources
Physical plant
Equipment/supplies
Personnel

another paper dealing specifically with the knowledge base for physicians who are to perform interventional procedures in adults with congenital and structural heart disease.[2]

Often, you may find a program that may be busy in one discipline or category of procedures but not in another. Therefore, the individual may seek further help/training from more than one program. The SCAI launched a survey in the United States of all programs that train physicians in congenital/structural heart disease.[3] In that survey, it was clear that not all institutions offer the entire spectrum in training. Further, the number of procedures performed in most institutions may not be large enough to train more than one individual. A similar survey is being arranged for European centers and perhaps other parts of the world.

Simulation/proctorship

The role of simulation in acquiring basic skills has seen dramatic increase in the last few years. Any new device that gets approval from the United States FDA includes in the regulatory process definition of a training program on how to use these devices once approved. Manufacturers and the FDA work together in setting the tone and process of device dissemination. For example, for atrial septal defect closure devices, prior to actually doing the case, the manufacturer requires the individual operator to attend a course. In that course, in addition to didactic lectures, there is a simulator where the operator gets trained on the device mechanics/techniques prior to doing any patient. Although, the simulators never exactly portray reality, they are the closest things to reality. The use of simulation in aviation training is well known.[4] There has been extensive experience with simulators in medicine, including anesthesiology for intubation and surgery for laparoscopic procedure training. For ASD closure, once the individual passes the training course, then the second phase moves to proctorship, where a certified proctor from the manufacturer visits and works with the individual on few cases. At the end of these training sessions, the proctor decides if the individual is ready to be an independent operator or he/she may require further training. This paradigm applies to the physician who is already out in practice, but does not provide a structure for training programs.

In contrast to coronary interventions, there are no published numbers to go by for certifying individuals in congenital/structural heart disease interventions. However, the American College of Cardiology/American Association for Thoracic Surgery (AATS)/Society of Thoracic Surgeons (STS)/SCAI have published a paper regarding transcatheter aortic valve implantation[5] in which a certain minimum number of procedures had to be acquired by the operators to be certified for the use of said valves. In that paper, the decision on certain numbers was not based on published evidence, but rather it was a consensus opinion. The published standards for coronary training create a paradox. The "magic number" for procedure volume for percutaneous coronary intervention (PCI) is 250 during an interventional fellowship. Congenital and structural procedure volumes are much lower than coronary, but many of the procedures are more complex. It is not possible to require even 100 cases during fellowship for most structural interventions.

Clinical research and clinical trials

One of the best avenues for training is participation in clinical trials. Many of the congenital and structural devices are new, and trials are ongoing to define their roles in practice, or to develop next-generation devices. Trial participation includes formal device training and also continued interaction with other operators regarding improvements in techniques and problem solving.

Institutional requirements

Any institution interested in offering patients transcatheter treatment for congenital and structural heart disease has to meet certain criteria. Obviously, the availability of cardiac surgery on the premises is essential. For congenital heart disease interventions, the presence of a program in congenital cardiac surgery is essential. This program should be performing all types of congenital cardiac surgery, from the simple to the most complex. Operations should be performed by at least one certified congenital cardiac surgeon. The need for a surgical program has less to do with surgery itself, and more to do with having an environment where decisions are made collaboratively. The institution should have a dedicated cardiac catheterization laboratory where cardiac catheterization (diagnostic/interventional) can be performed safely on such patients. For valvular heart transcatheter therapy, the presence of a hybrid suite is recommended with all the regulations that come with hybrid suites.[6] Detailed requirements have been determined by CMS (Centers for Medicare and Medicaid Services) for TAVR (transcatheter aortic valve replacement) procedures (Table 2.2).[7]

The cardiac catheterization/hybrid suite should be equipped with large inventory, including but not limited to:

Biplane fluoroscopy is preferable, but not essential; vascular closure devices and sheaths of varying sizes (from 6 to 24 Fr), length, and types, including Mullins sheaths; a wide variety of catheters (end holes, side holes, etc.); a variety of guide wires (hydrophilic, steerable, soft, stiff, extra stiff, and supra- and ultra-stiff), in regular length and exchange lengths; coronary and peripheral balloon dilation catheters of various sizes (balloon diameter and length), semi-compliant and noncompliant, low-pressure and high-pressure; stents of various sizes and design (open cell

Table 2.2 CMS operator and institutional requirement for TAVR

The patient (preoperatively and postoperatively) is under the care of a heart team: a cohesive, multidisciplinary team of medical professionals. The heart team concept embodies collaboration and dedication across medical specialties to offer optimal patient-centered care.

TAVR must be furnished in a hospital with the appropriate infrastructure that includes but is not limited to

1. On-site heart valve surgery program
2. Cardiac catheterization lab or hybrid operating room/catheterization lab equipped with a fixed radiographic imaging system with flat-panel fluoroscopy, offering quality imaging
3. Noninvasive imaging such as echocardiography, vascular ultrasound, computed tomography (CT), and magnetic resonance (MR)
4. Sufficient space, in a sterile environment, to accommodate necessary equipment for cases with and without complications
5. Post-procedure intensive care facility with personnel experienced in managing patients who have undergone open-heart valve procedures
6. Appropriate volume requirements per the applicable qualifications below

There are two sets of qualifications; the first set outlined below is for hospital programs and heart teams without previous TAVR experience and the second set is for those with TAVR experience.

Qualifications to begin a TAVR program for hospitals without TAVR experience:
The hospital program must have the following:

1. ≥50 total AVRs in the year prior to TAVR, including ≥10 high-risk patients
2. ≥2 physicians with cardiac surgery privileges
3. ≥1000 catheterizations per year, including ≥400 PCIs per year

Qualifications to begin a TAVR program for heart teams without TAVR experience:
The heart team must include:

1. Cardiovascular surgeon with:
   a. ≥100 career AVRs including 10 high-risk patients; or
   b. ≥25 AVRs in one year; or
   c. ≥50 AVRs in 2 years; and which include at least 20 AVRs in the last year prior to TAVR initiation
2. Interventional cardiologist with:
   a. Professional experience with 100 structural heart disease procedures lifetime; or
   b. 30 left-sided structural procedures per year of which 60% should be balloon aortic valvuloplasty (BAV). Atrial septal defect and patent foramen ovale closure are not considered left-sided procedures
3. Additional members of the heart team such as echocardiographers, imaging specialists, heart failure specialists, cardiac anesthesiologists, intensivists, nurses, and social workers
4. Device-specific training as required by the manufacturer

Qualifications for hospital programs with TAVR experience:
The hospital program must maintain the following:

1. ≥20 AVRs per year or ≥40 AVRs every 2 years
2. ≥2 physicians with cardiac surgery privileges
3. ≥1000 catheterizations per year, including ≥400 PCIs per year

Qualifications for heart teams with TAVR experience:
The heart team must include:

1. A cardiovascular surgeon and an interventional cardiologist whose combined experience maintains the following:
   a. ≥20 TAVR procedures in the prior year, or
   b. ≥40 TAVR procedures in the prior 2 years
2. Additional members of the heart team such as echocardiographers, imaging specialists, heart failure specialists, cardiac anesthesiologists, intensivists, nurses, and social workers

design vs. closed cell), short or long, bare and covered, and stent grafts for bail out dissections; snares of various sizes to retrieve foreign objects or to snare wires. Availability of valves of various sizes is a must if transcatheter valve replacement (aortic/pulmonic) is to be performed. The inventory is costly, and there are items that may not be used every 2 years, but their presence is essential. The cost of replacing expired inventory is part of "the cost of doing business," and this requires an institutional commitment. A failed procedure due to lack of proper equipment is no excuse!

Multidisciplinary team

The institution must have what is called a "heart team" on the premises. This concept has been adopted now by the major medical and surgical cardiovascular societies and is an integral part of the CMS requirements for institutions performing TAVR.[7] As stated in the CMS document, "The heart team concept embodies collaboration and dedication across medical specialties to offer optimal patient-centered care." The heart team should include interventional cardiologists who are trained and meet the procedure volume criteria for certification, cardiac and vascular surgeons who are also trained/certified, echocardiographers, CV anesthesiologists, perfusionists, nurse practitioners, and so on. The presence of other noncardiac services in the hospital is essential to manage these complex and often co-moribund patients, including pulmonologists, nephrologists, ID specialists, and others. The cardiology specialist has to develop considerable cross-specialty expertise as well, particulary with ultrasound and CT imaging.

Conclusion

Requirements for operator and institutional credentialing for congenital and structural interventions are largely undefined. The recent approval of TAVR has included criteria for this one procedure, and we will see more as other new devices are approved. In the meantime, some appreciation for a basic core curriculum[1] is essential, and each operator has a responsibility to pursue his or her training in the spirit of becoming competent for a given procedure with the welfare of the patient as the guide, rather than simply complying with some arbitrary numerical procedure requirement. The experience we gain in training programs is usually just the beginning of a program of lifelong learning, and it takes many years to become proficient in the wide array of congenital and structural interventions. Structural intervention should be a full-time job for those who practice it!

References

1. Ruiz CE, Mullins CE, Rochini AP, Radtke WAK, Hijazi ZM, O'Laughlin MP et al. Core curriculum for the training of pediatric invasive/interventional cardiologists: Report of the Society for Cardiac Angiography and Interventions Committee on Pediatric Cardiology Training Standards. *Cath Cardiovasc Diag* 1996; 37:409–24.
2. Ruiz CE, Feldman TE, Hijazi ZM, Holmes DR, Webb JG, Tuzcu EM et al. Interventional fellowship in structural and congenital heart disease for adults. *Catheter Cardiovasc Interv* 2010;76:E90–105.
3. Marmagkiolis K, Hakeem A, Cilingiroglu M, Bailey SR, Ruiz C, Hijazi ZM et al. The Society for Cardiovascular Angiography and Interventions Structural Heart Disease Early Career Task Force Survey Results: Endorsed by the Society for Cardiovascular Angiography and Interventions. *Catheter Cardiovasc Interv* 2012; 80:706–11.
4. Gallagher AG, Cates CU. Virtual reality training for the operating room and cardiac catheterisation laboratory. *Lancet* 2004 Oct 23–29;364(9444):1538–40.
5. Tommaso CL, Bolman III RM, Feldman T, Bavaria J, Acker MA, Aldea G et al. Multisociety (AATS, ACCF, SCAI, and STS) Expert Consensus Statement: Operator and institutional requirements for transcatheter valve repair and replacement, Part 1: Transcatheter aortic valve replacement. *J Am Coll Cardiol* 2012;59:2028–42; originally published online Mar 1, 2012.
6. Bashore TM, Balter S, Barac A, Byrne JG, Cavendish JJ, Chambers CE et al. 2012 American College of Cardiology Foundation/Society for Cardiovascular Angiography and Interventions Expert Consensus Document on Cardiac Catheterization Laboratory Standards Update. *Cathet Cardiovasc Interven* 2012;80:E37–49.
7. National Coverage Analysis (NCA) for Transcatheter Aortic Valve Replacement (TAVR) (CAG-00430N). http://www.cms.gov/medicare-coverage-database/details/nca-details.aspx?NCAId=257&NcaName=Transcatheter+Aortic+Valve+Replacement+%28TAVR%29&DocID=CAG-00430N&bc=gAAAAAgAAAAA&.

3

Angiography

Lee Benson and Haverj Mikailian

Introduction

Accurate anatomical and physiological diagnosis is the foundation of a successful catheter-based therapeutic procedure. As such, a number of complementary imaging modalities have been developed to define, in real time, specific aspects of the heart and circulation for interventional applications. In the evolution of our understanding of the cardiovascular system, angiography and fluoroscopy were the first to be developed, and the angiography suite remains the cornerstone around which the interventional suite is built.

This chapter will include a discussion of standard angiographic approaches and how to achieve them. Emphasis will be placed on the application of these projections as applied to interventional procedures. A detailed description of the physical principles of image formation is beyond the scope of this chapter and the interested reader is referred to other sources for more detailed information.[1]

Angiographic projections

In the therapeutic management of the child with a congenital heart lesion, the spatial orientation and detailed morphology of the heart and great vessels are of critical importance. As the operator enters the laboratory, an overall understanding of the anatomy should have been synthesized, based on information from other imaging modalities such as chest roentgenography echocardiography, and computed tomographic, and magnetic resonance imaging. As such, the angiographic projections used in the procedure will be "tailored" to outline the lesion to allow appropriate measurements and guide the intervention.

In most children, the heart is oriented obliquely, with the left ventricular apex being leftward, anterior and inferior, and then the heart base (Figure 3.1). The interventricular septum is a complex geometric three-dimensional structure that takes an "S" curve from the apex to base (Figure 3.2), the so-called sigmoid septum. From caudal to cranial, the interventricular septum curves through an arc of 100–120°. The right ventricle appears as an appliqué to the left. To address this unique topology, today's angiographic equipment allows a wide range of projections, incorporating caudocranial or craniocaudal angulations to outline or profile specific structures. The up-to-date laboratory of today consists of independent biplane-imaging chains, with which the proper selection of views minimizes overlapping and foreshortening of structures.[2]

Terminology

Angiographic projections are designated according to either the position of the recording detector (image intensifier or flat-panel detector) or the direction of the x-ray beam toward the recording device. Generally speaking, in cardiology the convention is the former, and all terminology discussed henceforth will use that convention. For example, when the detector is directly above a supine patient, the x-ray beam travels from posterior to anterior and the *angiographic projection* is designated posteroanterior (PA), but based on the detector *position*, it is called frontal, and the position of the detector by convention is at 0°. Similarly, when the detector is moved through 90°, to a position beside and to the left of the patient, a lateral (LAT) projection results. Between 0° and 90°, there are a multitude of projections termed left anterior oblique (LAO), and when the detector is moved to the right of the patient, a right anterior oblique projection (RAO) is achieved. As in the LAO projection, there are numerous RAO projections depending on the final angle from the midline. When the detector is posterior to the patient (the x-ray tube anterior), then a right (RPO) or left (LPO) posterior oblique projection occurs (Figure 3.3).

Standard detectors mounted on a C-arm or parallelogram, not only allow the above positions, but the detectors can be rotated around the transverse axis, toward the feet or head, expressed as caudal or cranial, respectively (Figure 3.4).

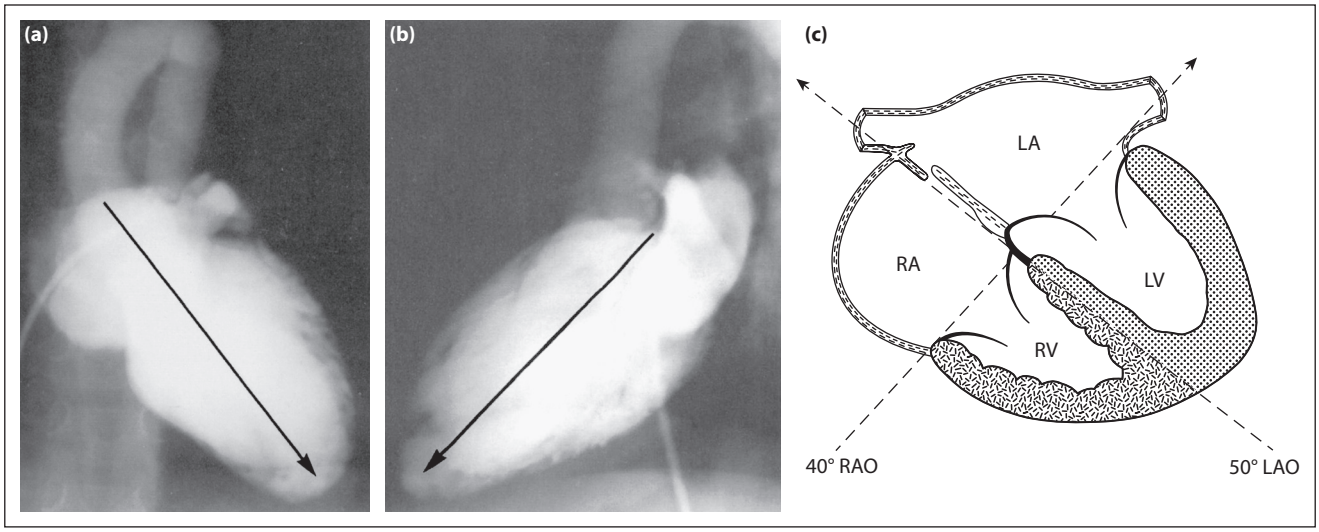

Figure 3.1 The typical lie of the heart in the chest. Panel (a)—frontal and (b)—LAT, projections of a left ventriculogram demonstrate the axis of the heart. The apex points anteriorly, inferiorly, and leftward. Panel (c) is a diagram of how standard mid-RAO and mid-LAO profile images of the axes of the heart. The RAO profiles the atrioventricular groove, and presents the ventricular septum en face. The mid-LAO view profiles the intraventricular septum, and separates the left and right ventricular and atrial chambers. (Modified from Culham JAG. Physical principles of image formation and projections in angiocardiography. In: Freedom RM, Mawson JB, Yoo SJ, Benson LN, Eds. *Congenital Heart Disease Textbook of Angiocardiography*. Chapter 2, figure 2-13. Armonk: Futura Publishing; 1997, pp. 39–93. With permission.)

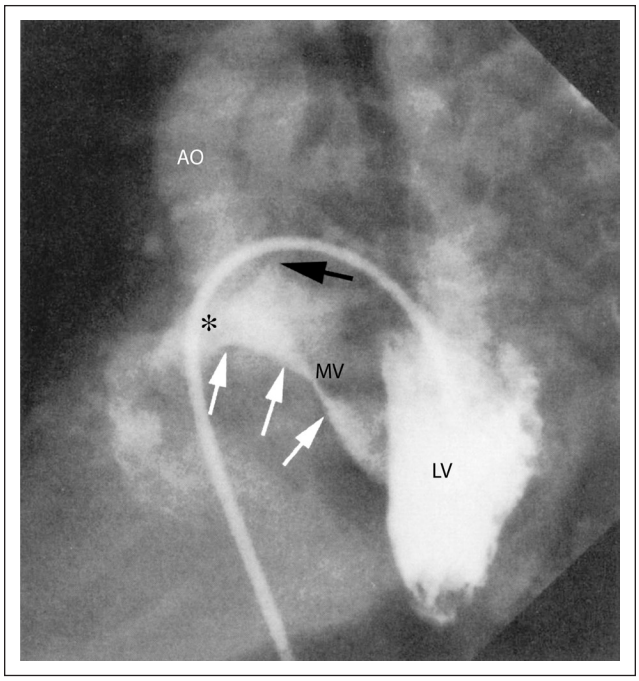

Figure 3.2 The sigmoid septum. A venous catheter is in the apex of the left ventricle through the mitral valve, in the long axis oblique projection. The sigmoid configuration of the septum is well seen (white arrows). Aortic–mitral continuity is noted (black arrow). Contrast is seen mixing across a ventricular defect (asterisk). (Modified from Culham JAG. Physical principles of image formation and projections in angiocardiography. In: Freedom RM, Mawson JB, Yoo SJ, Benson LN, Eds. *Congenital Heart Disease Textbook of Angiocardiography*. Chapter 2, figure 2-14. Armonk: Futura Publishing; 1997, pp. 39–93. With permission.)

In summary, the conventional terms RAO, LAO, PA, and left-LAT designate the position of the recording detector. The LAT position usually will have the detector to the left of the patient by convention, and will be so implied throughout this chapter. Finally, for clarification, while the term "projection" refers to the path of the x-ray beam, to be consistent with cardiological practice, projection or view will refer to the position of the detector.

Biplane angiography

As outlined in an earlier chapter discussing the ideal catheterization suite, dedicated interventional catheterization laboratories addressing congenital heart defects require biplane facilities.[3,4] Biplane angiography has the advantage of limiting contrast exposure and the assessment of evaluating the cardiac structures in real time in two projections simultaneously. However, this is at a cost, as these facilities are expensive, and with large flat-panel detectors, extreme simultaneous angulations can be compromised. The choice of a set of projections will depend on the information required, equipment capabilities, and the physical constraints to patient access. Standard biplane configurations include RAO/LAO, and frontal or LAT projections, with additional cranial or caudal tilt. The possible combinations are endless (Table 3.1 and Figure 3.5).

The cranial–LAO projections

A clear working understanding of these projections is of critical importance in developing a flexible approach to

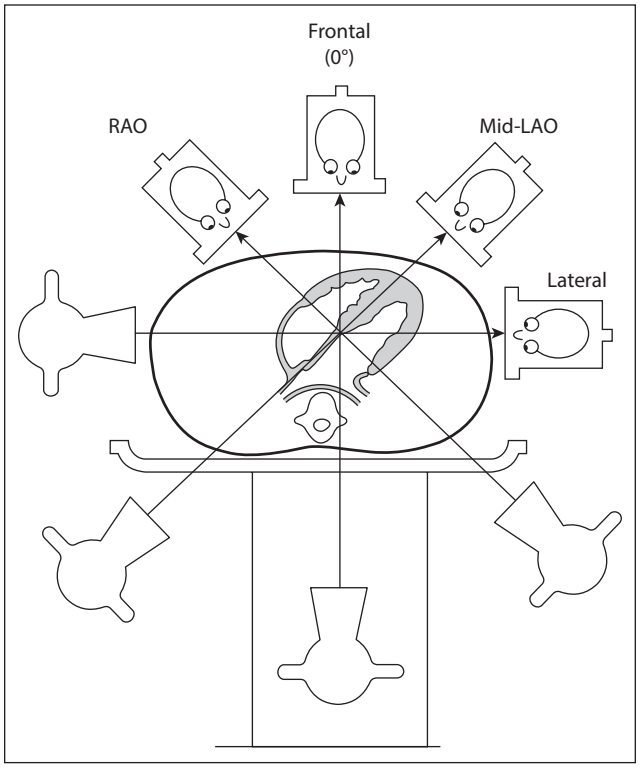

Figure 3.3 Naming the standard projections with the x-ray tube under the table. This diagrams the various positions of the detector/x-ray tube. The patient is supine, and the view is from the patient's feet, looking toward the head. (Modified from Culham JAG. Physical principles of image formation and projections in angiocardiography. In: Freedom RM, Mawson JB, Yoo SJ, Benson LN, Eds. *Congenital Heart Disease Textbook of Angiocardiography*. Chapter 2, figure 2-15. Armonk: Futura Publishing; 1997, pp. 39–93. With permission.)

congenital heart defect angiography and intervention. The practice of using "cookbook" projections for each case *may* allow acceptable diagnostic studies, but will fall short of the detail required to accomplish an interventional procedure. However, a comprehensive understanding of the normal cardiac anatomy, especially the interventricular septum, allows the operator to adjust the projection to optimize profiling the region of interest.

There are a number of "rules of thumb" that allow the operator to judge the steepness or shallowness of an LAO projection. Of importance is the relationship of the cardiac silhouette to the spine, the ventricular catheter, and the ventricular apex.

To optimize the profile of the midpoint of the *membranous ventricular septum*, (and thus the majority of perimembranous defects), two-thirds of the cardiac silhouette should be to the right of the vertebral bodies (Figures 3.6 and 3.7). This will result in a cranially tilted-left ventriculogram showing the left ventricular septal wall, the apex (denoted by the ventricular catheter) pointing toward the bottom of the image. A shallower projection will have more of the cardiac silhouette toward the left of the spine and profiles more of the inferobasal component of the septum, which is ideal for *inlet-type ventricular defects*. This projection allows for evaluation of atrioventricular valve relationships, inlet extension of perimembranous defects, and posterior muscular defects. A steeper LAO projection can be used to profile the *outlet extension of a perimembranous defect, and anterior muscular and apical defects*. As noted in Figure 3.6, the ventricular catheter in the cardiac apex can be used to help guide the projection, but only if it enters the chamber through the mitral valve. If catheter entry is through the ventricular defect or retrograde it tends to be more basal and left LAT.

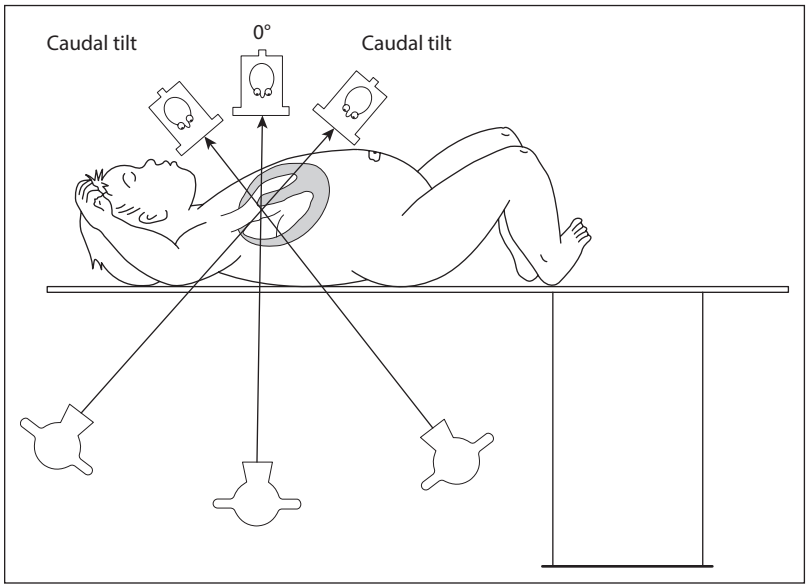

Figure 3.4 Naming the standard projections with the x-ray tube under the table. Cardiological convention is such that cranial and caudal tilt refers to the detector position. (Modified from Culham JAG. Physical principles of image formation and projections in angiocardiography. In: Freedom RM, Mawson JB, Yoo SJ, Benson LN, Eds. *Congenital Heart Disease Textbook of Angiocardiography*. Chapter 2, figure 2-16. Armonk: Futura Publishing; 1997, pp. 39–93. With permission.)

Table 3.1 Summary of projections

Projection	Angles	
Single-plane projections		
Conventional RAO	40° RAO	
Frontal	0°s	
Shallow LAO	1–30°	
Straight LAO	31–60°	
Steep LAO	61–89°	
Left-LAT	90° left	
Cranially tilted RAO	30° RAO + 30° cranial	
Cranially tilted frontal (sitting-up view)	30° or 45° cranial	
Cranially tilted shallow LAO	25° LAO + 30° cranial	
Cranially tilted mid-LAO (long-axis oblique)	60° LAO + 20° or 30° cranial	
Cranially tilted steep LAO (hepatoclavicular view)	45–70° LAO + 30° cranial	
Caudally tilted frontal	45° caudal	
Biplane combinations	**A plane**	**B plane**
AP and LAT	0°	Left-LAT
Long axial oblique (LXO)	30° RAO	*60° LAO + 20–30° cranial*
Hepatoclavicular view	*45° LAO + 30° cranial*	120° LAO + 15° cranial
Specific lesions		
RVOT-MPA (sitting up)	*10° LAO + 40° cranial*	Left- LAT
Long axial for LPA (biplane)	30° RAO	60° LAO + 30° cranial
LPA long axis (single plane)		60° LAO + 20° cranial
ASD	*30° LAO + 30° cranial*	
PA bifurcation and branches	*30° caudal + 10° RAO*	*20° caudal*

Note: Primary projections are in italics.
RAO = right anterior oblique, LAO = left anterior oblique, AP = anteroposterior, LAT = lateral, RVOT = right ventricular outflow tract, MPA = main pulmonary artery, LXO = long axis oblique, LPA = left pulmonary artery, ASD = atria septal defect, PA = pulmonary artery.

Modification of the cranial LAO projection will have to be made if there is a discrepancy in chamber sizes, and the septum rotated, such that a steeper or shallower projection may be required. Also, it is assumed that the patient is laying flat on the examining table, but if the head is turned to the right or a pad under the buttocks, it will rotate the thorax such that the LAO projection is steeper and the detector is caudal. This has to be compensated for during the setup for the angiogram. The clue in the former case is that more of the heart silhouette is over the spine.

The first step in setting up a cranial–LAO projection is to achieve the correct degree of steepness or shallowness. After that, the degree of cranial tilt has to be confirmed, so that the basal–apical septum is elongated. This can be estimated by seeing how much of the hemidiaphragm is superimposed over the cardiac silhouette; the more superimposition, the greater the cranial tilt. Additionally, the degree of cranial tilt can be determined by looking at the course of the ventricular catheter; it appears to be foreshortened or coming directly at the viewer as the degree of cranial angulation is decreased (Figure 3.8).

Three-dimensional rotational angiography

Digital imaging using flat-panel detectors allows the acquisition of cross-sectional images by rotating the detector on a C-arm around the object. The acquired volume data set can be manipulated on a workstation to generate a three-dimensional angiographic image and/or computerized tomography (CT)-quality soft-tissue imaging that can be used in real time during the procedure (Figure 3.9). The technology was first designed and applied for interventional neurovascular procedures.[5–7] However, its utility

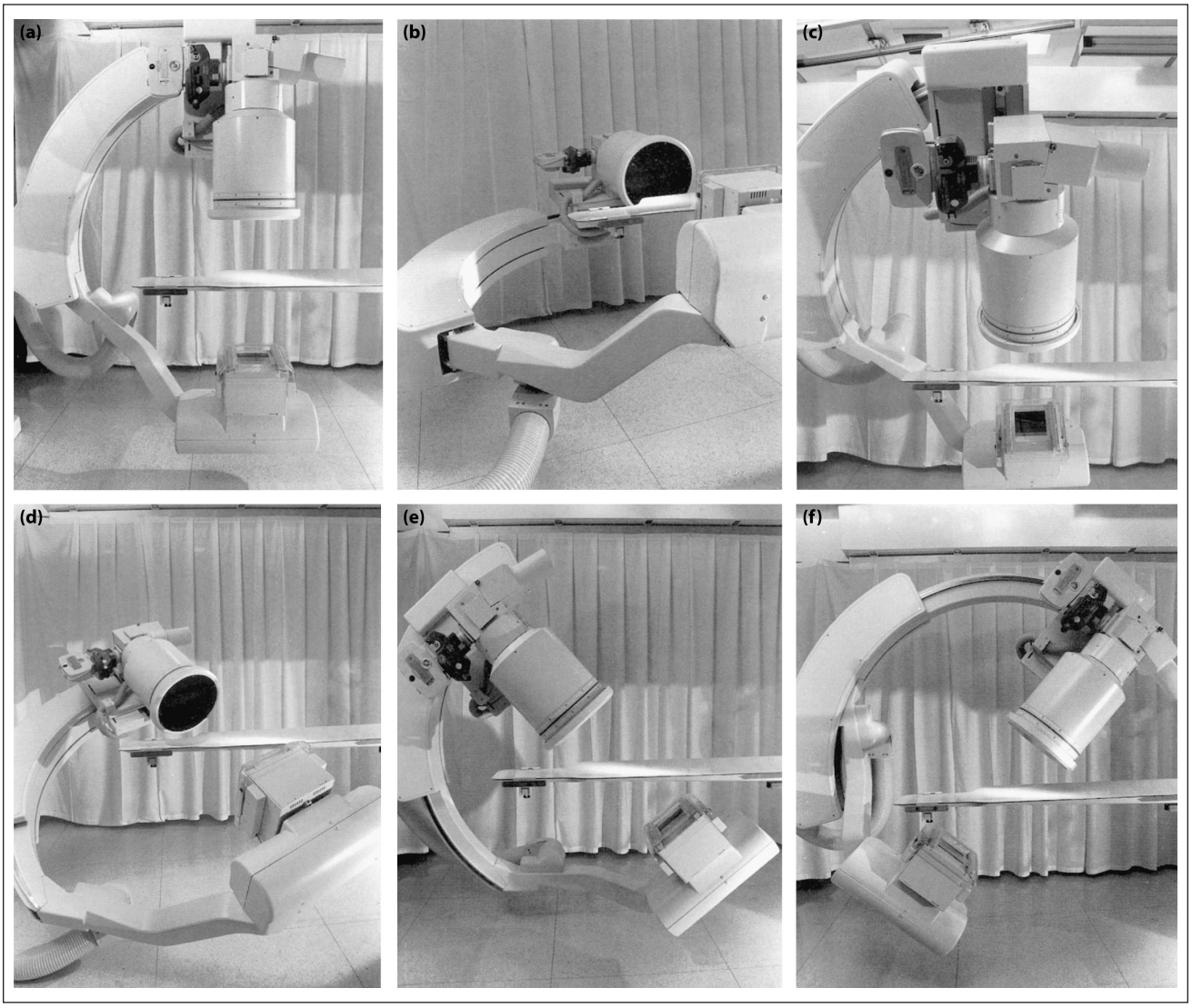

Figure 3.5 Standard projections. (a) Frontal (PA). (b) LAT. (c) RAO. (d) Mid-LAO with cranial tilt. (e) Cranially tilted frontal (sitting up). (f) Caudally tilted frontal. (Modified from Culham JAG. Physical principles of image formation and projections in angiocardiography. In: Freedom RM, Mawson JB, Yoo SJ, Benson LN, Eds. *Congenital Heart Disease Textbook of Angiocardiography*. Chapter 2, figure 2-17. Armonk: Futura Publishing; 1997, pp. 39–93. With permission.)

in obtaining a unique intraprocedural evaluation of the three-dimensional anatomy resulted in a rapid diffusion of the technology to other areas of interventional radiology. Until recently, its application outside interventional radiology was limited. In 2008, Noelker et al.[8] reported the use of 3-DRA for left atrial mapping during ablation procedures and Biasi et al.[9] reported its use in thoracic vascular interventions. In 2011, Glatz et al.[10] were the first to describe its application in children with congenital heart disease. In their study, 3-DRA was used for evaluation of the right ventricular outflow tract/central pulmonary arteries, cavopulmonary connection, pulmonary veins, and distal pulmonary arteries. A number of subsequent publications[11–15] have demonstrated the usefulness of 3-DRA in defining the three-dimensional relationship between structures poorly defined by two-dimensional angiography, and in guiding pediatric interventional procedures (Figure 3.10).[16] The acquisition programs will vary among vendors. However, the essential components consist of a 5–7 s rotation of the C-arm at which time dilute contrast is injected for 1 or 2 s before the rotation begins. The location of the injection and whether pacing is used depends on the chambers or vessels to be visualized.[17] For example, for an arch obstruction, right ventricular pacing

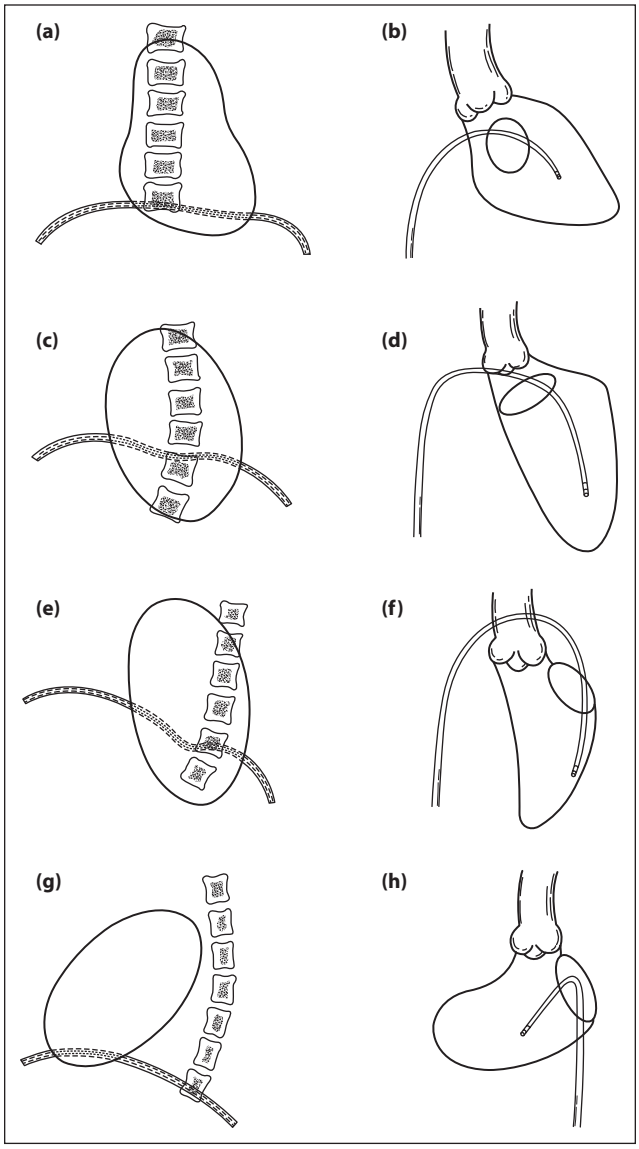

Figure 3.6 Setting up a standard LAO projection. To achieve the LAO projection, attempt to adjust the detector angle such that 2/3 of the cardiac silhouette is to the left of the spine as in (e). If a catheter is through the mitral valve in the left ventricular apex, it will point to the floor, as in (f). In this view, the intraventricular septal margin points toward the floor. The so-called four-chamber or hepatoclavicular view is achieved by having 1/2 the cardiac silhouette over the spine, as in (c). A catheter across the mitral valve will appear as in (d). A steep LAO projection will have the cardiac silhouette as in (g), and a transmitral catheter in the left ventricle will appear as in (h). (a) and (b) show the frontal projection. (Modified from Culham JAG. Physical principles of image formation and projections in angiocardiography. In: Freedom RM, Mawson JB, Yoo SJ, Benson LN, Eds. *Congenital Heart Disease Textbook of Angiocardiography*. Chapter 2, figure 2-19. Armonk: Futura Publishing; 1997, pp. 39–93. With permission.)

is typically used to reduce the stroke volume to allow the contrast to fill the vessel (Figure 3.11), while a nonpaced injection is used in the superior caval vein to examine a bidirectional cavopulmonary anastomosis (Figure 3.11). Diluted contrast is used (1:1 or 1:2) with 1–1.5 cm^3/kg contrast used for an injection, and if the patient anesthetized, it is used with a breath hold. Several acquisition programs are available that can be used to optimize three-dimensional (volume rendered) or soft-tissue images. Once the acquisition is acquired, it can be rapidly (>5 min) reconstructed on a workstation in the laboratory. As such, it can be a valuable tool in planning and accomplishing an interventional procedure. Details of the technology are beyond the scope of this section, and the reader is referred to other works.[18–20] With newer acquisition programs, lower radiation doses are possible compared with the traditional digital biplane cine acquisitions.[10]

Cardiac catheterization and radiation exposure

Cardiac catheterization in children has evolved from a purely diagnostic test to a critical component of therapy. As such, the principles of radiation safety must take a central role in the planning and execution of these procedures due to the possible repeated exposures over a lifetime, the known increased radiosensitivity of children, and a longer time for side effects to manifest. Radiation exposure can be very high in the pediatric patient due to complexity of interventions, small body size, higher heart rates (requiring faster frame rates), and wide anatomical variations. The precautions recommended for adult patients equally apply to children, and should include low fluoroscopy frame rates during catheter manipulation, grid-free magnification in smaller children, single-frame acquisition for position documentation, and application of the ALARA (as low as reasonably achievable) principle (see below). As children born with congenital heart disease frequently undergo numerous diagnostic and therapeutic catheterizations, there is an ever-present, potentially harmful occurrence of cumulative long-term effects of radiation exposure.[21,22] This is problematic as the complex three-dimensional anatomy of congenital structural lesions frequently necessitates multiple acquisitions, which increases the radiation exposure. Imaging equipment employed for pediatric procedures should be designed and configured for image acquisition modified to accommodate variable procedural requirements with a wide age and weight range as seen in the pediatric laboratory.[23] Strategies for radiation exposure reduction and image quality in the pediatric population are well described[24] and the importance of exposure reduction is emphasized in the Image Gently and Step Lightly campaigns.[25]

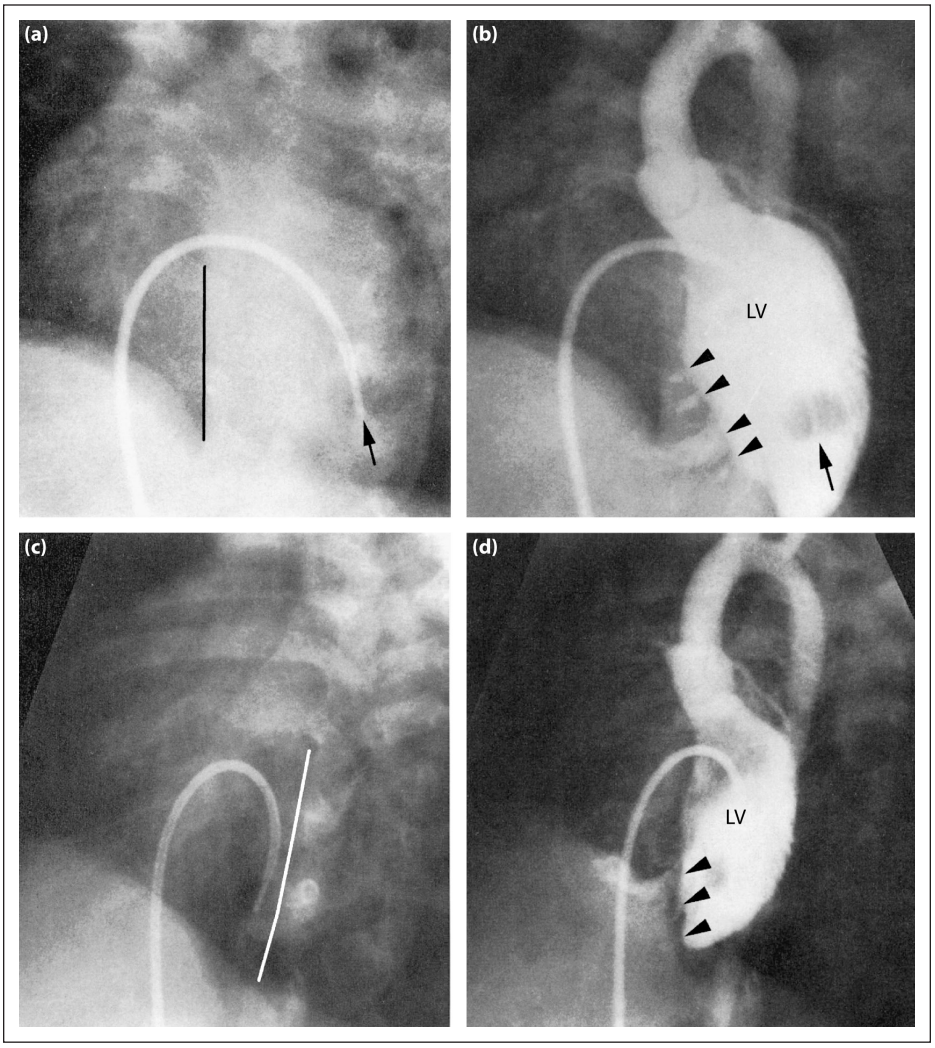

Figure 3.7 Achieving an LAO projection. (a): For a hepatoclavicular view, 1/2 of the cardiac silhouette is over or just left of the spine, with the catheter pointing toward the left of the image. During the injection, the apex and catheter (arrow) will point toward the bottom and left of the image. In this example, the basal (inlet) portion of the septum is intact. Multiple mid-muscular septal defects are not well profiled (arrowheads). In panel (c), the LAO projection is achieved with the catheter pointing toward the bottom of the frame, and the cardiac silhouette well over the spine. During the contrast injection (d), the mid-muscular defects are now better profiled. (Modified from Culham JAG. Physical principles of image formation and projections in angiocardiography. In: Freedom RM, Mawson JB, Yoo SJ, Benson LN, Eds. *Congenital Heart Disease Textbook of Angiocardiography*. Chapter 2, figure 2-20. Armonk: Futura Publishing; 1997, pp. 39–93. With permission.)

Specific lesions

Ventricular septal defect

The imaging of specific ventricular defects is beyond the scope of this chapter, but is commented upon in detail by various authors (Figure 3.12).[26] The injections to outline the septum and the lost margins, which circumscribe the defect(s), are best performed in the left ventricle using a power injector. Two orthogonal (right-angle) projections will give the best chance of profiling the lesion. However, in precatheterization, the location of the defect should be well characterized by other imaging modalities, such that the projections chosen would give the optimal profile, with little modification. Table 3.1 lists single and biplane angulations for the various projections. For the perimembranous defect, the mid-cranial LAO projection, at about 50–60° LAO, and as much cranial tilt as the equipment and patient position will allow (Figure 3.13) should be attempted. Additional projections can include a shallow LAO with cranial tilt (the so-called four-chamber or hepatoclavicular view) to outline the basal septum or inlet

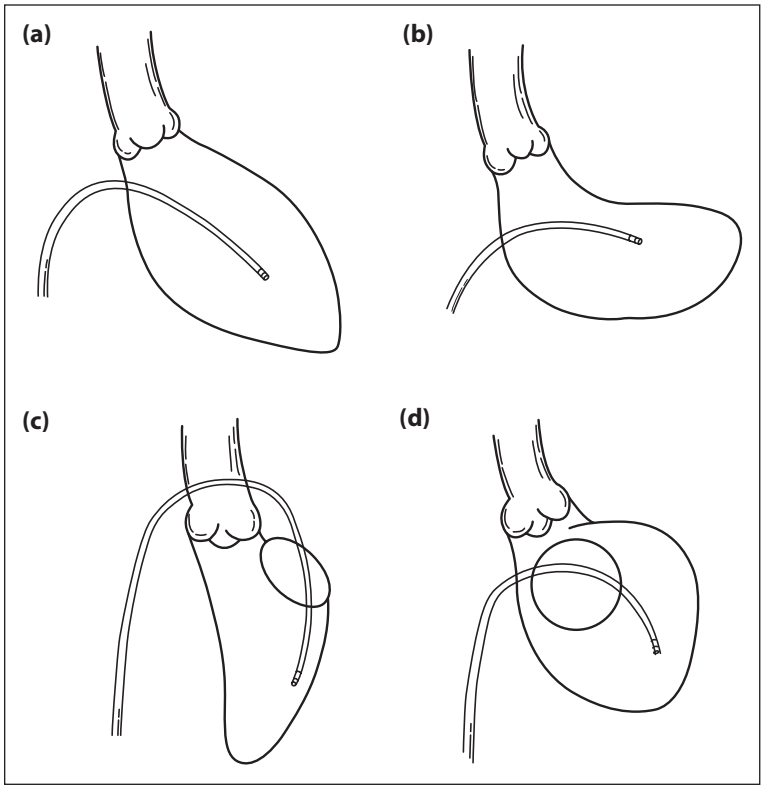

Figure 3.8 Obtaining the cranial tilt. In the standard RAO view, (a), the left ventricular apex points caudally and to the left. The LAO view will open the outflow from apex to base, as in diagram (c). If there is an upturned apex as in Fallot's tetralogy, the RAO view will appear as in (b). Adding cranial tilt to a mid-LAO projection will not effectively open the apex-to-base projection, and the appearance will be as looking down the barrel of the ventricles as in (d). (Modified from Culham JAG. Physical principles of image formation and projections in angiocardiography. In: Freedom RM, Mawson JB, Yoo SJ, Benson LN, Eds. *Congenital Heart Disease Textbook of Angiocardiography*. Chapter 2, figure 2-21. Armonk: Futura Publishing; 1997, pp. 39–93. With permission.)

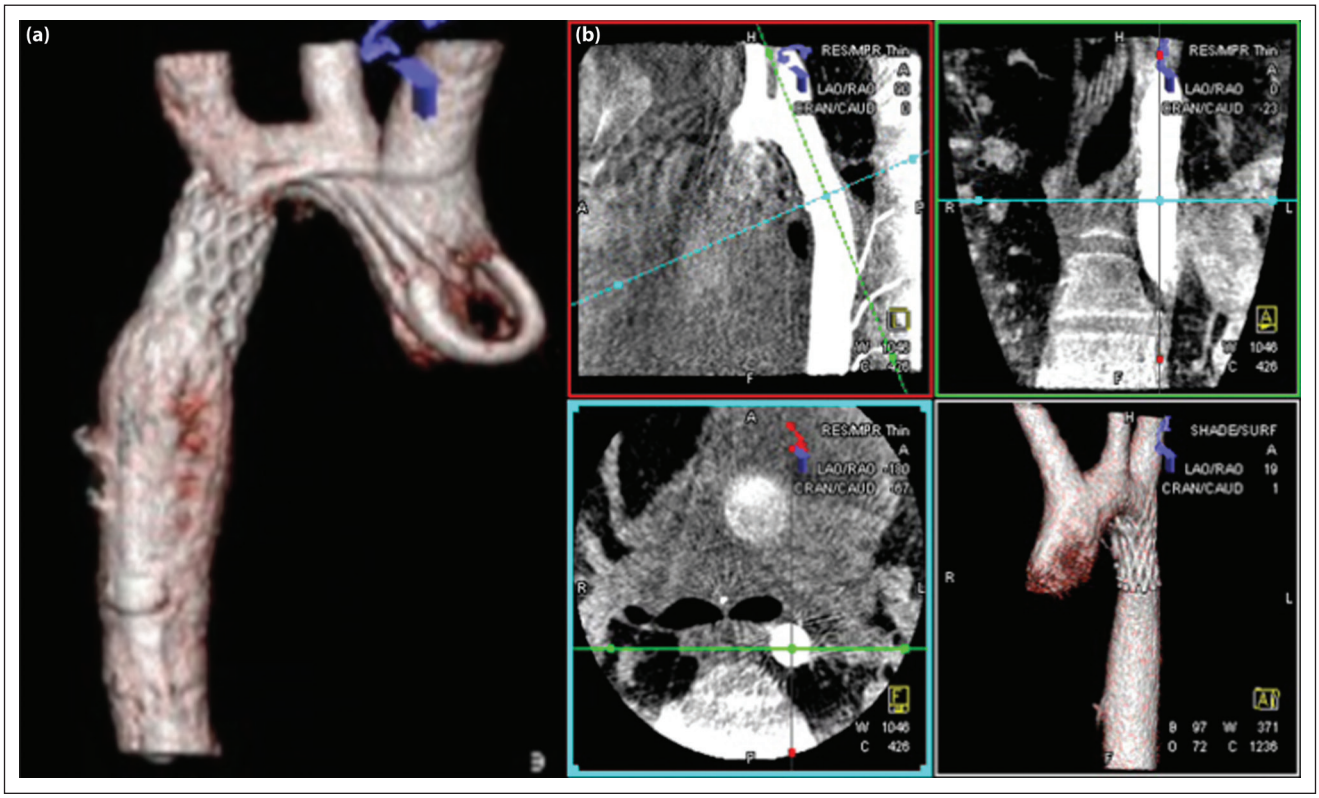

Figure 3.9 (**See color insert.**) Left panel (a), a volume-rendered image of a stented arch coarctation obtained from a rotational angiogram. In panel (b), from the same acquisition, the CT soft tissue images in the axial, coronal, and sagittal planes.

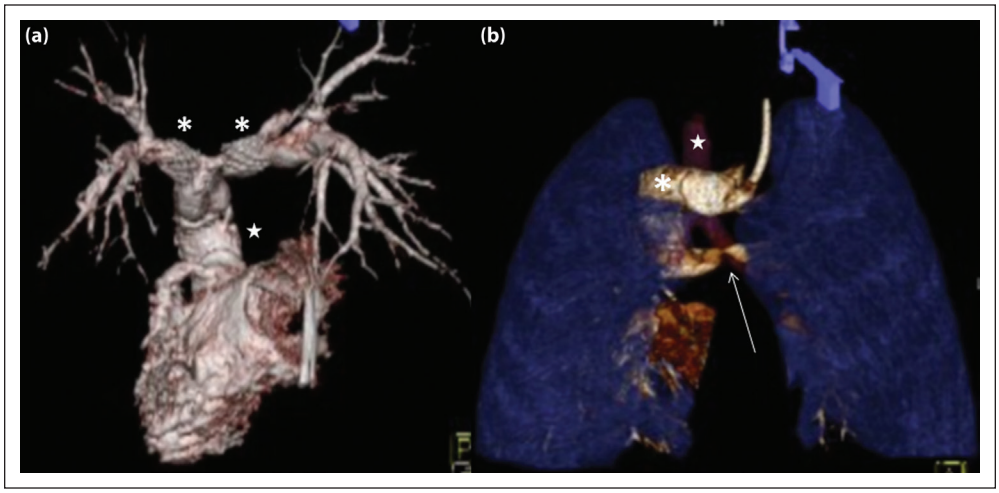

Figure 3.10 (**See color insert.**) Panel (a) A three-dimensional rotational angiogram from an injection in the right ventricle, viewed from the back (a projection not available in standard two-dimensional angiography), showing two endovascular stents (*) and the right ventricle to pulmonary artery conduit (star). Panel (b) shows a volume-rendered image from a cavopulmonary vein injection (*), reconstructed to show the relationship of the trachea (star) and a stenosis in the left pulmonary artery (arrow).

extension of a perimembranous defect. The RAO view will outline the high anterior and infundibular (outlet) defects.[27]

Coarctation of the aorta

Biplane angiography should be used to outline the arch lesion. Projections that can be used include LAO/RAO, PA and LAT, or a shallow or steep LAO (Figure 3.14). Our preference is a 30° LAO and left LAT, with 10–15° caudal tilt to minimize any overlapping structures, such as a ductal bump or diverticulum. Modifications to accommodate a right arch are generally mirror-image projections (i.e., 30° RAO and left LAT). The operator must be cautious to examine the transverse arch for associated hypoplasia, which may be foreshortened in the straight left-LAT projection. In such an instance, for a left arch, an LPO projection may elongate the arch. This is particularly important if an endovascular stent is to be implanted near the head and neck vessels.

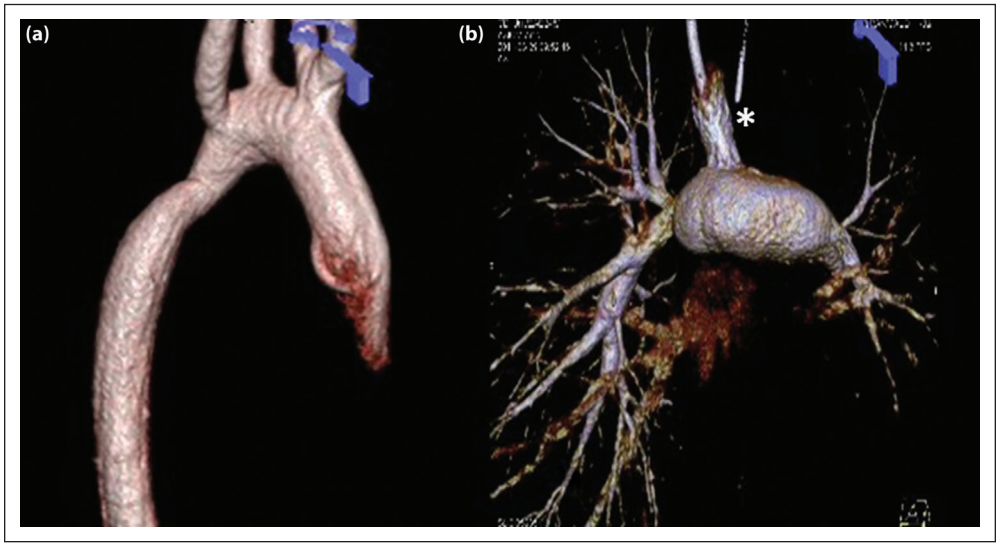

Figure 3.11 (**See color insert.**) Panel (a) is an image from a rotational angiogram from prior to stenting the arch obstruction. It was obtained during rapid right ventricular pacing to allow the diluted contrast time to fill the vessel throughout the time of acquisition. In panel (b), a cavopulmonary injection (*) is made without pacing, as the blood flow is slow, allowing filling of the anastomosis, and the proximal and distal pulmonary arteries during acquisition.

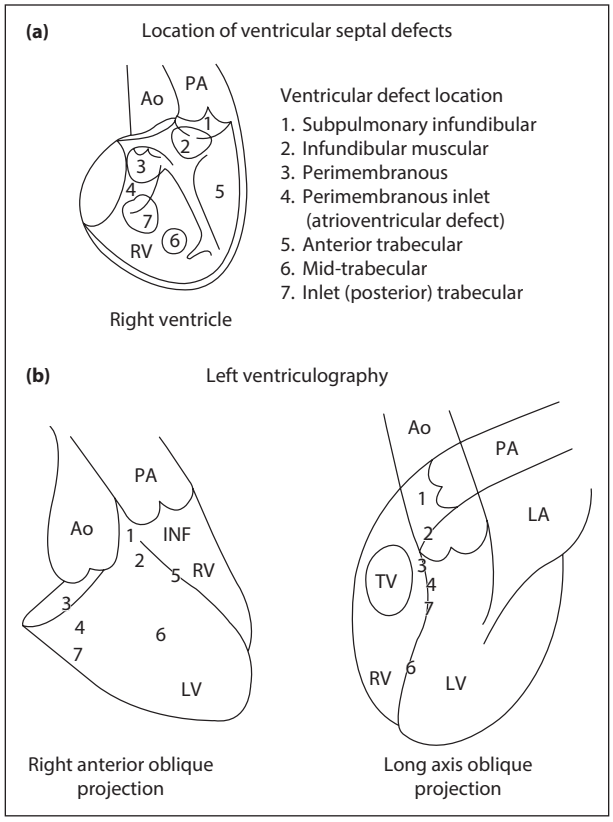

Figure 3.12 The locations of various ventricular defects are diagrammed in panel (a) viewed from the right ventricle. In panel (b), the locations of these defects are noted as seen in an RAO or LAO projection.

Aortic valve angiography

Assessment of the diameter of the aortic valve in the setting of normally related great arteries with ventricular arterial concordance for balloon dilation is best performed using biplane in the long axis and RAO projections (Figure 3.15) (Table 3.1). Our preference is to obtain the diameter of the aortic valve from a ventriculogram, which profiles the hinge points of the leaflets. Caution must be observed when using an ascending aortogram, as one of the leaflets of the valve may obscure the margins of attachment.

The Mustard baffle

Children who have had a Mustard operation may develop over time obstruction to one or both limbs of the venous baffle (Figure 3.16). As atrial arrhythmias are not uncommon in this population, particularly as adults, pacing systems are frequently required for management. In this regard, enlargement of a stenotic, although at times asymptomatic, superior baffle is frequently required. The optimum projection to outline superior baffle obstruction for potential stent implantation is a cranial-angulated LAO projection (30° LAO and 30° cranial). This view will elongate the baffle pathway, allowing accurate measurement prior to stenting. For inferior baffle lesions, a frontal projection will allow adequate localization of the lesion. Leaks along the baffle are more problematic and require modification of the projection. The initial approach

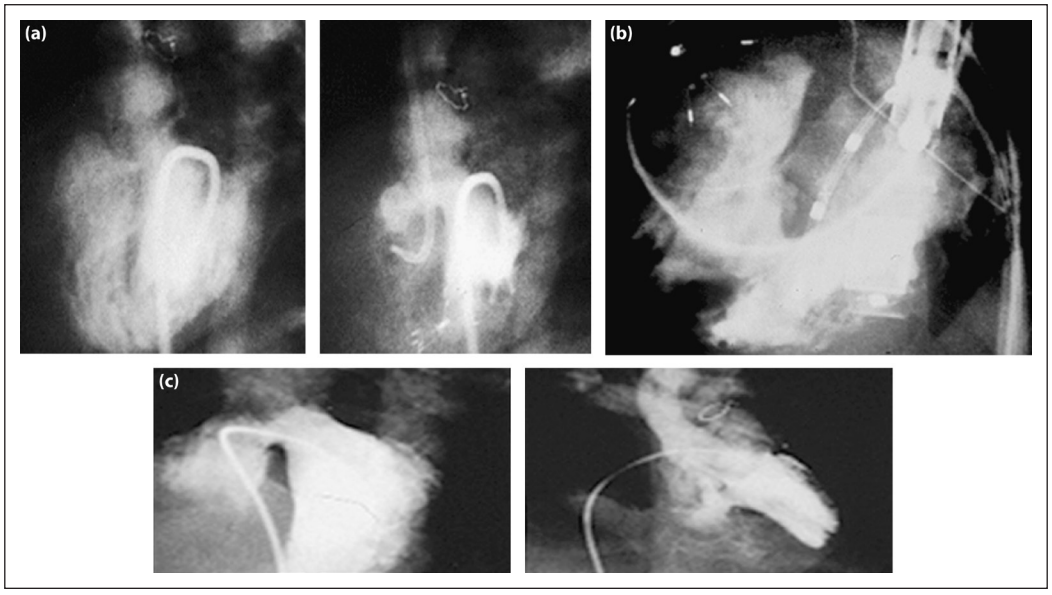

Figure 3.13 Panel (a) shows a left ventriculogram taken in the cranial–LAO projection. Note the apical, mid-muscular, and perimembranous septal defects. In panel (b), a modified hepatoclavicular view profiles a mid-muscular defect. Panel (c), left pane, is a left ventriculogram taken in the cranial–LAO view, with the catheter entering the ventricle through a perimembranous defect. Right pane, taken in the hepatoclavicular view with the catheter through the mitral valve, defines an inlet muscular defect in a child with a pulmonary artery band.

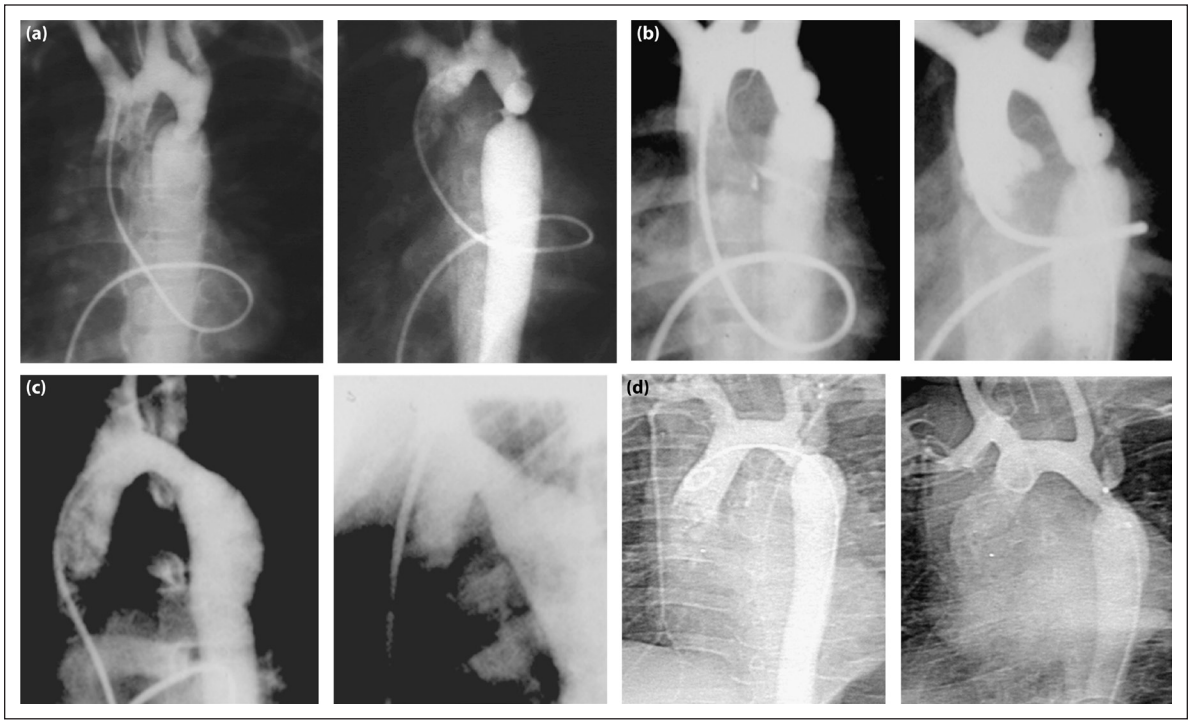

Figure 3.14 Panel (a), left pane, shows an ascending aortogram taken with a shallow-LAO projection without caudal angulation. The catheter was placed through a transeptal entry to the left heart. While the area of the coarctation can be seen, it is the caudal angulation that identifies the details of the lesion, including a small ductal ampulla, right pane. In panel (b), similar information is obtained, by employing caudal angulation to the frontal detector, right pane, while in the shallow-LAO projection in contrast to that information obtained without caudal angulation, left pane. In panel (c), left pane, hypoplasia of the transverse arch can be identified. However, in contrast, in the right pane, the degree of foreshortening is obvious. Panel (d), right pane, shows the standard LAO projection, of an ascending aortogram. In this case, there is overlap of the area of obstruction, transverse arch hypoplasia, and stenosis of the left subclavian artery, not defined until cranial angulation is employed, right pane.

should be a PA projection, with modifications in angulation made thereafter to best profile the lesion for device implantation, not too dissimilar to that of Fontan fenestration closure.

The secundum atrial septal defect and the fenestrated Fontan

Secundum atrial septal defects are best profiled in the 30° LAO with 30° cranial tilt (Figures 3.17 and 3.18). With the injection made in the right upper pulmonary vein, the sinus venous portion of the septum can be visualized, and anomalous pulmonary venous return can be ruled out. Additionally, any associated septal aneurysm can be outlined. With the application of transesophageal or intracardiac echocardiography, there is less fluoroscopic reliance on device positioning. When balloon sizing is performed, this projection will elongate the axis of the balloon for proper measurements.

The interventional management of the child with a fenestrated Fontan, whether an LAT tunnel or extracardiac connection, generally requires selective studies of the superior and inferior caval vein and pulmonary circulations to determine the presence or absence of obstructive or hypoplastic pathways and whether venous collaterals have developed. As such, they must be addressed by angioplasty, stenting, or embolization techniques before consideration of fenestration closure. The development of venous collaterals after an extracardiac Fontan will generally develop either from the innominate vein, or from the right upper hepatic/phrenic vein, toward the neo-left atrium, less frequently from the right hepatic veins to the pulmonary veins. The optimum projection to outline these lesions is in the AP and LAT projections, with selective power injections in the appropriate vessel. The location and dimensions of the fenestration may also be defined in these views, but for ideal profiling, some degree of right or LAO may be required.

The bidirectional cavopulmonary connection

Second-stage palliation for a number of congenital defects consists of a bidirectional cavopulmonary connection (aka, the bidirectional Glenn anastomosis) (Figure 3.19). Since

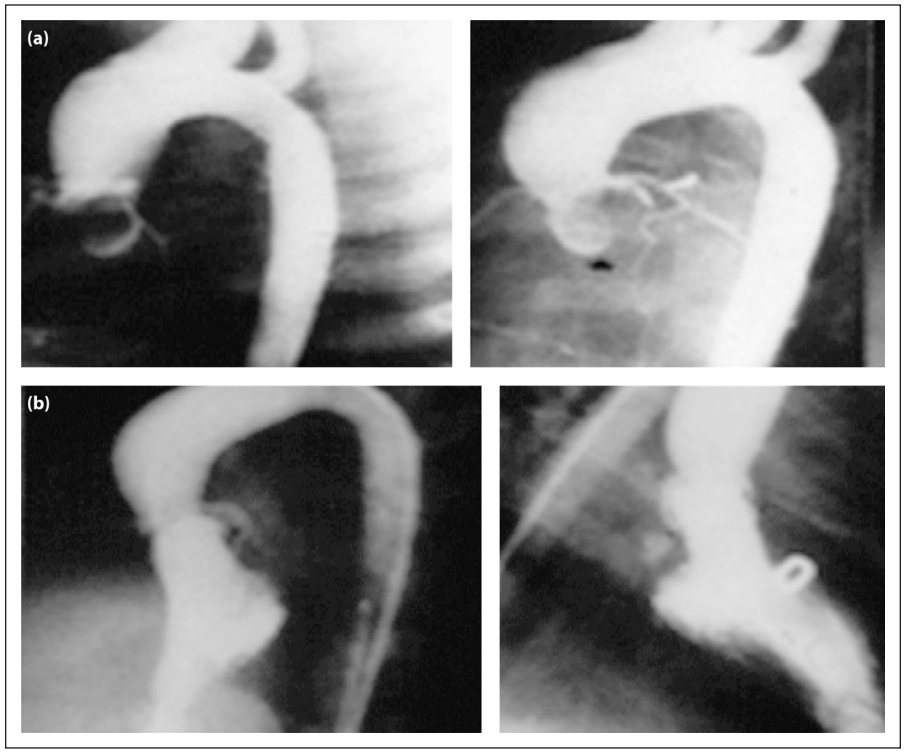

Figure 3.15 Intervention on the aortic valve requires accurate definition of the hinge points of the leaflets. In panel (a), long axis oblique views from an ascending aortogram, do not define the margins of the leaflets due to overlap of the cusps (bicuspid in these examples). In panel (b), long axis oblique (left) and RAO views, the left ventriculogram allows easier identification of the leaflet hinge points, where measurements can be made.

the caval to the pulmonary artery connection is toward the anterior surface of the right pulmonary artery (rather than on the upper surface), an AP projection will result in overlapping of the anastomotic site with the pulmonary artery. Therefore, to determine whether the anastomosis is obstructed, a 30° caudal with 10° LAO projection will generally open that region for better definition. Furthermore, this projection will outline the full extent of the right and left pulmonary arteries. The left-LAT projection with or without 10° caudal angulation will profile the anastomosis for its anterior–posterior dimension. Contrast injection must be made in the lower portion of the superior caval vein. The examination of venous collaterals can be performed from the AP and LAT projections in the innominate vein.

Pulmonary valve stenosis, Fallot's tetralogy, and pulmonary valve atresia with intact ventricular septum

Percutaneous intervention on isolated pulmonary valve stenosis is the assured procedure in the current era of catheter-based therapies (Figures 3.20 and 3.21). While angiographic definition of the right ventricular outflow tract and valve is not complicated, several features must be kept in mind when approaching the angiography for an interventional procedure. In the case of isolated pulmonary valve stenosis and other right ventricular outflow tract lesions, because the outflow tract can take a horizontal curve, a simple AP projection will foreshorten the structure. Therefore, a 30° cranial with 15° LAO will open up the infundibulum, allowing visualization of the valve and the main and branch pulmonary arteries. The best definition of the hinge points of the valve, to choose the correct balloon size, is from the left-LAT projection. Occasionally, 10° or 15° caudal angulation of the LAT detector can be used to separate the overlap of the branch vessels seen on a straight left-LAT projection. However, this is not recommended, as it will also foreshorten the outflow tract, and the valve will appear off-plane, giving incorrect valve diameters.

Branch pulmonary artery stenosis

Pulmonary artery interventions are most common, and represent the most difficult angiographic projections to separate out individual vessels for assessment and

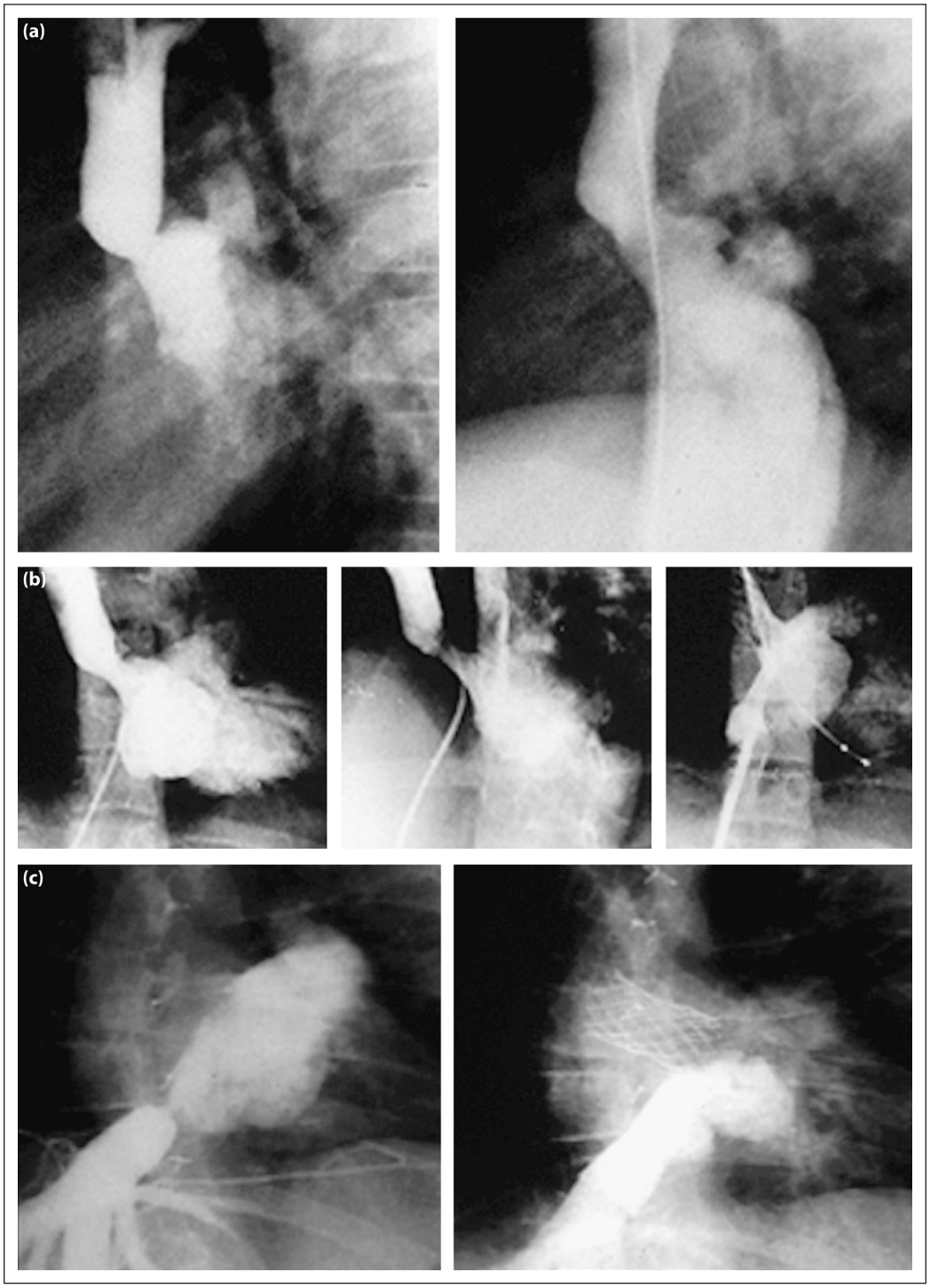

Figure 3.16 Baffle obstruction after a Mustard operation is, as the population ages, an increasingly common event. This is particularly so with the need to manage such patients with transvenous pacing devices. In panel (a), left pane, the presence of a superior baffle obstruction can be identified from the left-LAT projection. However, only with cranial angulation (cranial–LAO view), right pane, will the full extent of the lesion be detailed. This is particularly critical, as shown in panel (b), where the frontal view, left pane, does not show the full extent of the obstruction, and only from the angulated view will the length and diameter of the lesion be outlined (middle pane). A stent is placed, followed by a transvenous pacing system shown in the right pane from a frontal projection. For inferior baffle lesion, the frontal (PA) projection is optimal, panel (c), before (left) and after a stent is placed.

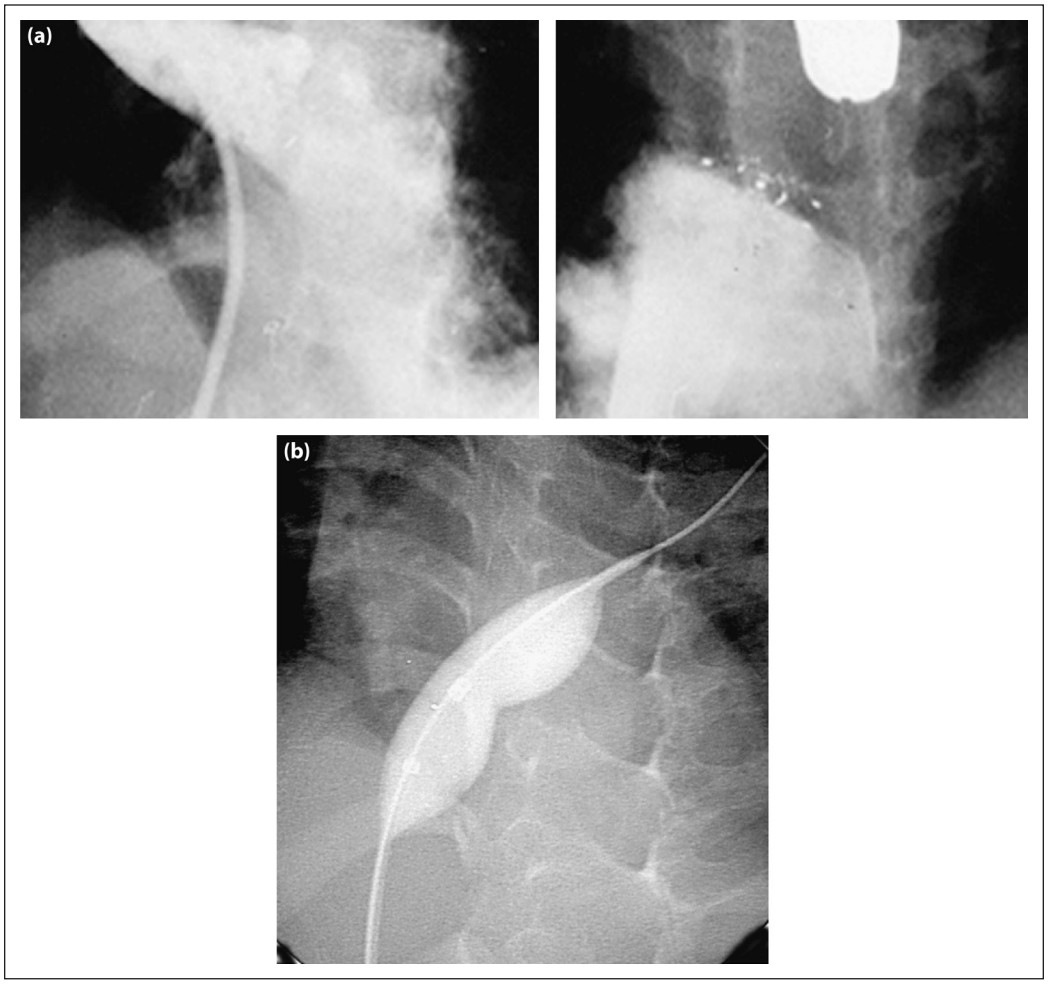

Figure 3.17 Use of angiography for septal defect definition and device placement in the setting of a secundum atrial septal defect has been supplanted by intracardiac and transesophageal techniques (panel a). However, fluoroscopy is still required for initial device localization, and in many laboratories, a short cine run is required to record the diameter of the static balloon to choose device size. In this case, we find the 30° LAO with 30° cranial tilt to best elongate the balloon to avoid foreshortening, panel (b).

potential intervention (Figures 3.22 through 3.24). A cranially tilted frontal projection with a left-LAT or RAO/LAO projection is frequently the first series of views that can be performed, as scout studies to map the proximal and hilar regions of the pulmonary circulation. The injection may be performed in either the ventricle or main pulmonary artery. Since there is frequent overlap to be seen in viewing the right ventricular outflow tract (see above), these standard views can be modified by increasing or decreasing the degree of RAO or LAO, and adding caudal or cranial tilt. Selective branch artery injections are best for detailed visualization, to plan the intervention. For the right pulmonary artery, a shallow-RAO projection with 10° or 15° cranial tilt will separate the upper- and middle-lobe branches, while a left-LAT with 15° caudal tilt will open up all the anterior vessels. Similarly, to maximize the elongated and posterior leftward-directed left pulmonary artery, a 60° LAO with 20° cranial is very effective, with a caudal tilt on the LAT detector. Occasionally, in small babies after surgical reconstruction of the branch pulmonary arteries, the main pulmonary artery is aneurysmal and obscures the confluence. In this case, a steep 30° caudal projection with the frontal detector with 10–20° RAO will open up the bifurcation.

Summary

This short introduction to interventional angiography will allow the reader a point of departure to visualize the most common lesions. However, many cases occur that do not fall into a standard categorization and the operator must be prepared to alter the imaging projection to optimally define the lesion. Successful outcomes require patience, perseverance, and the learned experience of others.

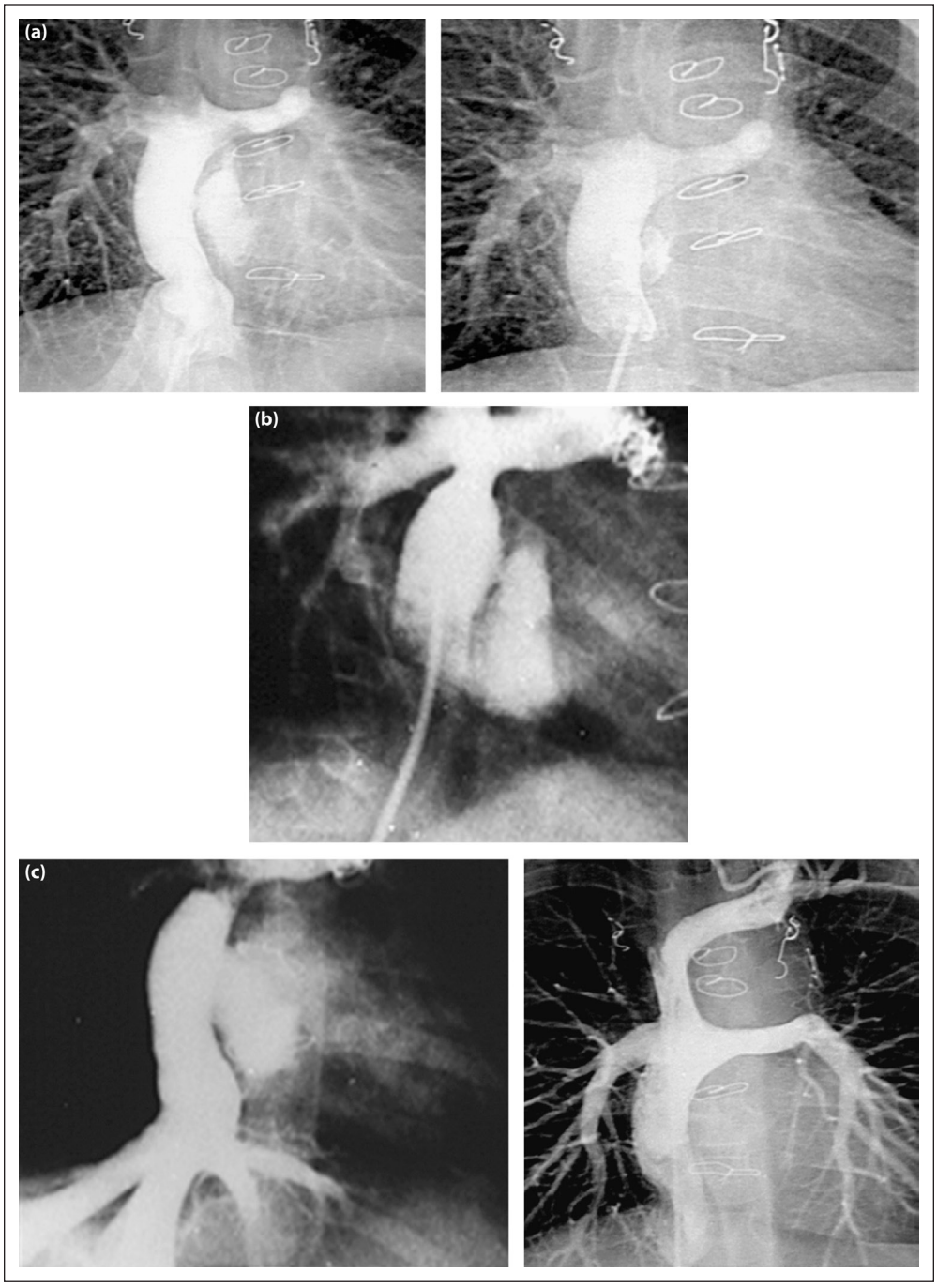

Figure 3.18 Panel (a) shows the appearance of a fenestrated extracardiac Fontan in the frontal projection, and its appearance after device closure. Generally, a frontal projection profiles the defect adequately, but at times, some angulation is required as seen in panel (b), where the defect is best profiled in a shallow-RAO view. Also note coils in the left superior caval vein, which developed after the Fontan procedure and required embolization. Occasionally, collateral vessels develop from the hepatic/phrenic vein (panel (c), left) or innominate vein (panel (c), right), where coils have been placed. The primary view is frontal (PA) and left-LAT.

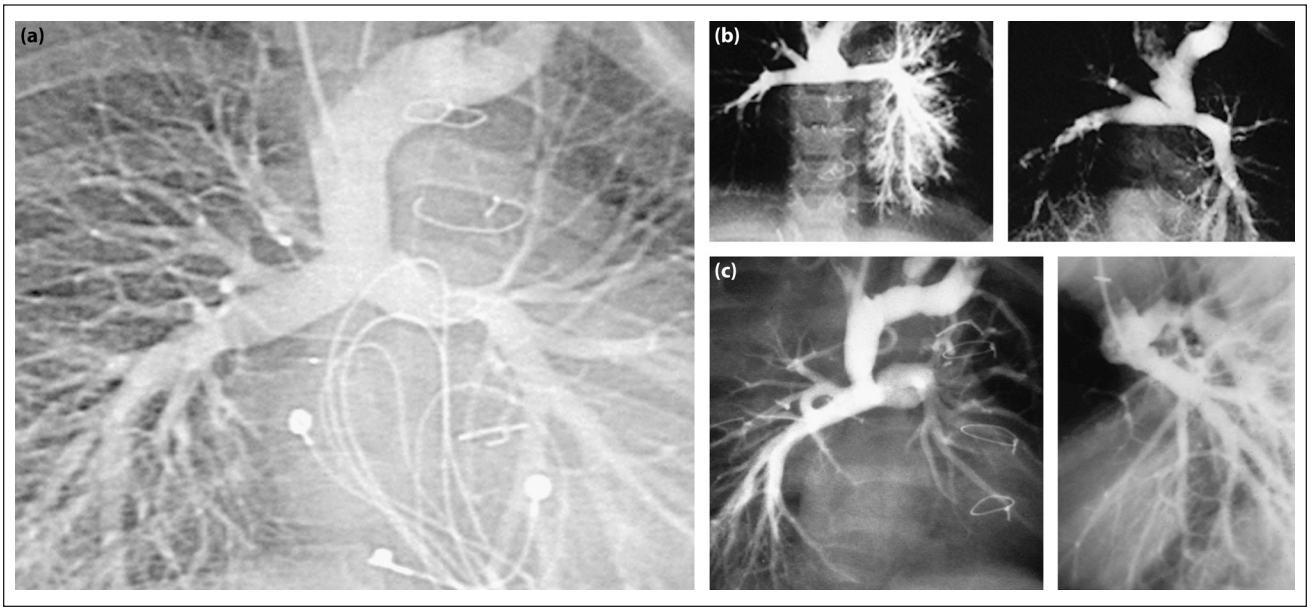

Figure 3.19 Because of an offset in the anastomosis between the superior caval vein and right pulmonary artery, the optimal view to see the anastomosis without overlap is shallow—with caudal tilt as seen in panel (a). Panel (b), left pane, is in the frontal projection, where overlap of the anastomosis obscures a potential lesion, as seen in the angulated view, right pane. The combination of an angulated frontal detector and caudal angulation of the LAT tube will allow definition of the anastomosis (left pane), and the pulmonary artery confluence (right pane), panel (c).

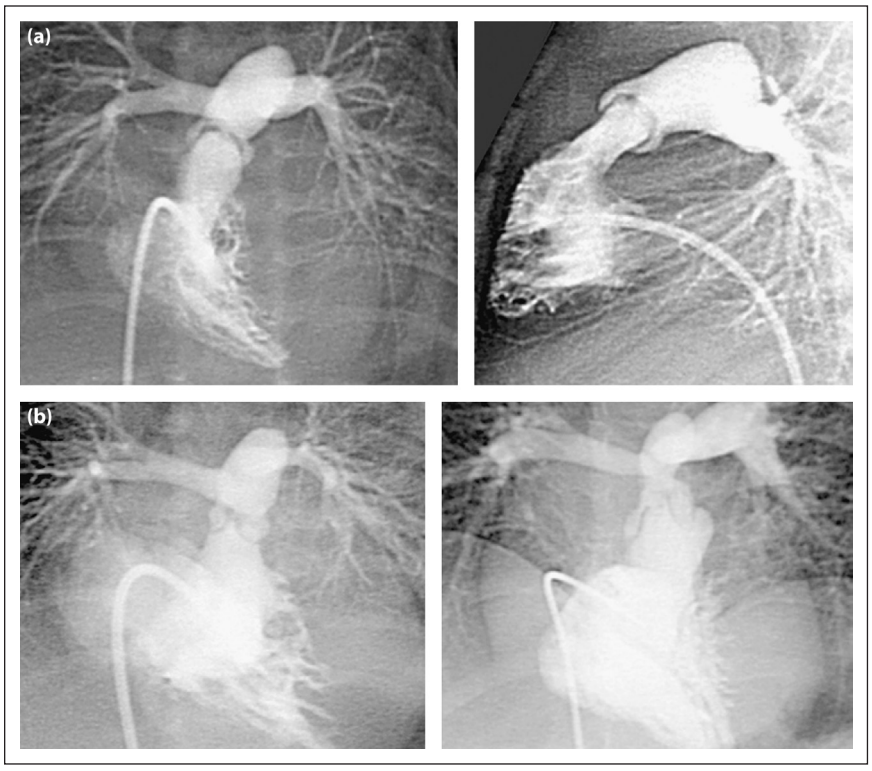

Figure 3.20 Panel (a) depicts the case of a typical isolated pulmonary valve stenosis in a neonate. The outflow tract is profiled in the cranially angulated frontal projection, with a slight degree of LAO angulation (left pane). The right ventriculogram outlines the form of the ventricle, the main pulmonary artery (and ductal bump) and the pulmonary artery confluence and branch dimensions. The LAT view (right pane) outlines the valve leaflets (thickened and doming) and allows accurate delineation of the valve structures for balloon diameter determination. In panel (b), two right ventriculograms in the cranially angulated slight LAO view depict the size of the annulus and main and branch pulmonary arteries (typical valve stenosis with left pulmonary hypoplasia, left pane; dysplastic valve stenosis, small nondilated main pulmonary artery, and proximal left branch pulmonary artery stenosis with poststenotic dilation, right pane).

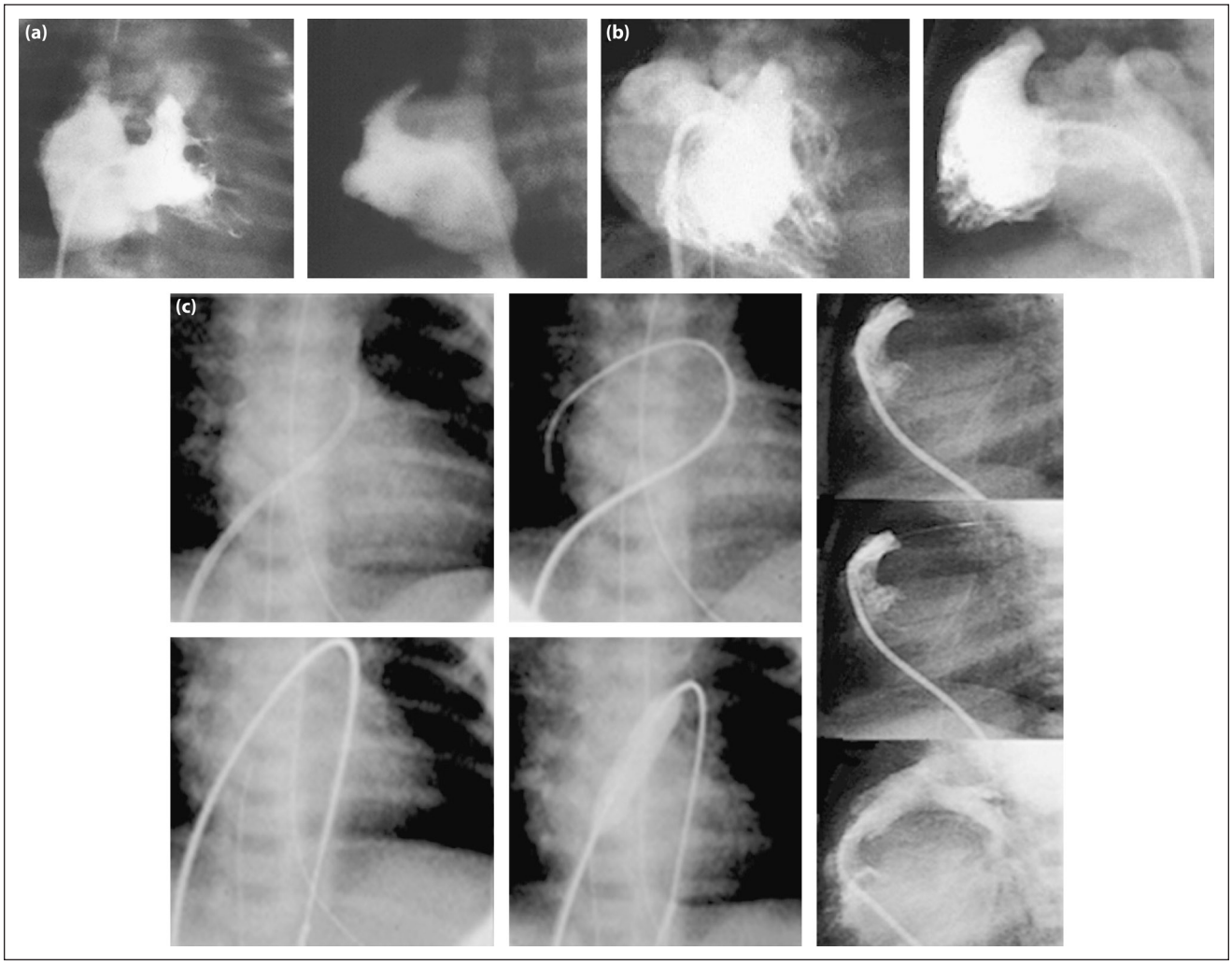

Figure 3.21 Angiographic projections for intervention in pulmonary atresia with intact septum are similar to that of isolated pulmonary valve stenosis. In panels (a) and (b), cranial angulation is critical to image the valve plate (left panes); while a left LAT will suffice for imaging the anterior–posterior aspects of the outflow tract. In valve perforation, it is critical to have visual control in two orthogonal planes, to avoid inadvertent infundibular perforation. A series of images during valve perforation is seen in panel (c). The left upper pane shows the catheter position; right upper pane, perforation and wire in the right pulmonary artery; left lower pane, the wire guide across the duct for stability; and in the right lower pane, balloon dilation of the valve. In the accompanying panel, viewed from the left-LAT projection, a series of images taken during perforation in the main pulmonary artery; top pane, position confirmation; middle pane, radio-frequency perforation; lower pane, angiography.

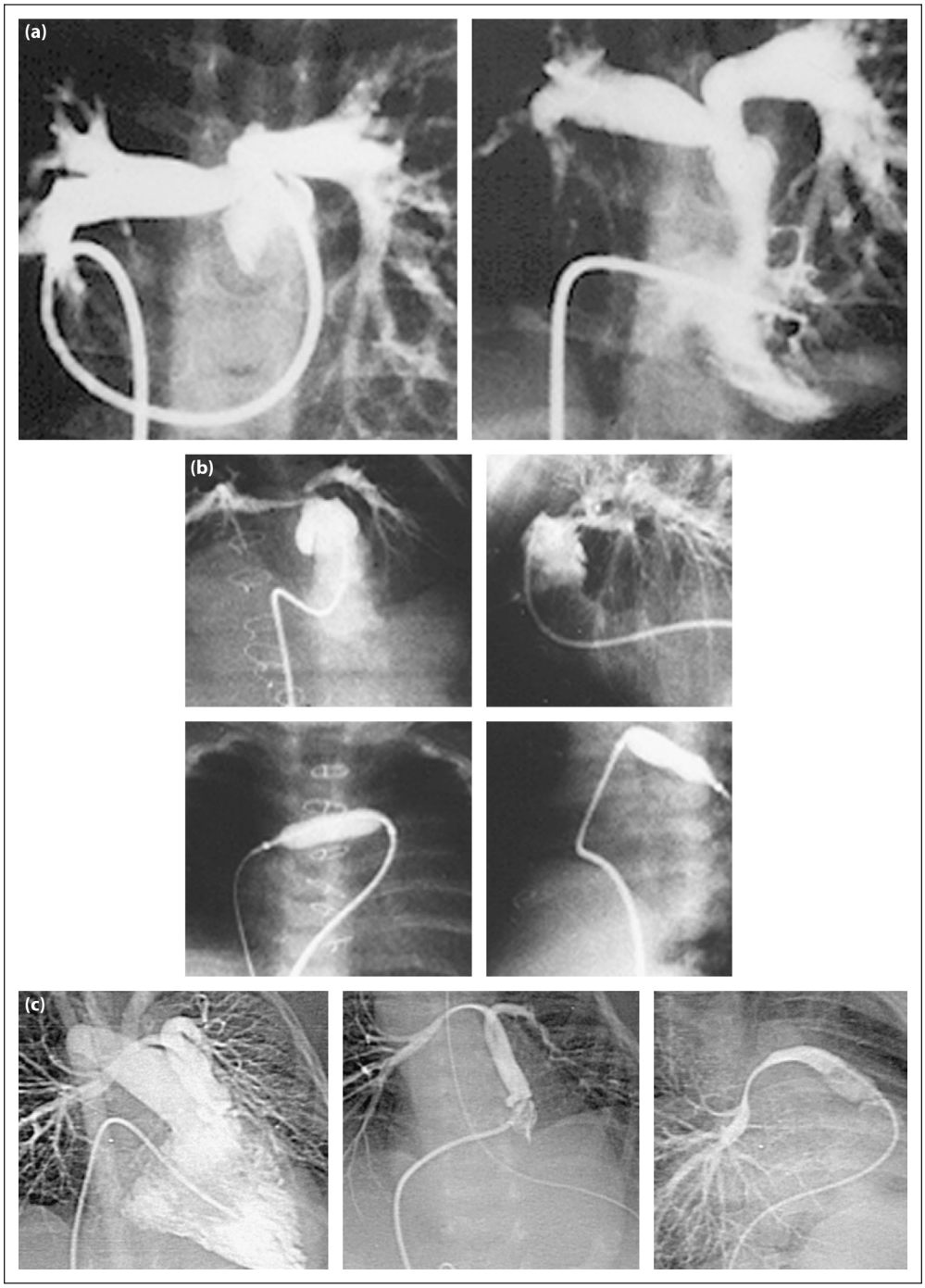

Figure 3.22 Angiography for selective intervention on the branch pulmonary arteries can be most difficult due to overlapping of structures. No single projection is totally representative and multiple views are frequently required. In panel (a), left pane, a scout film is taken in the main pulmonary artery; in the right pane, the right ventricle. Both images are taken in the cranial–LAO projection and in these examples clearly outline the outflow tracts and branch confluences. In panel (b), the dilated main pulmonary artery would have obscured the branch pulmonary artery confluence, and this cranial–LAO (left upper pane) and caudal left LAT (right upper pane) nicely details the anatomy for subsequent intervention (lower panes). In panel (c), an LAO-cranial projection outlines the crossed pulmonary arteries (left pane), as does a main pulmonary artery injection in the cranial projection (middle pane). The right pane identifies a stenotic lesion in the vessel from an RAO-cranial projection.

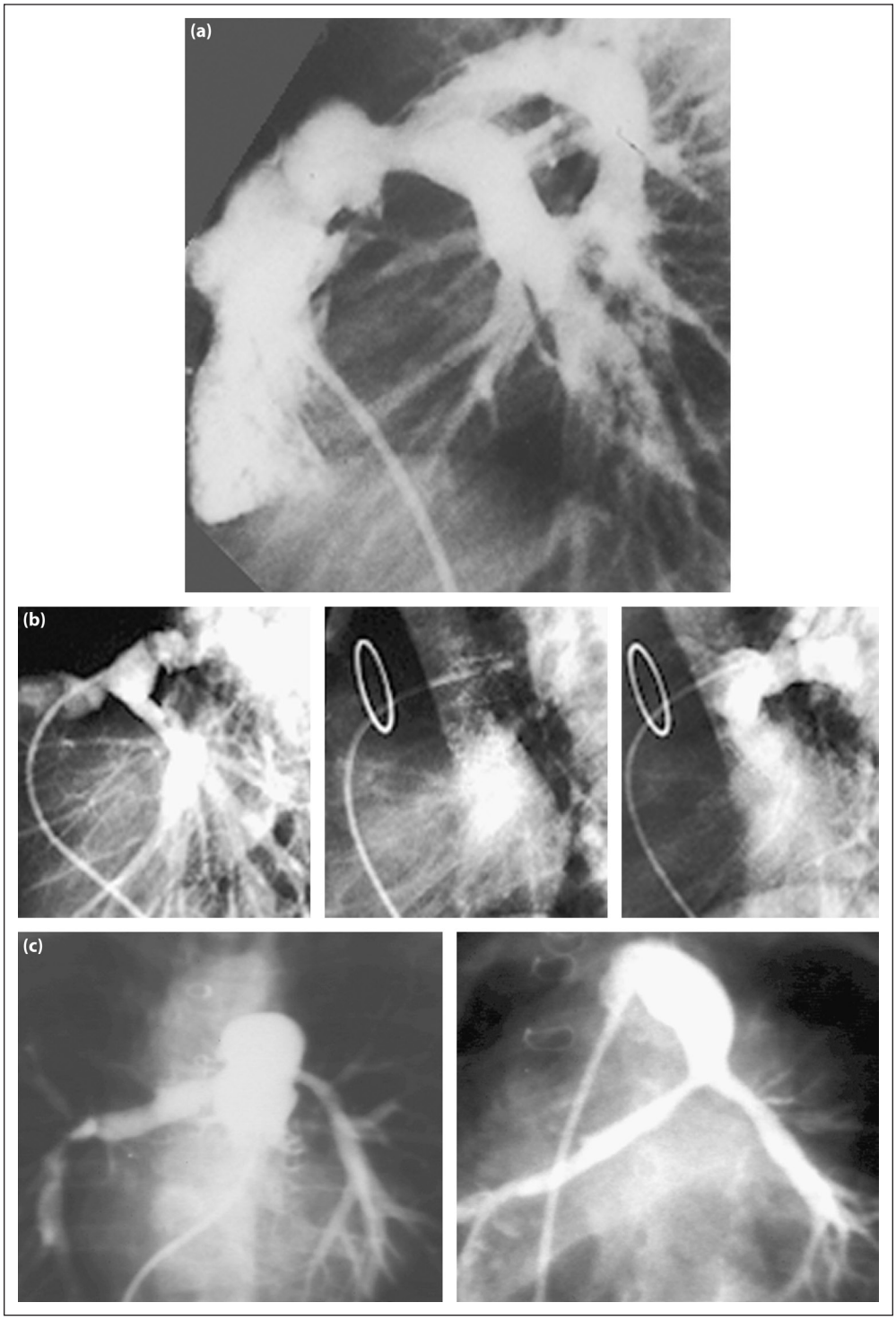

Figure 3.23 In panel (a), the image is taken from a left-LAT projection with caudal tilt. These will separate the proximal right and left pulmonary artery branches, and detail the main pulmonary artery. The outflow tract is foreshortened, and this view will mislead the operator when examining the diameter of the valve, and infundibulum. If such detail is required, a straight left LAT should be performed. In the caudal–LAT projection, the left pulmonary branch will sweep superiorly and toward the upper right corner of the image, while the left pulmonary artery will appear more medial and in the center of the image. In panel (b), the child had severe bilateral branch stenosis, (left pane), which persisted after surgical repair and valve insertion. Using the left-LAT view, stents could be placed in each branch (middle and right panes). In panel (c), severe main pulmonary artery dilation has obscured the confluence and very hypoplastic pulmonary arteries (left pane) in this child shortly after surgery. In this case, steep caudal angulation of the frontal tube with 10° or 15° LAO has detailed the lesion for the intervention (right pane).

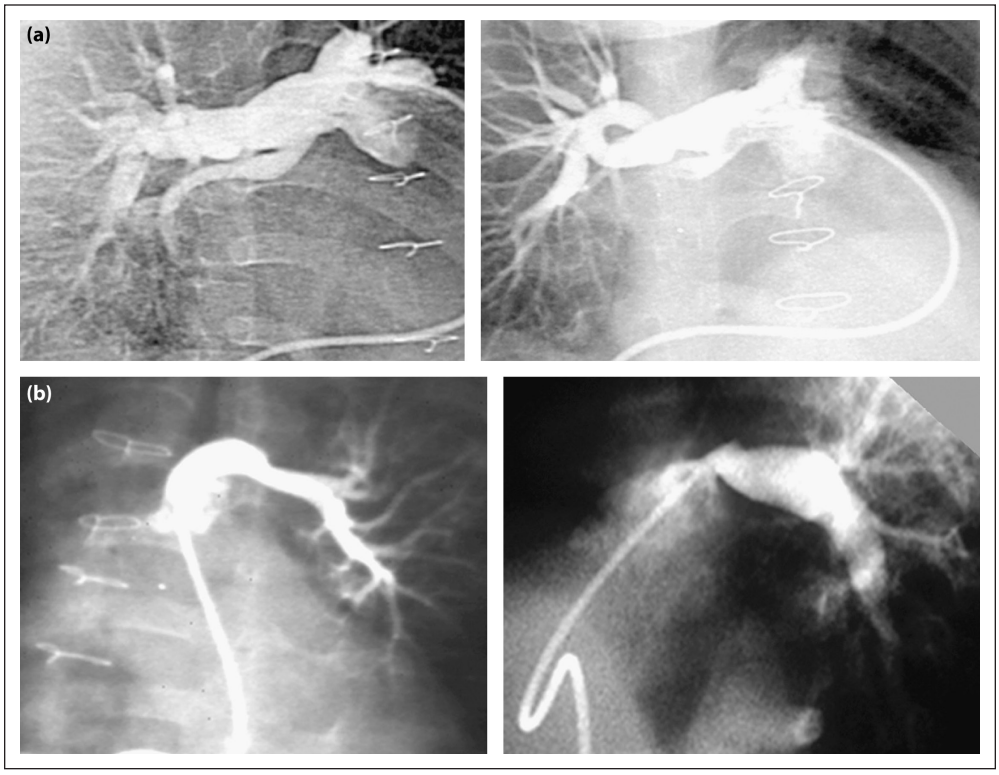

Figure 3.24 Selective injection into a branch pulmonary vessel will give the best-detailed image. However, overlapping the intrahilar branching vessels will interfere with interpretation if the lesion, as seen in panel (a), left pane, is taken in the RAO projection. By adding caudal tilt, as in this example, the tortuous path of the intrahilar vessel can be seen. In panel (b), left and right panes, cranial–LAO projection details the length of the left pulmonary artery and proximal areas of potential stenosis.

References

1. Culham JAG. Physical principles of image formation and projections in angiocardiography. In: Freedom RM, Mawson JB, Yoo SJ, Benson LN, Eds. *Congenital Heart Disease Textbook of Angiocardiography*. Armonk: Futura Publishing; 1997. pp. 39–93.
2. Freedom RM, Culham JAG, Moes CAF. *Angiocardiography of Congenital Heart Disease*. New York: Macmillan; 1984. pp. 10–16.
3. Beekman RH 3rd, Hellenbrand WE, Lloyd TR, Lock JE, Mullins CE, Rome JJ et al. ACCF/AHA/AAP recommendations for training in pediatric cardiology. Task force 3: Training guidelines for pediatric cardiac catheterization and interventional cardiology endorsed by the Society for Cardiovascular Angiography and Interventions. *J Am Coll Cardiol* 2005;46(7):1388–90.
4. Qureshi SA, Redington AN, Wren C, Ostman-Smith I, Patel R, Gibbs JL et al. Recommendations of the British Paediatric Cardiac Association for therapeutic cardiac catheterisation in congenital cardiac disease. *Cardiol Young* 2000;10(6):649–6.
5. Fahrig R, Fox AJ, Lownie S, Holdsworth DW. Use of a C-arm system to generate true three-dimensional computed rotational angiograms: Preliminary *in vitro* and *in vivo* results. *AJNR Am J Neuroradiol* 1997;18:1507–14.
6. Heran NS, Song JK, Mamba K, Smith W, Niimi Y, Berenstein A. The utility of DynaCT in neuroendovascular procedures. *AJNR Am J Neuroradiol* 2006;27:330–2.
7. Richter G, Engelhorn T, Struffert T et al. Flat panel detector angiographic CT for stent-assisted coil embolization of broad-based cerebral aneurysms. *AJNR Am J Neuroradiol* 2007;28:1902–8.
8. Noelker G, Gutleben KJ, Marschang H et al. Three-dimensional left atrial and esophagus reconstruction using cardiac C-arm computed tomography with image integration into fluoroscopic views for ablation of atrial fibrillation: Accuracy of a novel modality in comparison with multislice computed tomography. *Heart Rhythm* 2008;5:1651–7.
9. Biasi L, Ali T, Thompson M. Intraoperative DynaCT in visceral–hybrid repair of an extensive thoracoabdominal aortic aneurysm. *Eur J Cardiothorac Surg* 2008;34:1251–2.
10. Glatz AC, Zhu X, Gillespie J, Hanna BD, Rome JJ. Use of angiographic CT imaging in the cardiac catheterization laboratory for congenital heart disease. *J Am Coll Cardiol Img* 2010;3:1149–57.
11. Berman DP, Khan DM, Gutierrez Y, Zahn EM. The use of three-dimensional rotational angiography to assess the pulmonary circulation following cavo-pulmonary connection in patients with single ventricle. *Cath Cardiovas Interv* 2012;80:922–30.
12. Schwartz JG, Neubauer AM, Fagan TE, Noordhoek NJ, Grass M, Carroll JD. Potential role of three-dimensional rotational angiography and C-arm CT for valvular repair and implantation. *Int J Cardiovasc Imaging* 2011;27:1205–22.
13. Glockler M, Halbfab J, Koch A, Achenbach S, Dittrich S. Multimodality 3D-roadmap for cardiovascular interventions in congenital heart disease—A single-center, retrospective analysis of 78 cases. *Catheter Cardiovasc Interv* 2013;82:436–42 [Epub ahead of print].
14. Glöckler M, Koch A, Halbfaß J, Greim V, Rüffer A, Cesnjevar R, et al.. Assessment of cavopulmonary connections by advanced imaging: Value of flat-detector computed tomography. *Cardiol Young* 2013;23:18–26.

15. Glöckler M, Koch A, Greim V, Shabaiek A, Rüffer A, Cesnjevar R et al. The value of flat-detector computed tomography during catheterisation of congenital heart disease. *Eur Radiol* 2011;21:2511–20.
16. Fagan T, Kay J, Carroll J, Neubauer A. 3-D guidance of complex pulmonary artery stent placement using reconstructed rotational angiography with live overlay. *Catheter Cardiovasc Interv* 2012;79:414–21.
17. Noble S, Miro J, Yong G, Bonan R, Tardif JC, Ibrahim R. Rapid pacing rotational angiography with three-dimensional reconstruction: Use and benefits in structural heart disease interventions. *EuroIntervention* 2009;5:244–9.
18. Gupta R, Cheung AC, Bartling SH, et al. Flat-panel volume CT: Fundamental principles, technology, and applications. *Radiographics* 2008;28:2009–22.
19. Kalender WA, Kyriakou Y. Flat-detector computed tomography (FD-CT). *Eur Radiol* 2007;17:2767–79.
20. Kyriakou Y, Struffert T, Dorfler A, Kalender WA. Basic principles of flat detector computed tomography (FD-CT). *Radiologe* 2009;49:811–9.
21. Andreassi MG, Ait-Ali L, Botto N, Manfredi S, Mottola G, Picano E. Cardiac catheterization and long-term chromosomal damage in children with congenital heart disease. *Eur Heart J* 2006;27:2703–8.
22. de Gonzalez AB, Mahesh M, Kim K, et al. Projected cancer risks from computed tomographic scans performed in the United States in 2007. *Arch Intern Med* 2009;169:2071–7.
23. Strauss KJ. Pediatric interventional radiography equipment: Safety considerations. *Pediatr Radiol* 2006;36(Suppl 2):126–35.
24. Justino H. The ALARA concept in pediatric cardiac catheterization: Techniques and tactics for managing radiation exposure. *Pediatr Radiol* 2006;36(Suppl 2):146–53.
25. Sidhu MK, Goske MJ, Coley BJ, et al. Image Gently, Step Lightly: Increasing radiation exposure awareness in pediatric interventions through an international social marketing campaign. *J Vasc Interv Radiol* 2009;20:1115–9.
26. Ventricular septal defect. In: Freedom RM, Mawson JB, Yoo SJ, Benson LN, Eds. *Congenital Heart Disease Textbook of Angiocardiography*. Armonk: Futura Publishing; 1997. pp. 189–218.
27. Brandt PW. Axially angled angiocardiography. *Cardiovasc Intervent Radiol* 1984;7(3–4):166–9.

4

Hemodynamics

Mustafa Al-Qbandi and Ziyad M. Hijazi

Introduction

Hemodynamics, by definition, is the study of the motion of blood through the vascular system. In simple clinical application, this may include the assessment of a patient's heart rate, pulse quality, blood pressure, capillary refill, skin color, skin temperature, and other parameters.[1] As the complexity of the patient's status increases, invasive hemodynamic monitoring may be utilized to provide a more advanced assessment and to guide therapeutic interventions.

Invasive hemodynamic monitoring is now used routinely in many critical-care and intermediate-care units to assist in the assessment of single and multisystem disorders and their treatment. Hemodynamic monitoring might include waveform and numeric data derived from the central veins, right atrium (RA), right ventricle (RV), pulmonary artery, left atrium (LA), left ventricle (LV), aorta, and peripheral arteries.

Pressure itself is defined as force per area. This can be expressed in a variety of ways, such as pounds per square inch or kilograms per square centimeters. The standard international unit (SI) is the pascal (Pa). One pascal equals one newton per square meter. In practice, millimeters of mercury (mmHg) is the most commonly used unit of measure of blood pressure. One mmHg is the pressure exerted by a column of mercury that is 1 mm high at zero celsius at standard atmospheric pressure and equals 133.3 Pa.

$$1 \text{ mmHg} = 133.3 \text{ Pa} \quad \text{at zero Celsius}$$

Intra-arterial or direct arterial pressure measurement

The three components or characteristics of intravascular pressures measured through a fluid-filled catheter are

- Residual or static pressure inside the fluid-filled vessel.
- Dynamic pressure, which is caused by the imparted kinetic energy of the moving fluid (similar to the encountered fluid in arterial pressures when the catheter tip is directly facing the flow of fluid).
- Hydrostatic pressure, which results from the difference between the ends of the fluid-filled tubes (the tip of the catheter and the air-reference port of the transducer).

The most desired measurement during hemodynamic monitoring is residual or static pressure within the vessel or chamber being assessed. To achieve this goal, both dynamic and hydrostatic pressure components need to be eliminated. As stated above, dynamic pressures are encountered only in high or frequent flow rates or when the catheter tip is directed into the flow. This component is greatly reduced when assessing arterial blood pressure by the use of dampening services.

The hydrostatic pressure is the component to most consistently interfere with the accuracy of pressure measurements obtained through fluid-filled systems. Placement of the air-reference port at the level of the RA eliminates the effects of hydrostatic pressure within the fluid-filled column and provides accurate measurement within the peripheral artery.

All biomedical devices consist of three basic components:[1]

1. A transducer or device that detects the physiological event.
2. An amplifier that increases the magnitude of the signal from the transducer.
3. A recorder, meter, oscilloscope, or monitor to display the signal.

Right-sided pressure waveforms

Right-sided pressures

Hemodynamic data require examination of not only individual pressure waves, but also their timing to events on the electrocardiogram (ECG), particularly the QRS complex.[2] Correct interpretation of normal right heart pressure waveforms and careful examination of the unusual right heart hemodynamics and their timing in the cardiac cycle may reveal unanticipated pathophysiologic mechanisms.

Abnormalities of the waveforms can occur in the presence of arrhythmia or ventricular pacing. This must be considered when interpreting hemodynamic data. Therefore, ECG correlation is required for correct identification of these events.

Right atrium

In the RA, there is an 80–100 ms delay in the detection of mechanical events from their appearance on the ECG due to the length of tubing in the system.[1,3] During inhalation, the right atrial pressure falls, while in exhalation, the right atrial pressure increases (Table 4.1).

The right atrial pressure waveform consists of two major positive deflections, the "a" and "v" waves (Figure 4.1 and Tables 4.2 and 4.3).

The "a" wave results from right atrial contraction and immediately follows the P wave on the surface of ECG. Following the "a" wave and right atrial contraction, the pressure declines, defining the "x" descent. A small positive deflection, known as the "c" wave, may be seen reflecting closure of the tricuspid valve. Thereafter, the "x" descent continues as right atrial pressure declines due to right atrial relaxation. After full atrial relaxation and the nadir of the

Table 4.1 Normal physiologic respiratory effect on right atrial pressure

Inhalation: Intrathoracic pressure falls → RA pressure falls
Exhalation: Intrathoracic pressure increases → RA pressure increases

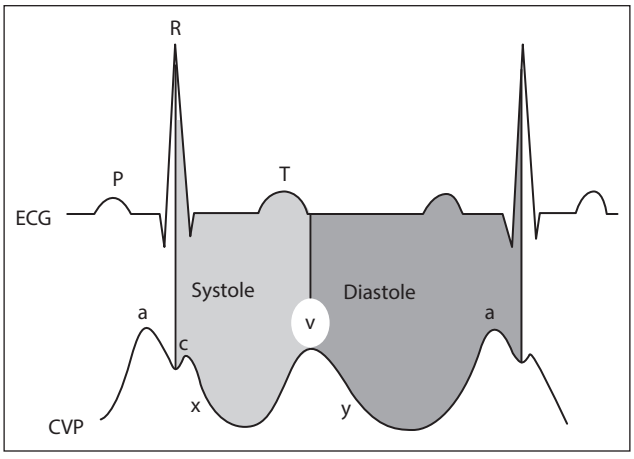

Figure 4.1 RA pressure tracing in a normal person. The "a" wave occurs simultaneously with atrial contraction; the "v" wave occurs during atrial filling; the "c" wave is coincident with the onset of ventricular contraction; the "x" descent corresponds to the fall in pressure after atrial contraction and the continued fall during early systole ("x"); and the "y" descent occurs after the opening of the tricuspid valve and with early diastolic filling. (From Internet: University of Iowa Children's Hospital. Home page section of arterial blood and central venous pressure monitoring devices. With permission.)

Table 4.2 Normal right atrial pressure waves

a Wave	1—Rise in pressure due to atrial contraction. 2—a Waves are larger in the presence of any resistance to RV filling (TS, RV failure, and cardiac tamponade), because resistance will increase pressure as the atrium attempts to contract and eject blood.
x Descent	Fall in pressure due to atrial relaxation.
c Wave	Rise in pressure due to ventricular contraction and bulging of the closed tricuspid valve.
v Wave	Rise in pressure during atrial filling.
y Descent	Fall in pressure due to the opening of the tricuspid valve and the beginning of ventricular filling.

Table 4.3 Abnormalities in right atrial tracings

Low mean atrial pressure	Hypovolemia Improper zeroing of the transducer
Elevated mean atrial pressure	Right ventricular failure Valvular disease (TS, TR, PS, and PR) Myocardial disease (RV ischemia, cardiomyopathy) Left heart failure (MS, MR, AS, AI, and cardiomyopathy) Increased PVR (PE, COPD, and primary pulmonary HTN) Pericardial effusion with tamponade physiology Atrial myxoma
Elevated a wave	Tricuspid atresia/stenosis Decreased RV compliance due to RV failure
Cannon a wave	A–V asynchrony (3rd degree AVB, VT, and V-pacer)
Absent a wave	Atrial flutter or fibrillation
Elevated v wave	TR RV failure Reduced atrial compliance (restrictive myopathy)
Equal a and v waves	Tamponade Constrictive physiology
Prominent x descent	Tamponade Subacute/chronic constriction RV ischemia
Prominent y descent	TR Constrictive pericarditis Restrictive myopathy
Blunted x descent	Atrial fibrillation RA ischemia
Blunted y descent	TS RV ischemia Tamponade
M or W waves	Diagnostic for RV ischemia, pericardial constriction, or CHF

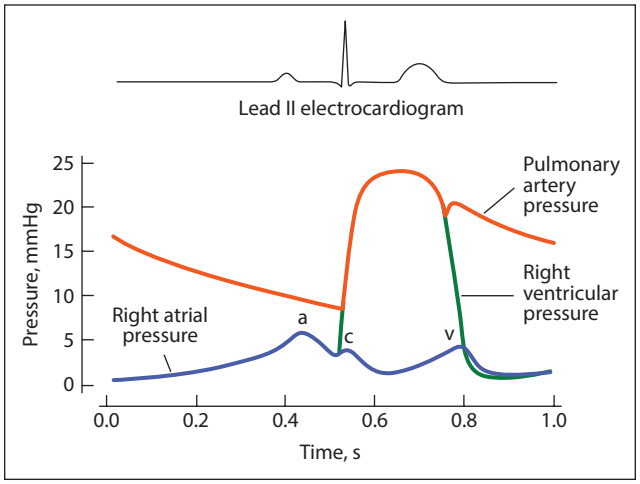

Figure 4.2 (**See color insert.**) The right ventricular pressure tracing is similar to that generated by the left ventricle except that the pressures are lower. (Courtesy of McGraw Hill.)

"x" descent, right atrial pressure rises due to increased volume from peripheral venous return. With right ventricular systole and the rapid increase in the right ventricular pressure, the tricuspid valve closes. The increasing right atrial pressure during right ventricular systole is the "v" wave; it reaches maximal amplitude just prior to the opening of the tricuspid valve. When the pressure in the RV falls below that of the RA, the tricuspid valve opens.

After the tricuspid valve opens, at the beginning of right ventricular diastole, the pressure in the RA rapidly falls, defining the "y" descent. After the "y" descent, the pressure in the RA equals the right ventricular end-diastolic pressure (RVEDP) since the tricuspid valve is opened; it slowly increases as the RV fills.

The normal mean right atrial pressure is between 1 and 8 mmHg.

Jugular venous pulsations

The jugular venous pulse closely reflects changes in right atrial pressure, and also parallels changes observed in the vena cavae.[4,5] The variations in pressure within the RA are principally reflected by a change in volume for the venous system.

The venous pulse "a" and "c" waves have an average delay from the RA of approximately 60 ms, while the "v" wave delay is 80 ms; by comparison, the "y" trough delay is 90 ms, and the "x" trough is 110 ms. It also requires 60 ms for the right atrial "a" wave to reach the RV and cause a positive defection in this chamber. These delays should be considered when examining the jugular venous pulse, as well as inferior vena caval pressure waves as a reflection of the right atrial pressure.[6]

Right ventricle

The RV pressure tracing (Figures 4.2 and 4.3) normally exhibits a peak systolic pressure equal to the one in the main pulmonary artery (PA) and is ≤30 mmHg. Generally, the RA and RV diastolic pressures are equal. The RV pressure during the first one-third of the diastole rises rapidly during the period of early diastolic filling. At the beginning of diastasis (this is the third phase of diastole) in which the RA and RV pressures are almost equal, filling is mainly the result of venous flow with the RA acting as a passive conduit. Also termed as the slow-filling period, the resistance to filling significantly increases, and the pressure

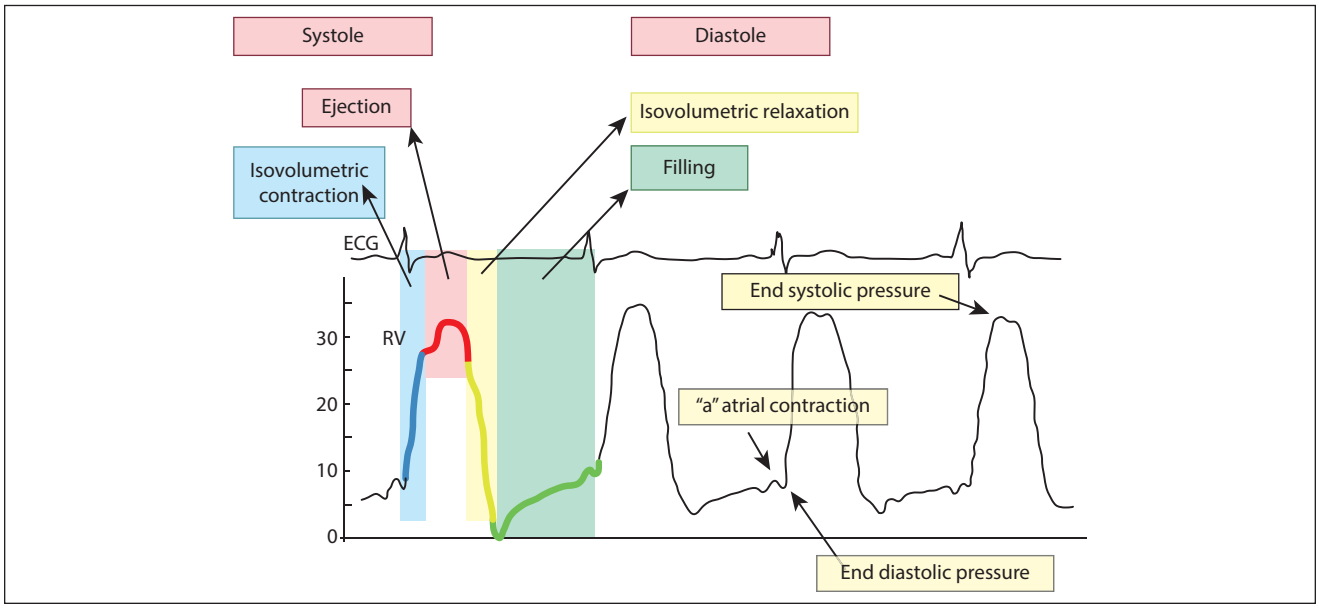

Figure 4.3 Example of RV pressure tracing in a normal person. The "a" wave represents atrial contraction. The shaded areas represent the contraction, ejection, relaxation, and filling periods.

then rises much more slowly until the onset of atrial systole "a" (Figure 4.2). This diastasis period is much shorter with rapid heart rates and the rapid-filling phase is immediately followed by atrial contraction.

The right ventricular waveform consists of the systole, a result of right ventricular contraction, and diastole occurring with right ventricular relaxation (Figure 4.3). During right ventricular systole, the pressure rapidly rises; when it is higher than that of the RA, the tricuspid valve closes. When the pressure exceeds that of the pulmonary artery, the pulmonic valve opens. The systolic waveform is rapid in upstroke and rounded in morphology; it occurs simultaneously with or immediately after the QRS complex on the surface ECG. The peak or maximal amplitude of this waveform is the right ventricular systole pressure. At the end of the systole, there is right ventricular relaxation and a rapid fall in pressure back to the baseline. This is the initiation of right ventricular diastole. When the pressure in the RV is lower than that of the pulmonary artery, the pulmonic valve closes. As the right ventricular pressure falls further, it becomes lower than that of the RA and the tricuspid valve opens.

Diastole consists of three periods generating three waveforms (Tables 4.4 and 4.5):

The first period, occurring at the onset of the tricuspid valve opening, produces an early rapid-filling wave during which approximately 60% of ventricular filling occurs.

Following this is a slow-filling period, accounting for approximately 15% of ventricular filling. Right atrial systole, which accounts for approximately 25% of right ventricular diastolic filling, produces an "a" wave that is simultaneous with and identical in morphology and amplitude to the "a" wave on the right atrial pressure tracing, since the tricuspid valve is opened and creates essentially one chamber. The pressure at the end of the "a" wave is termed the RVEDP.

The right ventricular pressure tracing is similar to that generated by the left ventricle, except that the pressures are lower.

The normal right ventricular diastolic pressure is 1–8 mmHg and the peak systolic pressure is 15–30 mmHg.

Pulmonary artery

The pulmonary artery waveform reflects systolic pressure resulting from rapid flow of blood into the pulmonary artery from the RV during right ventricular systole. Since the pulmonic valve is opened, the waveform in the systole is identical in morphology and amplitude to that of right ventricular systole (Figure 4.4).

Table 4.4 Right ventricular waves in systole and diastole

Systole
1. Isovolumetric contraction from TV closure to PV opening
2. Ejection from PV opening to PV closure

Diastole
1. Isovolumetric relaxation from PV closure to TV opening
2. Filling from TV opening to TV closure
   - Early rapid phase
   - Slow phase
   - Atrial contraction ("a" wave)

Table 4.5 Causes of right ventricular pressure changes

RV systolic pressure overload	RV systolic pressure reduced
Pulmonary HTN	Hypovolemia
Pulmonary valve stenosis	Cardiogenic shock
Right ventricular outflow obstruction	Tamponade
Supravalvular obstruction	
Significant shunt, ASD or VSD, TAPVC, and so on	
Increased PVR	
End-diastolic pressure overload	**End-diastolic pressure reduced**
Hypervolemia	Hypovolemia
CHF	TS
Diminished compliance	
Hypertrophy	
Tamponade	
TR	
Pericardial constriction	

As right ventricular ejection ends, the pressure in the pulmonary artery falls in a similar manner to that in the RV. However, as right ventricular pressure falls below that of the pulmonary artery, the pulmonic valve closes, resulting in an incisura, or dicrotic notch, on the downslope of the pressure tracing. Pressure in the pulmonary artery continues to fall gradually as blood flows through the pulmonary arteries and veins into the left side of the heart, reaching a nadir or the end-diastolic pulmonary artery pressure.

Thereafter, the pressure falls during diastole to the level that is nearly equivalent to the mean LA pressure (or PCWP). Exceptions to the equivalency of PA diastolic pressure and mean LA pressure are

1. Rapid heart rate (the PA pressure does not have time to fall to the level of LA pressure during diastole)
2. Elevated pulmonary vascular resistance (PVR) with vasoconstriction

The mean PA pressure or diastolic PA pressure is elevated in response to any condition that (Table 4.6)

1. Increases LA or PCWP (e.g., LV diastolic dysfunction, MS, and mitral valve regurgitation [MR])
2. Increases PVR at the arterial level
3. Selectively obliterates a significant portion of pulmonary vascular bed upstream to the arteriolar level (e.g., multiple or large thromboemboli)

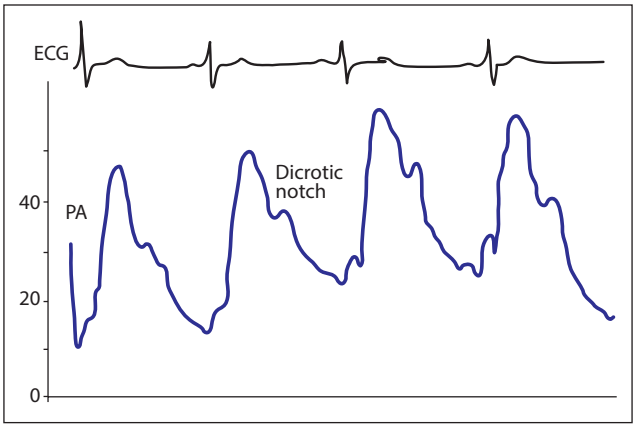

Figure 4.4 (**See color insert.**) Example of a PA pressure tracing in a normal person. Note the variation in peak systolic and diastolic pressures with respiration. The dicrotic notch appears shortly after the end of ejection and the closure of the pulmonic valve.

Table 4.6 Causes of change in pulmonary artery pressure

Elevated systolic PA pressure	**Reduced systolic PA pressure**
Primary pulmonary hypertension	Hypotension
Mitral stenosis	Pulmonary artery stenosis
Mitral regurgitation	Pulmonary valve stenosis/ atresia
Congestive heart failure	Supra- or subvalvular pulmonary stenosis
Restrictive cardiomyopathy	Ebstein anomaly
Left-to-right shunt	Tricuspid valve stenosis/ atresia
Pulmonary disease	
Reduced pulse pressure	**PA diastolic pressure > PCW pressure**
Right heart ischemia	Pulmonary disease
Tamponade	Pulmonary embolus
RV infarction	Tachycardia
Pulmonary embolism	

The waveform of the pulmonary artery is similar in morphology to that of the aorta. It is biphasic, but the pressure is lower.

The normal pulmonary artery systolic pressure is 15–30 mmHg and the normal pulmonary artery diastolic pressure is 4–12 mmHg.

Pulmonary artery capillary wedge pressure and left atrium

The pulmonary artery capillary wedge pressure (PCWP) (Figure 4.5) is an occluded pressure reflecting downstream

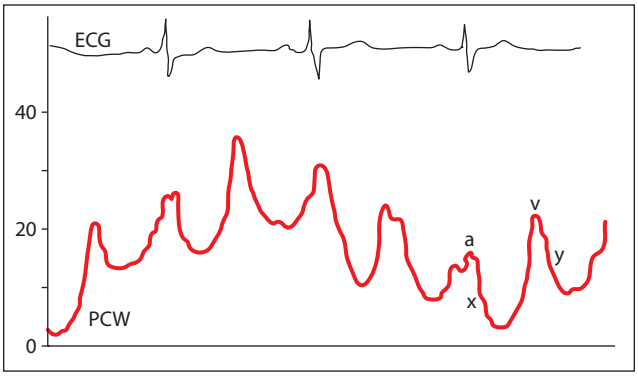

Figure 4.5 (**See color insert.**) Example of PCWP tracing, reflecting the LA pressure, in a normal person.

LA pressure provided there is proper positioning and there are no intervening anatomic obstructions (e.g., pulmonary venous obstruction, cor triatriatum). There is a time delay between the PCWP and the LA tracings of about 140–200 ms (Figure 4.6). The normal waveform consists of an "a" wave due to atrial contraction, a "v" wave reflecting left atrial filling during left ventricular contraction, a "c" wave (which may not be apparent on the PCWP tracing) due to mitral valve closure, and an "x" and "y" descent due to left atrial relaxation and left ventricular diastole, respectively. In the normal situation, the mean PCWP and end-diastolic PA pressure are approximately equal.

The normal mean left atrial pressure (and pulmonary capillary wedge pressure) is between 4 and 15 mmHg. When compared with the RA pressure tracing, LA pressure is always higher than RA pressure and the LA pressure pulse exhibits a normally dominant "v" wave (<15 mmHg) and a subordinate "a" wave (<12 mmHg). Tables 4.7 and 4.8 show the PCWP waves and the causes of change in PCWP waves.

Left ventricle

The pressure pulse (Figure 4.7) is characterized by a peak systolic pressure nearly equal to the peak aortic pressure (there may be a small mid-systolic or late-systolic pressure

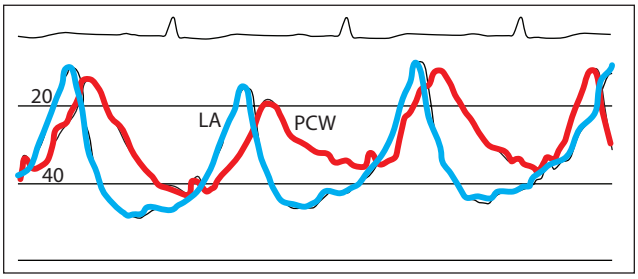

Figure 4.6 (**See color insert.**) PCW tracing (red tracing) "approximates" actual LA tracing (blue tracing) but is slightly delayed since pressure wave is transmitted retrograde through pulmonary veins.

Table 4.7 Causes of change in pulmonary artery pressure changes

PACWP Waves
"a" Wave: Atrial systole
High in MS, decreased LV compliance due to LV failure/valve disease
Cannon a waves: AV asynchrony (3rd degree AN block, V-pacer, and VT)
Absent a: Atrial flutter or fibrillation
Equal a and v: Tamponade and constrictive pericarditis
"c" Wave: Protrusion of MV into LA
"x" Descent: Relaxation of LA, downward pulling of mitral annulus by LV contraction
Prominent: Tamponade and constrictive pericaritis
Blunted: Atrial fibrillation and LA ischemia
"v" Wave
LV contraction
Height related to atrial compliance and amount of blood return and higher than a wave
High in VSD/MR/left or right ventricular failure
"y" Descent MV opening and LA emptying into LV
Prominent: MR, constrictive pericarditis, and restrictive cardiomyopathy
Blunted: MS, LV ischemia, and tamponade

Table 4.8 PCWP and LVEDP

PCWP not equal to LV end-diastolic pressure
• Mitral stenosis
• Atrial myxoma
• Cor triatriatum
• Pulmonary venous obstruction
• Decreased ventricular compliance
• Increased pleural pressure

gradient). In the absence of any obstruction to LV outflow, this peak pressure occurs at the end of the first third of systole. The peak-positive rate of rise of LV pressure (*dP/dt*) occurs before the opening of the aortic valve (AV); the peak-negative *dP/dt* occurs simultaneously with closure of the AV and marks the beginning of isovolumetric relaxation in the LV. Following AV closure, the LV pressure declines until decreasing the pressure differential between LV and LA causes the opening of mitral valve (MV). At end diastole, the pressure rises quickly in response to atrial systole. The LVEDP immediately precedes the beginning of isovolumetric contraction in the LV pressure pulse. In general, the mean PCWP, mean LAP, and LVEDP are all nearly equivalent in magnitude.

Comparing left-sided to right-sided pressures

- Diastolic amplitude similar between RV and LV tracings
- Systolic amplitude higher for LV than RV
- Duration of systole, isovolumetric contraction, and isovolumetric relaxation are longer for LV compared with RV
- Duration of ejection is shorter for LV than RV

Important abnormalities of left ventricular tracings

- Systolic pressure overload
  - Systemic hypertension
  - Aortic valve stenosis
  - Left ventricular outflow obstruction
  - Supravalvular obstruction
  - Coarctation of aorta
  - Significant atrial (ASD) or ventricular septal defect (VSD)
- Systolic pressure reduced
  - Hypovolemia
  - Cardiogenic shock
  - Tamponade

The LVEDP is elevated (>12 mmHg) in

1. LV diastolic volume overload (e.g., MR, aortic valve regurgitation [AR], and a large left-to-right shunt)
2. Concentric hypertrophy (decreased compliance), for example, aortic valve stenosis (AS) or long-standing HTN
3. Decreased myocardial contractility (dilated LV)
4. Restrictive or infiltrative cardiomyopathy
5. Constrictive pericardial disease (or a high-pressure pericardial effusion)
6. Ischemic heart disease (acute or chronic secondary-to-noncompliance, scar)

However, LVEDP is low in

1. MS
2. Hypovolemia

Ascending aorta

During ejection, normal pressure in the ascending aorta parallels LV pressure (Figure 4.7). Once the AV closes, the aortic pressure declines somewhat more slowly than the LV pressure. This reflects the accumulated pressure waves from the thoracic aorta and its tributaries as well as the capacitance of the aorta. Following the dicrotic notch, there is a brief increase in pressure due to some retrograde flow from the periphery into the ascending the aorta and the elastic recoil of the ascending aorta. Then as the blood runs off into the periphery, there is a gradual decline in the systolic arterial pressure until the next cardiac cycle. The rate and

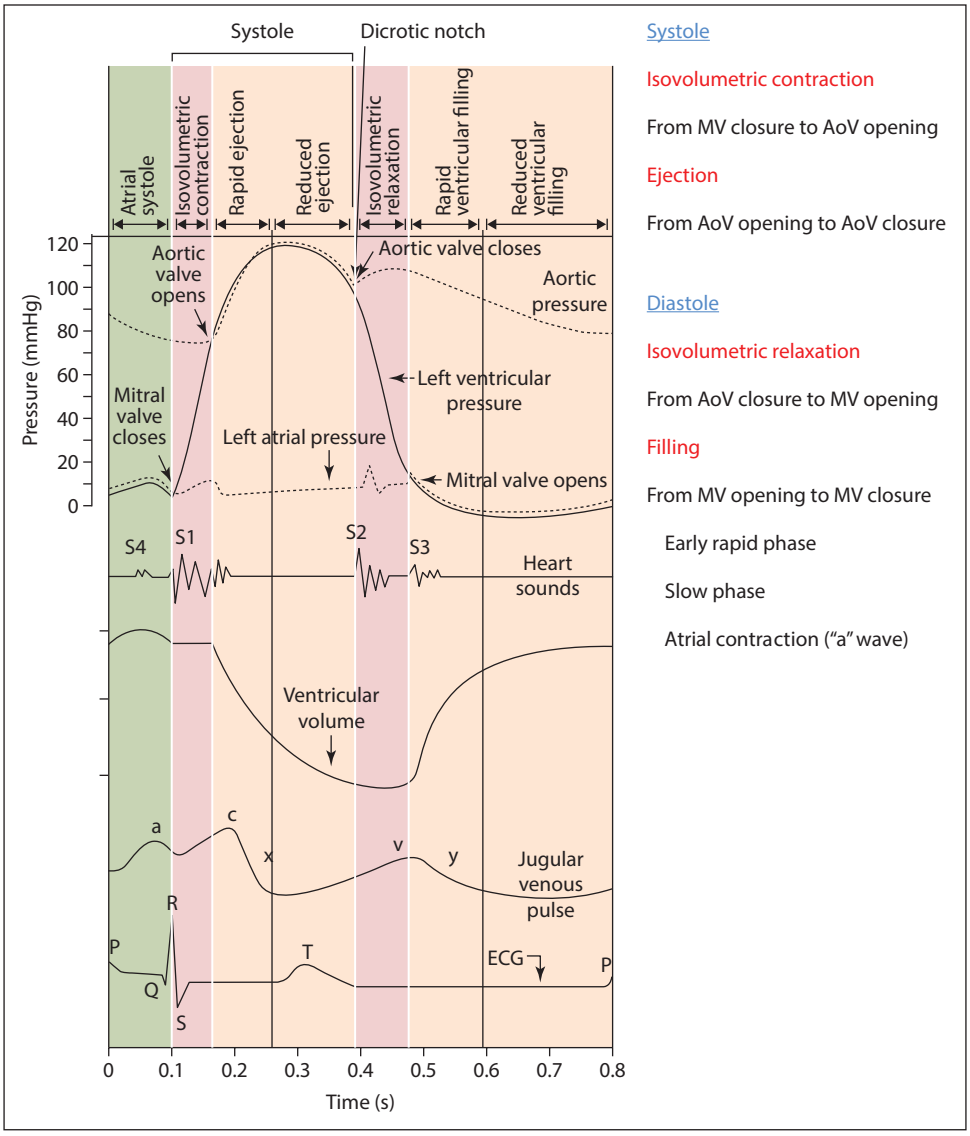

Figure 4.7 (**See color insert.**) Normal left and right pressure waves in correlation to ECG. The isovolumetric contraction and relaxation times are shaded in pink.

magnitude of decline of aortic pressure during diastole are dependent on

1. Aortic valve integrity (aortic insufficiency)
2. Capacitance and resistance of the peripheral circuit
3. Presence or absence of abnormal connection of aorta and the pulmonary circulation or the right heart (e.g., PDA)
4. Presence or absence of a large arteriovenous fistula

Pulse pressure (PP) is defined as the systolic minus the diastolic pressure

$$PP = \text{Systolic BP} - \text{Diastolic BP}$$

There are many causes of change in pulse pressure (Table 4.9).

Femoral or peripheral arterial pressure is not, and usually should not be equal to central aortic pressure. The overshoot of femoral artery pressure is due to summation of the pressure wave reflections generated by the expansion and recoil characteristics of the central aortic and large-artery elasticity. The peripheral or femoral artery pressure is almost always higher than the central aortic pressure (Figure 4.8).[7]

Pulsus bisferiens

The normal carotid arterial pulse tracing and the central aortic pulse waveform consist of an early component, the percussion wave, which results from rapid left ventricular ejection, and a second smaller peak, the tidal wave,

Table 4.9 Causes of change in aortic pressure

Widened pulse pressure	Reduced pulse pressure
Systemic hypertension	Tamponade
Aortic insufficiency	Heart failure
Significant patent ductus arteriosus	Cardiogenic shock
	Aortic stenosis
Ruptured sinus of Valsalva aneurysm	
Systolic pressure elevated	**Systemic pressure reduced**
Systemic hypertension	Hypovolemia
Atherosclerosis	Aortic stenosis
Aortic insufficiency	Heart failure
Coarctation of aorta	

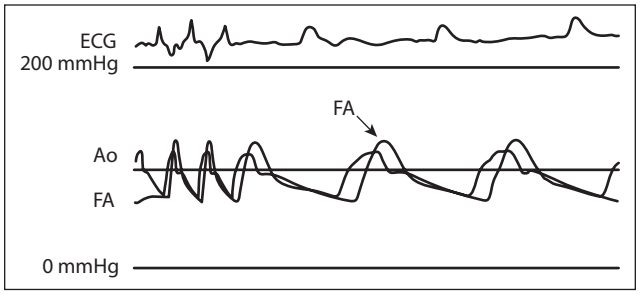

Figure 4.8 Simultaneously recorded pressures from the aortic root (Ao) and femoral artery (FA) demonstrating delayed transmission and a higher systolic pressure in the femoral artery. There is smoothing of the waveform and loss of the dicrotic notch.

presumed to represent a reflected wave from the periphery. The tidal wave may increase in amplitude in hypertensive patients or in those with elevated systemic vascular resistance. Radial and femoral pulse tracings demonstrate a single sharp peak in normal circumstances. Pulsus bisferiens is characterized by two systolic peaks of the aortic pulse during left ventricular ejection separated by a mid-systolic dip (Figure 4.9). Both percussion and tidal waves are accentuated. It is difficult to establish with certainty that the two peaks are occurring in the systole with simple palpation (pulsus bisferiens) versus one peak in the systole and the other in the diastole (dicrotic pulse).[8–10]

Pulsus bisferiens (Figure 4.9) is frequently observed in patients with hemodynamically significant (but not mild) aortic regurgitation. In patients with mixed aortic stenosis and aortic regurgitation, bisferiens pulse occurs when regurgitation is the predominant lesion. The absence of pulsus bisferiens does not exclude significant aortic regurgitation.

In most patients with hypertrophic cardiomyopathy, the carotid pulse upstroke is sharp and the amplitude is normal; pulsus bisferiens is rarely palpable but often recorded. The rapid upstroke and prominent percussion wave result from

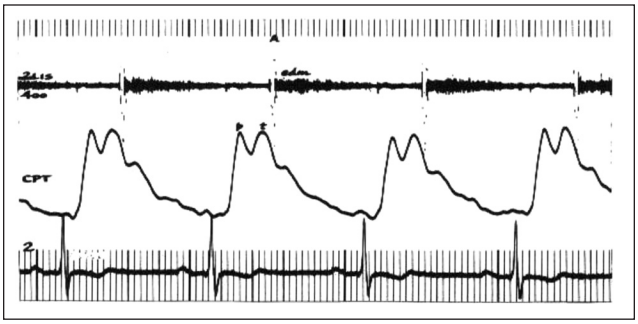

Figure 4.9 Pulsus bisferiens.

rapid left ventricular ejection into the aorta during early systole. This is followed by a rapid decline as left ventricular outflow tract obstruction ensues, a result of midsystolic obstruction and partial closure of the aortic valve. The second peak is related to the tidal wave. Occasionally, a bisferiens pulse is not present in the basal state but can be precipitated by the Valsalva maneuver or by inhalation of amyl nitrate.

Pulsus bisferiens is occasionally felt in patients with a large patent ductus arteriosus or arteriovenous fistula. A bisferiens quality of the arterial pulse is also rarely noted in patients with significant mitral valve prolapse and very rarely in normal individuals, particularly when there is a hyperdynamic circulatory state.

The mechanism of pulsus bisferiens is not clear. It appears to be related to a large, rapidly ejected left ventricular stroke volume associated with increased left ventricular and aortic *dp/dt*.

It is mainly seen in hypertrophic obstructive cardiomyopathy and aortic insufficiency.[8]

Pulsus alternans

Pulsus alternans (also termed mechanical alternans) is a variation in pulse amplitude occurring with alternate beats due to changing systolic pressure (Figure 4.10). The precise mechanism for pulsus alternans remains unclear; alternating preload (Frank–Starling mechanism) and incomplete relaxation have been proposed. Changes in afterload, which is lower before the strong beat because of the lower output during the weak beat, may also contribute. Pulsus alternans should not be diagnosed when the cardiac rhythm

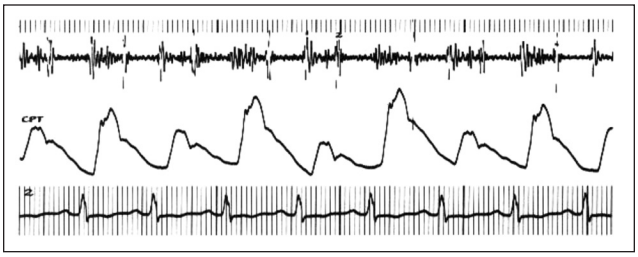

Figure 4.10 Pulsus alternans.

is irregular. Pulsus alternans is more common with faster heart rate.

It has also been suggested that a change in ventricular contractility is the primary mechanism. Changes in sarcoplasmic calcium pumps with alternate strong and weak beats appear to be the mechanism for changes in contractility. Thus, pulsus alternans may primarily result from an alternating contractile state of the ventricle. The magnitude of the alteration of pressure and stroke volume during pulsus alternans, indices of pump function, reflects the interaction of an alternating contractile state with changes in preload and afterload.[11,12]

Some of the causes of pulsus alternans are pericardial effusion, cardiomyopathy, congestive heart failure, and severe aortic regurgitation with left ventricular dysfunction.

Pulsus paradoxus

Systolic arterial pressure normally falls during inspiration, although the magnitude of decrease usually does not exceed 8–12 mmHg. These changes in pulse amplitude are not usually appreciated by palpation but can be established with the sphygmomanometer.

A more marked inspiratory decrease in arterial pressure exceeding 20 mmHg is termed pulsus paradoxus (Figure 4.11).[13] In contrast to the normal situation, this is easily detectable by palpation, although it should be evaluated with a sphygmomanometer. When the cuff pressure is slowly released, the systolic pressure at expiration is first noted. With further slow deflation of the cuff, the systolic pressure during inspiration can also be detected. The difference between the pressures during expiration and inspiration is the magnitude of pulsus paradoxus. The inspiratory decrease in systolic pressure is accentuated during very deep inspiration or Valsalva; thus, assessment of pulsus paradoxus should be made only during normal respiration.

In addition to tamponade, pulsus paradoxus can occur in chronic obstructive pulmonary disease, hypovolemic shock, and infrequently in constrictive pericarditis and restrictive cardiomyopathy. It is rarely observed in pulmonary embolism, pregnancy, marked obesity, and partial obstruction of the superior vena cava.

In hypertrophic obstructive cardiomyopathy, arterial pressure occasionally rises during inspiration (reversed pulsus paradoxus); the precise mechanism for this phenomenon is unclear.[13] In addition to changes in the amplitude, configurational changes of the carotid pulse may occur.

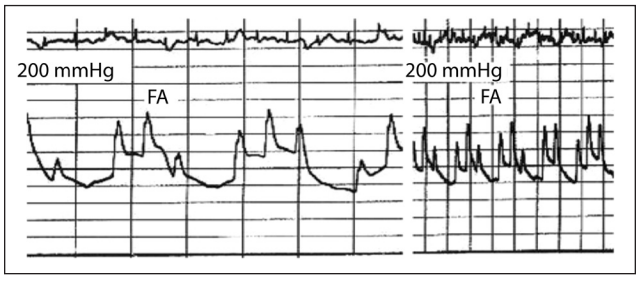

Figure 4.11 Pulsus paradoxus.

Cardiac output

In the cardiac catheterization laboratory, the cardiac output is usually determined by one of two methods: (1) measurement of oxygen consumption, or (2) the indicator-dilution method. Each of these techniques will be reviewed further.

Measurement of oxygen consumption (Fick method)

Adolph Fick initially described this technique in 1870.[14] The principle used is that the uptake of a substance by any organ system is the product of the arteriovenous concentration difference of that substance and the blood flow to that organ. Hence, if the lungs are used as the end organ, the pulmonary blood flow (which is equal to the systemic blood flow in the absence of an intracardiac shunt) can be determined by measuring the arteriovenous difference in the oxygen across the lungs and the uptake of oxygen by the lungs. Oxygen content is calculated by estimating the oxygen-carrying capacity of the patient's blood, as hemoglobin-bound oxygen. This is the volume of oxygen that could be carried on hemoglobin at 100% saturation. This is calculated by

$$\text{Hb (g/L)} \times 1.36.$$

Usually, this is in the order of 200 mL/L, although it varies with Hb. The content of each sample is then computed by multiplying by the saturation. Thus, if Hb is 140 g/L and saturation in a sample is 70%, then oxygen-carrying capacity is

$$140 \times 1.36 = 190 \text{ mL/L}$$

and oxygen content will be

$$190 \times 70\% = 133 \text{ mL/L}.$$

The left ventricular oxygen content:

$$1.36 \times \text{Hemoglobin concentration} \times \text{LV oxygen saturation}.$$

The mixed venous (pulmonary artery) oxygen content:

$$1.36 \times \text{Hemoglobin concentration} \times \text{PA oxygen saturation}.$$

The value 1.36 is derived from the fact that 1 g of hemoglobin, when 100% saturated, combines with 1.36 mL of oxygen.

Therefore,

$$\text{CO(L/min)} = \frac{\text{O}_2 \text{ consumption (mL/min)}}{\text{Ao} - \text{PA O}_2 \text{ content (mL/L)}}$$

There are two techniques traditionally used for the determination of oxygen consumption:

1. Douglas bag method
2. Metabolic hood or the polarographic method

However, it is important to remember that no matter what method is used, the patient needs to be breathing comfortably at a steady state. The other source of error is the use of supplemental oxygen by the patient during the procedure; this makes it difficult to calculate the oxygen content of inspired air. To minimize this error, it is suggested that supplemental oxygen therapy must be discontinued for at least 15 min prior to determination of cardiac output by the Fick method. Alternatively, VO_2 can be estimated as 3 mL O_2/kg/min or 125 mL/min/m^2.

Indicator-dilution method

This method uses the mean concentration and transit time of an artificial substance that is added to the bloodstream. The most commonly used method is cold saline (thermodilution) injected into the RA and the resulting temperature change is detected in the PA. Another indicator not commonly used these days is the indocyanin green dye. The dye is injected into the central circulation (preferably PA) and is then detected in a systemic artery.

Thermodilution

Room temperature (or iced) normal saline solution is injected into the SVC or RA through the proximal port of the Swan–Ganz catheter, the thermistor that is located at the tip of the catheter is inserted in the PA.[15,15–17] If room-temperature saline is used, there must be at least 10°C difference between the injectate and body temperature. A dilution curve is then constructed as cool saline passes the thermistor tip. The CO is then calculated by the computer using the area under the curve as done for the dye indicator technique (total of 3–5 outputs should be done). In a number of studies, this method has shown good correlation with the Fick method for calculation of cardiac output.

CO is calculated by the following formula:

$$\text{CO (mL/s)} = \frac{\text{Volume injected (mL)} \times \text{Temperature difference (°C)}}{\text{Area under the curve (°C.s)}}$$

To get the CO in L/min, the above value is multiplied by 0.06. MR or AR does not directly influence the downslope of the indicator-dilution curve. However, severe TR results in poor mixing in the RA and subsequent loss of the indicator to the body tissue before it reaches the PA.

Important hemodynamic equations:

1. Mixed venous oxygen saturation:[18]

$$\text{MV sat} = \text{Sat SVC} - \frac{\text{Sat SVC} - \text{Sat IVC}}{4}$$

Usually, it is in the range of 60–80%.

2. Cardiac output

$$\text{CO} = \text{SV} \times \text{HR}$$

$$\text{CO} = \frac{\text{Oxygen consumption (mL/min)}}{\text{AVO}_2 \text{ difference (mL O}_2\text{/L blood)}}$$

AVO_2 is the difference between arterial and mixed venous (pulmonary artery) O_2 content

$$O_2 \text{ content} = \text{Saturation} \times 1.36 \times \text{Hemoglobin concentration}$$

3. Simple shunt calculation Qp:Qs

$$\text{Qp:Qs} = \frac{\text{Sat Ao} - \text{Sat MV}}{\text{Sat PV} - \text{Sat PA}}$$

4. Cardiac index (L/min.m^2)

$$\text{CI} = \frac{\text{CO (L/min)}}{\text{BSA (m}^2\text{)}}$$

Normal 2.5–4.2 L/min.m^2.

5. Stroke volume (mL)

$$\text{SV} = \frac{\text{CO(mL/min)}}{\text{HR}}$$

6. Stroke index (mL/beat.m^2)

$$\text{SI} = \frac{\text{SV(mL/beat)}}{\text{BSA (m}^2\text{)}}$$

7. Stroke work

$$\text{SW} = (\text{Mean LV systolic P} - \text{Mean LV diastolic P}) \times \text{SV} \times 0.0144$$

8. Pulmonary artery resistance (Wood units)

$$\text{PAR} = \frac{\text{Mean PAP} - \text{Mean LAP (or PCWP)}}{\text{Qp}}$$

You can use CO instead of Qp in the absence of intracardiac shunting. Multiply by 80 for results in metric units (dynes.s.cm^{-5}) (i.e., PVRI). Normal range for PVRI is 225–315 dynes.s.cm^{-5}

$$\text{Mean PAP} = \text{PAD} + \frac{\text{PAS} - \text{PAD}}{3}$$

The normal range of mean pulmonary artery pressure (PAP) is 11–18 mmHg.

9. Total pulmonary resistance (Wood units)

$$\text{TPR} = \frac{\text{Mean PAP}}{\text{CO}}$$

Multiply by 80 for results in metric units (dynes.s.cm^{-5}) (i.e., TPRI).

10. Systemic vascular resistance (Wood units)

$$\text{SVR} = \frac{\text{Mean systemic arterial BP} - \text{Mean RAP}}{\text{CO}}$$

Multiply by 80 for results in metric units (dynes.s.cm^{-5}) (i.e., obtain the SVRI). The normal range for SVRI is 1970–2390 dynes.s.cm^{-5}.

$$\text{Mean AP} = \text{DBP} + \frac{\text{SBP} - \text{DBP}}{3}$$

The normal range for mean atrial pressure (MAP) is 80–100 mmHg.

Vascular resistance

Vascular resistance is the impediment offered by the vascular bed to flow. The greatest resistance occurs at the site of the greatest drop in pressure (arterioles). Whether it is on the left or right side, it is a measurement of ventricular afterload.

The percentage of total vascular resistance estimated for each region of the systemic vascular is: aorta and larger arteries: 9%; small arteries and branches: 16%; arterioles: 41%; capillaries: 27%; venules: 4%; small veins: 1%; and large veins: 2%.

However, vascular resistance is dependent on the properties of the vessel and its contained fluid, with a pattern of unidirectional and constant blood flow (microcirculation). Vascular impedance is the impediment offered to flow at the input of a vascular bed where pulsatile flow is involved (aorta and arteries).

Estimation of vascular resistance

The hemodynamic expression of Ohms's law helps one to understand how the circulation is controlled. Similarly, the Poiseuille equation for flow of homogeneous fluids states

$$\text{Resistance} = \frac{\text{P}}{\text{Q}} = \frac{8\eta L}{r4}$$

where

Q = volume flow
P = change in pressure
r = radius of tube
L = length of tube
η = viscosity of the fluid

In the vascular system, the key factor is the radius of the vessel. The smaller the vessel diameter, the greater the resistance.

This can be simplified to

$$\text{Flow (Q)} = \frac{\text{Pressure}}{\text{Resistance}}$$

Arterial pressure = Cardiac output × Vascular resistance

The resistance is a ratio, relating pressure and flow, and reflects the vasomotor tone in arterioles, terminal arterioles, and precapillaries sphincter (Tables 4.10 and 4.11).

$$\text{Vascular resistance (mmHg/L/min)} = \frac{\text{Arterial pressure (mmHg)}}{\text{Cardiac output (L/min)}}$$

Data in these formulae are expressed in liters per minute (blood flow), and pressures are in millimeters of mercury. These equations yield resistance in arbitrary resistance units (R units). They may be converted into dyne.cm.s^{-5} by using the conversion factor 80. mmHg/L/min is termed as a hybrid unit or Wood unit. If multiplied by 80, then the unit will be in dyne.cm.s^{-5}.

Table 4.10 Normal values for systemic and pulmonary vascular resistance

	Normal reference values Wood units	dyne.cm.s^{-5}
Systemic vascular resistance SVR = (Mean Ao – Mean RA)/Qs	10–20	770–1500
Pulmonary vascular resistance PVR PVR = (Mean PA – Mean LA)/Qp	0.25–1.5	30–180

Table 4.11 Causes of change in pulmonary and systemic vascular resistance

Increased systemic vascular resistance	Decreased systemic vascular resistance[19]	Increased PVR
Systemic HTN	Inappropriately high cardiac output	Primary lung disease
Cardiogenic shock with compensatory arteriolar constriction	Arteriovenous fistula	Eisenmenger syndrome
	Severe anemia	Elevated pulmonary venous pressure
	High fever	Left-sided myocardial dysfunction
	Sepsis	Mitral/aortic valve disease
	Thyrotoxicosis	Left-sided obstructive chd

$$\text{Systemic vascular resistance (SVR)} = \frac{(\text{Mean Ao} - \text{Mean RA})}{\text{Qs}}$$

$$\text{Pulmonary vascular resistance (PVR)} = \frac{(\text{Mean PA} - \text{Mean LA})}{\text{Qp}}$$

Qs: systemic blood flow; Qp: pulmonary blood flow.

Shunt detection and measurements

Shunt detection

1. Indocyanine green method
   - Indocyanine green (1 cm^3) is injected as a bolus into the right side of the circulation (pulmonary artery).
   - Concentration is measured from peripheral artery.
   - Appearance and washout of dye produces initial first-pass curve followed by recirculation in normal adults.
   - Nowadays, this method is not used in modern cardiac catheterization laboratories.
   - However, there is resurgence using this method to accurately detect right-to-left shunt in patients with patent foramen ovale.
2. Oximetric method
   - Obtain O_2 saturations in sequential chambers, identifying both step-up and drop-off in O_2 sat. It is important that the samples used for this calculation are acquired with the patient breathing air or an oxygen-enriched mixture not exceeding 30%. If higher concentrations of oxygen (50% or greater) are to be used (e.g., to test for pulmonary vascular reactivity), then the calculation of pulmonary blood flow (and Qp:Qs ratio) should involve measurement of pO_2 on at least the pulmonary vein sample (preferably also the pulmonary artery sample). This allows inclusion of dissolved oxygen in the calculation (a more complex calculation, which necessitates calculation of the oxygen content of the samples). The oximetric method is not very sensitive for small shunts (<1.3:1). As the RA receives blood from several sources, SVC, IVC, and coronary sinus:
   - SVC: Saturation most closely approximates true systemic venous saturation
   - IVC: Highly saturated because kidneys receive 25% of CO and extract minimal oxygen
   - Coronary sinus: Markedly desaturated because heart maximizes O_2 extraction

$$\text{MV sat} = \frac{3 \times \text{sat SVC} + \text{sat IVC}}{4}$$

   - Oxygen saturation samples should be taken from
   - IVC (at L4–5 and diaphragm levels)
   - SVC (at innominate vein level and RA level)
   - RA (high, mid, and low levels)
   - RV (mid, apex, and outflow tracts)
   - PA (MPA and left and right PAs)
   - LV (left ventricle)
   - AO (ascending, descending below ductus)

Shunt measurement

Pulmonary-to-systemic blood flow Qp:Qs

Estimation of oxygen content = $1.36 \times \text{Hgb} \times O_2$ saturation

$$\text{Systemic blood flow (SBF)} = \frac{O_2 \text{ consumption}}{\text{Ao } O_2 - \text{MV}O_2}$$

$$\text{Pulmonary blood flow (PBF)} = \frac{O_2 \text{ consumption}}{\text{Pv } O_2 - \text{Pa } O_2}$$

Oxygen consumption VO_2 measured either by

Resting oxygen uptake = Basal metabolic rate by Douglas bag method or

Formula $VO_2 = 2 \times 125$ mL O_2/min = 250 mL O_2/min

In children, the largest source of error is in the assessment of oxygen consumption.[19–23] Traditionally, this has been measured using a hood and gas pump that extracts all exhaled air and passes it through a mixing system before measuring the oxygen content. The difference between inhaled oxygen content and exhaled oxygen content, coupled with the flow maintained by the pump, allows estimation of oxygen consumption. This method involves several assumptions. First, it assumes that the pump caters for all exhaled air and that none is "lost." Second, it assumes effective mixing before the oxygen measurement. Third, it assumes (at least with some equipment) that the volume of exhaled air is the same as that of inhaled air, which is only true if carbon dioxide production is identical with oxygen uptake (in some labs, a respiratory quotient—respiratory exchange ratio [RER]—of 0.8 is assumed). It also requires very accurate measurements of flow through the pump. Additionally, it requires very precise measurements of the oxygen level in exhaled air, which has in the past required the use of large and cumbersome equipment (a mass spectrometer). Patients being catheterized under anesthesia may require a closed-circuit method, which is also laborious and time-consuming to perform. In either case, it is essential that the medical and technical personnel involved be very familiar with the equipment and the methodology, and that they perform such measurements on a regular basis.

Oxygen consumption is not measured routinely; when measurements are required, it is often difficult or impossible to obtain satisfactory measurements—for example, because the staff who are familiar with the apparatus are unavailable, and the personnel involved with the procedure are unfamiliar with the equipment and lack confidence/competence in obtaining the necessary data. Normal values for oxygen consumption obtained from children of varying age and sex and at different heart rates have allowed the use of "assumed oxygen consumption."[22]

Gradients and valve stenosis

Aortic valve stenosis

Stenosis of the aortic valve causes obstruction to blood flow from the left ventricle to the aorta. As a result, there is a systolic pressure gradient across the valve with a higher pressure in the left ventricle than the aorta.

Echocardiography has largely reduced the need for cardiac catheterization in the evaluation and monitoring of patients with aortic stenosis (Table 4.12). The 2006 American College of Cardiology/American Heart Association (ACC/AHA) guidelines on the management of valvular heart disease included recommendations for the diagnostic evaluation of adolescents and young adults with congenital aortic stenosis and the use of echocardiography for the evaluation and monitoring of older patients with aortic stenosis.[24,25]

Table 4.12 Severity of aortic stenosis in adults

	Aortic jet velocity (m/s)	Mean gradient (mmHg)	Valve area (cm^2)
Normal	≤2.0	<5	3.0–4.0
Mild	<3.0	<25	>1.5
Moderate	3.0–4.0	25–40	1.0–1.5
Severe	>4.0	>40	<1.0[a]

Source: Adapted from Bonow RO. *Circulation* 2008;118:e523.
Note: Critical aortic stenosis has been hemodynamically defined as a valve area <0.75 cm^2 and/or an aortic jet velocity >5.0 m/s. However, the decision about valve replacement is not solely based on hemodynamics, as some patients who meet these criteria are asymptomatic, while others with less severe measurements are symptomatic. In patients with severe aortic stenosis who also have a low cardiac output state, the aortic jet velocity and mean gradient may be lower than that indicated above (low-gradient aortic stenosis)
[a] Severe aortic stenosis is also considered to be present if the valve area indexed by body surface area is <0.6 cm^2/m^2.

The guidelines recommended cardiac catheterization for hemodynamic assessment in older adults in only one setting: in symptomatic patients in whom noninvasive tests are inconclusive or provide discrepant results from clinical findings regarding the severity of aortic stenosis. There may be a larger role in adolescents and young adults with congenital aortic stenosis. Also, with the emergence of percutaneous transcatheter aortic valve replacement, patients undergo full hemodynamic assessment of the gradient prior to and after valve implantation.

A precise assessment of the aortic valve gradient can be obtained by the simultaneous measurement of the aortic pressure (as assessed with a pigtail catheter above the aortic valve or a long 5 F or 6 F long sheath), and the left ventricular pressure (measured using the transseptal technique or longer 4 F pigtail catheter inserted into the long sheath). However, if the aortic pressure is obtained from the peripheral artery, realignment of the pressure tracing is necessary, since the peripheral arterial pressure is delayed temporarily compared with the central aortic pressure.

Determining the transvalvular gradient is done by simultaneous measurement of pressures obtained from a catheter in the aorta and one in the left ventricle positioned via a transseptal approach. However, it is more common for the left ventricular catheter to be placed retrogradely via the aorta. With this technique, after measurements are made in the left ventricle, the catheter is quickly pulled back to a level just above the aortic valve and the aortic pressure is measured. However, the transvalvular gradient may increase by the presence of a catheter across the stenotic aortic valve, thereby reducing the effective antegrade orifice area.[3] This effect is proportional to the severity of the underlying aortic stenosis.

The time-honored method of evaluating the severity of aortic stenosis (Figure 4.12) is a calculation of the

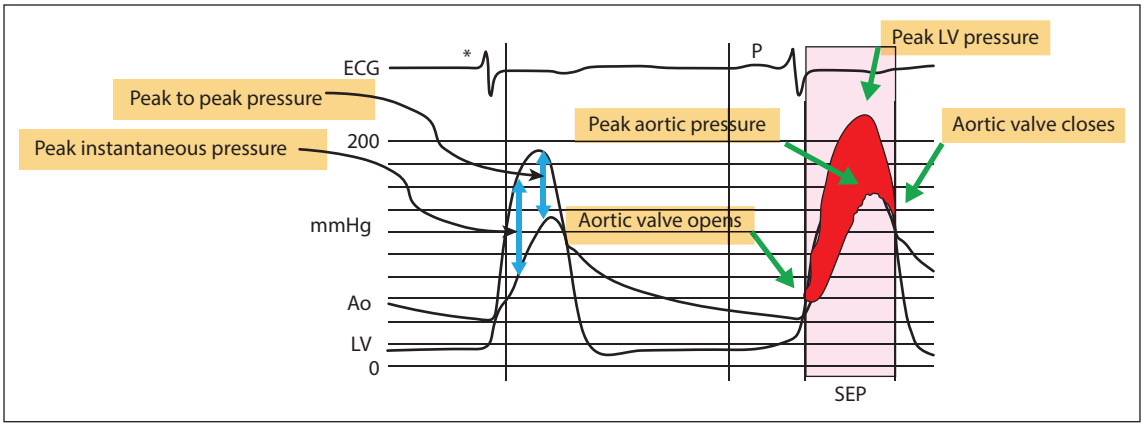

Figure 4.12 (**See color insert.**) Simultaneously recorded pressures from the left ventricle (LV) and aorta (Ao) in a patient with aortic stenosis. There is a systolic pressure gradient (red shaded area) in which the LV systolic pressure is greater than that in the aorta. The pressure gradient and systolic ejection period (SEP, in s/beat) are used in the Gorlin formula to calculate the aortic valve area (aortic valve area = cardiac output ÷ [44.3 x SEP x HR x square root mean gradient]). The peak instantaneous gradient is the maximal pressure difference between Aorta and LV when the pressures are measured at the same moment. The peak-to-peak gradient is the difference between the maximal pressure in the aorta and the maximal pressure in LV. (Redrawn from Kern MJ (ed). *Cardiac Catheterization Handbook*, 2nd ed. St. Louis: Mosby-Year Book; 1995. With permission.)

aortic valve area (AVA in cm^2) based on the formulations described by Cannon and Gorlin[26,27] and Hakki et al.:[28]

AVA by Gorlin

$$= \frac{\dfrac{\text{CO in cc/min}}{\text{SEP} \times \text{HR}}}{\text{K} \times 44.3 \times \sqrt{\text{Mean aortic valve gradient in mmHg}}}$$

where CO = cardiac output (mL per beat), SEP = systolic ejection period (s per beat), and it is measured from the time the semilunar valves open, and ventricular contraction propels blood into the great arteries, to the point of when the semilunar valves close. SEP is calculated by measuring at 100 mm/s paper speed. K is the combined constant and is 1.0 for aortic, pulmonic, and tricuspid valves, and 0.85 for the mitral valve.

For example: CO = 4.3 L/min, HR = 95 beats/min, SEP = 0.22 s/beat, and mean gradient = 40 mmHg

$$\text{AVA} = \frac{(4.3 \times 1000/0.22 \times 95)}{44.3 \times \sqrt{40}} = \frac{205.7}{279.1} = 0.7\ \text{cm}^2$$

A more simplified formula is

AVA by Hakki[29] formula

$$= \frac{\text{CO}}{44.3 \times \sqrt{\text{Peak-to-peak gradient}}} = \frac{\text{CO in mL/min}}{44.3 \times \sqrt{P1 - P2}}$$

*P*1 = peak LV pressure, *P*2 = peak Ao pressure.

A reduced aortic pressure and the existence of a pressure gradient between the left ventricle and the aorta are the principal findings relating to the aortic pressure among patients with aortic valvular stenosis. In addition, the rise in aortic pressure is slow and delayed compared with the pressure rise in the left ventricle.

In addition to an increased systolic pressure, abnormalities of diastolic pressure may be observed because of left ventricular hypertrophy with reduced compliance. Although the mean left ventricular diastolic pressure may be normal or elevated, the left ventricular end-diastolic pressure is most commonly elevated, a result of atrial contraction and filling of the noncompliant left ventricle. Thus, there is usually a prominent "a" wave with increased amplitude.

The left atrial pressure tracing shows large "a" waves because of the combination of a hypertrophied left atrium and a stiff or noncompliant left ventricle; this reflects the increased pressure generated during atrial contraction and filling of the left ventricle.

Low-gradient valvular aortic stenosis

An important group of patients with aortic stenosis consists of symptomatic patients who have low-gradient aortic stenosis, defined as a small transvalvular gradient (<30 mmHg), and a low cardiac output, with a calculated AVA of ≤0.7 cm^2.[29] In these patients, there is often doubt about whether the aortic valve is sufficiently stenotic to account for the symptoms or the patient has only mild aortic valvular disease and the symptoms are resulting from a significant reduction in left ventricular function due to a myopathic problem.

The concern about low-gradient aortic stenosis is justified, since the Gorlin formula is flow dependent and tends to underestimate the valve area when the cardiac output is low, that is, <3 L/min.[26,30,31] Since cardiac output measured

at the time of cardiac catheterization greatly influences the clinical evaluation and subsequent management decisions, a pharmacologic stimulation of cardiac output (such as Dobutamine)[32] is often required for further evaluation to facilitate the decision regarding surgery in these patients. Maneuvers that increase cardiac output will almost always increase the calculated valve area, except in truly severe aortic stenosis. Aortic valve resistance calculations are rarely used for clinical decision making.

Common maneuvers that have been employed in the cardiac catheterization laboratory to induce left ventricular outflow tract (LVOT) gradients include:

- Valsalva maneuver—Valsalva lowers preload due to reductions in venous return.
- Administration of nitroglycerin that lowers preload through venodilation.
- Postextrasystolic potentiation—Postextrasystolic potentiation produces an increase in left ventricular inotropy and contractility, which may result in an increase in systolic anterior motion (SAM) and outflow obstruction, and a decrease in aortic pulse pressure (Brockenbrough effect).
- Isoproterenol infusion—Isoproterenol infused at an initial rate of 1 μg/min and then increased by 1 μg every minute until a heart rate of 120–150 beats/min is reached or the LV outflow pressure gradient reaches 55 mmHg. Isoproterenol is no longer used in the catheter lab.

Acute aortic valve regurgitation

Acute AR does not allow sufficient time for myocardial adaptation, and LV moves quickly up its diastolic pressure–volume curve, causing a marked elevation of LVEDP and early closure of the mitral valve. The left ventricular pressure tracing reveals a steep rise in diastolic pressure and a markedly elevated left ventricular end-diastolic pressure (which is equivalent to the aortic end-diastolic pressure). There is minimal increase in LVED volume or fiber length, and the total stroke volume cannot increase sufficiently to compensate for the regurgitant volume; thus, forward SV and CO fall. The high LVEDP also serves to minimize the runoff into LV; therefore, the diastolic pressure in the aorta may remain near normal and the arterial pulse pressure increases very little, if at all.[3]

Chronic aortic valve regurgitation

In this case, the LV has time to adapt to the volume overload by using the Frank–Starling mechanism (increased fiber stretch). The hemodynamic and afterload conditions in chronic AR resemble those of chronic MR with two important differences: (1) the total SV is ejected into a high-impedance circuit (the aorta and systemic arteries), and because the total forward SV is augmented, the LV and aortic systolic pressures are elevated (>160 mmHg); and (2) because the AV is incompetent, the diastolic pressure in the aorta falls to subnormal levels during diastole, thereby reducing the diastolic perfusion pressure across the coronary arterial bed. The pulse pressure, which is defined as the systolic minus the diastolic pressure, is therefore widened. Since eccentric myocardial hypertrophy is associated with a sizable increase in total myocardial oxygen demand, patients with AR are particularly prone to develop angina in the absence of coronary artery disease (CAD).

In aortic regurgitation, the left ventricular stroke volume (A) (measured angiographically) is greater than the forward stroke volume (F) (determined by the Fick cardiac output); the difference is the regurgitant fraction (RF) that leaks back into the left ventricle during each cardiac cycle.

$$\text{RF} = \frac{[\text{Stroke volume (A)} - \text{Stroke volume (F)}]}{\text{Stroke volume (A)}}$$

The ACC/AHA guidelines[24,25] for the management of patients with valvular heart disease recommended cardiac catheterization in patients with aortic regurgitation in only one setting: when noninvasive tests are inconclusive or provide discrepant results from clinical findings. Cardiac catheterization should be performed with aortic root angiography and measurement of left ventricular pressure to assess the severity of the regurgitation, aortic root size, and left ventricular function.

Mitral valve stenosis

Regardless of the cause, there is impairment of blood flow from the left atrium into the left ventricle, resulting in a pressure gradient between the two chambers during diastole.

The ACC/AHA guidelines on the management[24,25] of valvular heart disease included recommendations for the use of cardiac catheterization for hemodynamic evaluation in patients with mitral stenosis (Table 4.13).

The severity of mitral stenosis as reflected by the mean mitral valve gradient (MVG) is measured during diastole by the simultaneous comparison of the left ventricular pressure (obtained with a left ventricular catheter positioned retrogradely from the aorta), and the left atrial pressure directly measured using a transseptal catheter or indirectly with a pulmonary artery catheter measuring the capillary wedge pressure. In most cases, a gradient is present, although it decreases during diastole because of slow but continuous left atrial emptying. With atrial systole, however, the gradient increases and is markedly higher than the left ventricular end-diastolic pressure. The volume of blood in the left atrium and the mean left atrial pressure are both increased during this period. After mitral valve opening, the pressure only gradually decreases and the "y" descent is gradual. The "a" wave, which is due to left atrial contraction, is markedly increased because of the stenosis.[3,7]

Table 4.13 ACC/AHA guideline summary: cardiac catheterization in mitral stenosis

Class I—There is evidence and/or general agreement that cardiac catheterization for hemodynamic evaluation is useful in patients with MS in the following settings:

- To assess the severity of MS if noninvasive tests are not conclusive or there is a discrepancy between the results of noninvasive tests and clinical findings related to the severity of MS.
- When there is a discrepancy between MVA and the Doppler-derived mean gradient, catheterization should include left ventriculography to evaluate the severity of mitral regurgitation.

Class IIa—The weight of evidence or opinion is in favor of usefulness of cardiac catheterization for hemodynamic evaluation in patients with MS in the following settings:

- To assess the exercise-induced hemodynamic response of the pulmonary artery and left atrial pressures when there is a discrepancy between clinical symptoms and hemodynamics at rest.
- To assess the cause of severe pulmonary arterial hypertension if it is out of proportion to the severity of MS determined by noninvasive testing.

Class III—There is evidence and/or general agreement that cardiac catheterization for hemodynamic evaluation in patients with MS is not useful in the following settings:

- To assess mitral valve hemodynamics when two-dimensional and Doppler echocardiographic findings are consistent with clinical findings.

Source: Data from Bonow RO. *J Am Coll Cardiol* 2006; 48:e1.

Since the diastolic filling period is important in the assessment of MVGs (Figure 4.13), the heart rate's effect upon the MVG is important. The gradient is higher with a faster heart rate since less time is available for left atrial emptying with a reduced diastolic period. By comparison, the gradient is lower with a slower heart rate.

A simplified method for estimating the mean MVG has been developed in which mean left ventricular diastolic pressure is estimated as LVEDP/2,[33] thus

$$\text{MVG} = \text{Mean LAp} - \frac{\text{LVEDP}}{2}$$

The calculation of mitral valve area (MVA in cm^2) based on the formulations described by Gorlin and Gorlin is [27]

$$\text{Mitral VA by Gorlin} = \frac{\dfrac{\text{CO in cc/min}}{\text{DFP} \times \text{HR}}}{\text{K} \times 44.3 \times \sqrt{\text{Mean mitral valve gradient in mmHg}}}$$

where CO = cardiac output (mL per min), DFP = diastolic filling period (s per beat), and K is the constant factor for the mitral valve 0.85 (for aortic, pulmonary, or tricuspid valves, K = 1). The Gorlin formula is best applied to patients in sinus rhythm without mitral regurgitation, normal left ventricular function, and no other concomitant valve lesions.

Acute mitral regurgitation

With acute mitral regurgitation, the left ventricle and (more importantly) the left atrium have not had time to adapt to the regurgitant volume overload, resulting in low compliance chambers. As a result, with the onset of systole and the large volume of regurgitant blood flow, the left atrial pressure rises abruptly, causing a very tall "v" wave. Because of this "v" wave, the pressure gradient between the left atrium and left ventricle declines by the end of the systole; the amplitude of the "v" wave and that of the left ventricular systole are nearly equivalent. The diastolic pressure of the left ventricle is increased because of an increase in the end-diastolic volume within an undilated and noncompliant chamber.[7]

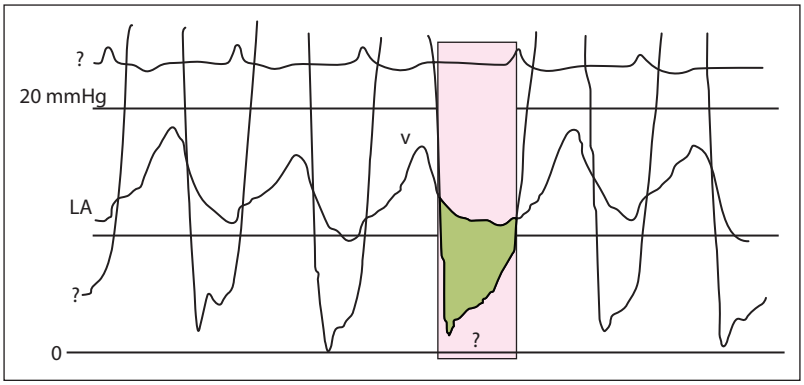

Figure 4.13 (**See color insert**.) LA and LV pressure tracings in a patient with MS. Shaded area represents the mitral valve gradient. DFP = diastolic filling period. The planimetered area (green shaded) is used to calculate mean valve gradient (MVG).

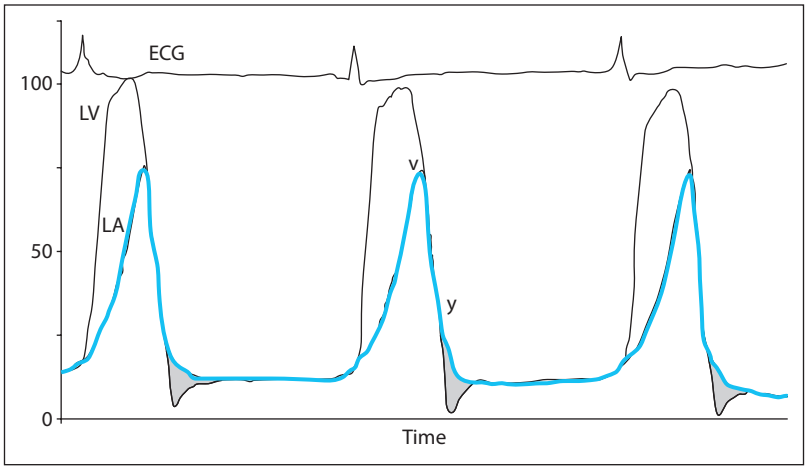

Figure 4.14 (**See color insert**.) LV and LA pressure tracings in isolated, severe MR and atrial fibrillation. The "a" and "c" waves in the LA tracing (blue pressure tracing) are not evident and the "v" wave is accentuated.

Chronic mitral regurgitation

Normal MV closure, which prevents the systolic backflow of blood into the LA, depends on the complex interaction of each of the components of the valve apparatus (LA wall, the annulus, the MV leaflets, the chordae, the papillary muscles, and the LV wall). Abnormalities in the anatomy and function of any of these components lead to valvular regurgitation. The regurgitant flow produces a large left atrial pressure wave immediately with the onset of ventricular systole. During the initial part of diastole, the left atrium rapidly decompresses with a large antegrade flow to the left ventricle.

Pressure measurements (Figure 4.14) either in the PCW or LA positions usually reveal an elevated "v" wave (>20 mmHg peak value), followed by a relatively rapid "y" descent as the MV opens and an excessive inflow of blood traverses the MV.[34] There is commonly a small pressure gradient across the MV during early diastole, reflecting functional MS in the presence of increased flow. If the MR is relatively acute and severe, a very large "v" wave is generated owing to the fact that the LA remains relatively normal sized and noncompliant and LV shortening remains normal to supranormal. Conversely, in long-standing severe MR, the "v" wave may be extremely small owing to massive dilatation of the LA and a significant increase in its capacitance. When myocardial contractility becomes severely diminished, depression of the total stroke volume may also contribute to the lack of generation of a significantly elevated "v" wave.

The left ventricle is volume overloaded due to the excess blood volume (generated during the prior systolic regurgitant beat) flowing during diastole from the left atrium. However, since the compliancy of the left ventricle increases, the left ventricular systolic and diastolic pressures are normal or only slightly increased. Although the left ventricular stroke volume is increased, the forward stroke volume is normal because a part of the stroke volume regurgitates back into the left atrium. The left ventricular pressure waveforms in systole and diastole are therefore normal.

The effective CO depends on the severity of the regurgitation, the acuteness versus chronicity of the process, the adaptation of the LV to the volume overload, and the maintenance of normal myocardial contractility.

In combined MS/MR, significant dilatation of the LA is seen owing to the combined pressure and volume overload of the chamber. In this setting, the pressure recordings from the left heart reveal an early and mid-diastolic pressure gradient across the MV, but if the DFP is sufficiently long, the LA and LV pressures equilibrate during the period of slow ventricular filling. The "v" wave is often dominant, reflecting the augmented systolic expansion and dilatation of the LA. The amount of regurgitation is calculated as the difference between total LV stroke volume (measured on contrast LV angiogram) and the stroke volume calculated from a Fick or indicator-dilution CO and the resting HR.

The left ventricular stroke volume (A) (measured angiographically) is greater than the forward stroke volume (F) (determined by the Fick cardiac output); the difference is the RF that leaks back into the left atrium during each cardiac cycle:

$$\text{RF} = \frac{[\text{Stroke volume (A)} - \text{Stroke volume (F)}]}{\text{Stroke volume (A)}}$$

Pulmonary valve stenosis

Diagnostic cardiac catheterization is rarely required in patients with pulmonic stenosis (PS) due to the extensive characterization of valvular structure, severity of stenosis, and right ventricular size and function derived from echocardiography. Invasive hemodynamic measurements and ventriculography may be useful when the severity of

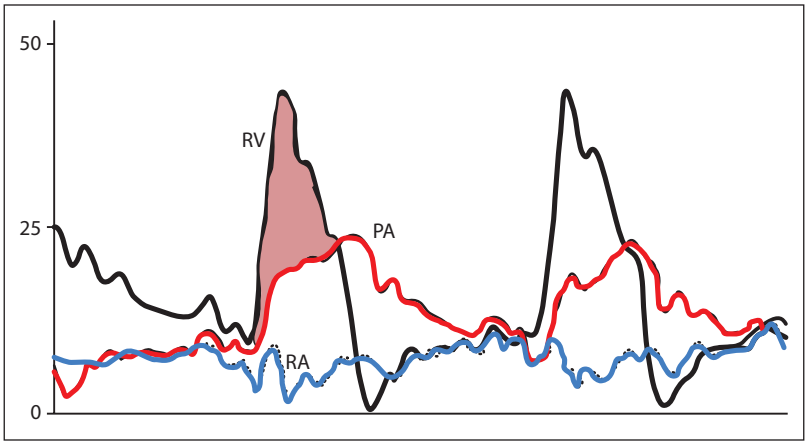

Figure 4.15 (**See color insert**.) Simultaneous pressure recordings from RV, PA (red tracing), and RA (blue tracing) in a patient with pulmonic valve stenosis. The shaded area is the pulmonic valve stenosis gradient.

stenosis is unclear or a significant secondary infundibular stenosis is suspected in addition to the valvular stenosis (Figure 4.15).

The ACC/AHA guidelines recommended cardiac catheterization for evaluation of the severity of PS in only one condition (Table 4.14): if the peak jet velocity on the Doppler echocardiography is >3 m/s (estimated peak systolic gradient >36 mmHg).[24,25] Balloon valvotomy is usually performed during the same procedure, if clinically indicated (Table 4.13).

PS is congenital in 95% of cases; rare causes include carcinoid syndrome and rheumatic valve disease. Although PS can be a feature of other types of congenital heart disease (e.g., tetralogy of Fallot), 80% of cases are isolated as PS. The abnormal valve is classified as unicommissural (with prominent systolic doming of leaflets and eccentric orifice), bicuspid (with fused commissures), or dysplastic (severely thickened and deformed leaflets). Rarely, PS can be associated with the aneurysm of the PA.

Cardiac catheterization in a moderate-to-severe obstruction of the PV places a pressure overload on the RV that, in turn, leads to significant right ventricular hypertrophy (RVH). The pressure tracings from RV and PA (Figure 4.15) can be used to calculate the mean gradient similar to the method used for AS. Pulmonic valve area can also be calculated by the Gorlin[27] formula as follows:

$$\text{Pulmonary valve area by Gorlin} = \frac{\dfrac{\text{CO in cc/min}}{\text{SEP} \times \text{HR}}}{\text{K} \times 44.3 \times \sqrt{\text{Mean RV to PA gradient in mmHg}}}$$

Table 4.14 ACC/AHA guideline summary: balloon valvotomy for pulmonic stenosis in adolescents and young adults

Class I—There is evidence and/or general agreement that balloon valvotomy should be performed in adolescents and young adults with PS in the following settings:

- Symptoms of angina, syncope, or dyspnea on exertion with an RV-to-pulmonary artery peak-to-peak gradient >30 mmHg at cardiac catheterization.
- Asymptomatic patients with an RV-to-pulmonary artery peak-to-peak gradient >40 mmHg at cardiac catheterization.

Class IIb—The weight of evidence or opinion is less well established for the usefulness of balloon valvotomy in adolescents and young adults with PS in the following setting:

- Asymptomatic patients with an RV-to-pulmonary artery peak-to-peak gradient of 30–39 mmHg at cardiac catheterization.

Source: Data from Bonow RO. *J Am Coll Cardiol* 2006; 48:e1.

Pulmonary valve regurgitation

The basic cardiac defect in pulmonary regurgitation (PR) is retrograde leakage of blood from the main PA into the RV during diastole. Unless the pulmonary artery diastolic pressure (PADP) is severely elevated, the driving force between the PA and RV is not large, and the RF of the stroke volume remains relatively small. Moreover, the RV can tolerate a relatively large volume overload, and thus, the patient with PR commonly exhibits no impairment of CO either at rest or during exercise. Also, the RVEDP and RAP are not elevated unless there is an associated pressure overload on RV, or PR is long-standing.

Tricuspid valve stenosis

Tricuspid stenosis (TS) is a rare clinical condition, with rheumatic disease accounting for more than 90% of cases. In patients with rheumatic MV disease, only 3–5% have concurrent TS.

Tricuspid valve regurgitation

Secondary tricuspid regurgitation (TR) is much more common than primary TR. Functional TR resulting from pulmonary HTN is seen in patients with significant left-sided heart disease, those with primary pulmonary HTN, and those with pulmonary disease leading to cor pulmonale. Functional TR also occurs in patients with RV dilatation as seen with RV infarction or an ASD. TR occurs in as many as 30–50% of patients with rheumatic mitral valve disease.

The normal tricuspid valve (TV) orifice area is 8–12 cm^2; significant symptoms and signs of TS may be seen when the valve area is compromised to ≤2 cm^2. As with MS, the gradient across the valve is dependent on the diastolic filling period and cardiac output. Thus, exercise is associated with a significant increase in the gradient across the valve. The RA pressure pulse in TS is characterized by an exaggerated "a" wave (if in sinus rhythm). As with MS, there is slowing of the "y" descent and the absence of diastasis between the RA and RV pressure pulses (Figure 4.15). HR influences the pressure gradient as it does in MS. These effects are subtle though, since in most cases the valve gradient is not more than 5–8 mmHg.

Cardiac Tamponade

The pericardial space normally contains 5–10 mL of fluid that may be detected by echocardiography. This fluid serves as a lubricating material to allow normal rotation and translation of the heart during the cardiac cycle. A wide variety of disorders can result in pericardial effusion. When the intrapericardial (IP) pressures exceed the pressures in the cardiac chambers, impaired cardiac filling occurs; this is known as tamponade physiology. As the pericardial pressures increase, filling of each cardiac chamber is affected sequentially, starting with lower-pressure chambers (atria). The compressive effect of the fluid is seen best in the phase of cardiac cycle when pressure is lowest in that chamber (diastole for the ventricle and systole for atrium). In severe tamponade, diastolic pressures in all cardiac chambers are equal and elevated.

Diastolic equilibration or pressures are the hallmark of cardiac tamponade. Hence, accurate measurement of pressures in right- and left-sided chambers is mandatory when tamponade is suspected, although this is rarely necessary these days with the advent of echocardiography. The pressure tracings should be recorded simultaneously, along with the respiratory cycle. Ideally, both right and left heart catheterization should be done to show the equalization of diastolic pressures in these chambers. However, if PCWP tracings are of good quality, and if clinical, noninvasive, and hemodynamic data are consistent with tamponade, left heart catheterization may be omitted. When the IP pressure has increased to equal RA pressure, cardiac tamponade begins.

With the rise in IP pressure, the venous pressure rises to maintain intracardiac volume. In early cardiac tamponade without preexisting heart disease, the IP and RA pressures are equal but only slightly elevated. Furthermore, PCWP (or LA pressure) remains higher than the RA pressure. When cardiac tamponade becomes more severe, the RA and IP pressures remain equal and rise progressively as the tamponade gets more severe. The point at which the RA, and PCWP (or LA pressure) become equal defines classic cardiac tamponade (this finding is not pathognomonic; other conditions can cause this equalization such as constrictive pericarditis). RA and PCWP should be recorded simultaneously rather than sequentially. The height to which the venous pressure is elevated depends on the severity of tamponade. In milder cases, these pressures range from 7 to 10 mmHg. In moderate cases, pressures are 10–15 mmHg and are often accompanied by reduction in cardiac output and arterial BP.

Severe tamponade is characterized by pressures in the range of 15–30 mmHg usually accompanied by profound reduction in CO and arterial BP, which at this stage will demonstrate pulsus paradoxus (Figure 4.11). Often, there is a narrow pulse pressure before the drop in peak systolic pressure. In establishing the diagnosis of cardiac tamponade, special attention should be paid to the waveform of RA and PCWP tracings. Inspiratory decrease in RA pressure should be observed. Cardiac tamponade exerts its abnormal pressure on heart chambers throughout the cardiac cycle. However, ventricular ejection is faster than venous return, causing cardiac volume to decrease. With this event, there is a slight decline in IP pressure. For this reason, venous return is confined to the period of ventricular systole that translates to prominence of "x" descent and absence of "y" descent of venous pressure. Thus, in typical tamponade, RA pressure is elevated and equal to PCWP and shows an inspiratory drop and absence of "y" descent. This is in contrast to constrictive pericarditis that demonstrates a sharp "x" and "y" descents.

References

1. Baim DS, Grossman W. *Cardiac Catheterization, Angiography, and Intervention*. 5th ed. Baltimore: Williams & Wilkins; 2005.
2. Kern MJ. Hemodynamic rounds series II: Pitfalls of right-heart hemodynamics. *Cathet Cardiovasc Diagn* 1998;43:90–4.
3. Kern MJ, Feldman T, Bitar S. Hemodynamic data. In: *The Cardiac Catheterization Handbook*. 5th ed. St. Louis: Mosby-Year Book; 2011. pp. 126–7.
4. Morgan BC, Abel FL, Mullins GL, Guntheroth WG. Flow patterns in cavae, pulmonary artery, pulmonary vein, and aorta in intact dogs. *Am J Physiol* 1966;210:903–9.
5. Brecher GA, Hubay CA. Pulmonary blood flow and venous return during spontaneous respiration. *Circ Res* 1955;3:210–14.
6. Tavel ME. Normal sounds and pulses: Relationships and intervals between the various events. In: *Clinical Phonocardiography and External Pulse Recording*. 2nd ed. Chicago: Year Book Medical Publishers; 1972. p. 35.

7. Kern MJ, Lim MJ, Goldstein JA. *Hemodynamic Rounds: Interpretation of Cardiac Pathophysiology from Pressure Waves Analysis*. 3rd ed. Philadelphia: Wiley-Blackwell; 2009. pp. 86–7.
8. Fleming PR. The mechanism of the pulsus bisferiens. *Brit Heart J* 1957;19:519–24.
9. Lewis T. The pulsus bisferiens. *Brit Med J* 1907;1:918–20.
10. Talley JD. Recognition, etiology, and clinical implications of pulsus bisferiens. *Heart Dis Stroke* 1994;3:309–11.
11. Lab MJ, Seed WA. Pulsus alternans. *Cardiovasc Res* 1993;27:1407–12.
12. Lablanche JM, Thieuleux FA, Bertrand ME. Pulsus alternans: Alternation of relaxation parameters. *Arch Mal Coeur Vaiss* 1984;77:1540–6.
13. Massumi RA, Mason DT, Vera Z, Zelis R, Otero J, Amsterdam EA. Reversed pulsus paradoxus. *N Engl J Med* 1973;289:1272–5.
14. Acierno LJ. Adolph Fick: Mathematician, physicist, physiologist. *Clin Cardiol* 2000;23:390–1.
15. Wood EH. Diagnostic applications of indicator-dilution technics in congenital heart disease. *Circ Res* 1962;10:531–68.
16. Freed MD, Keane JF. Cardiac output measured by thermodilution in infants and children. *J Pediatr* 1978;92:39–42.
17. Sibille L, Prasquier R, Vallois JM, Gaudebout C, Pocidalo JJ. Cardiac output measurement with a simplified thermodilution technique. Comparison with the Fick method. *Biomedicine* 1975;23:64–7.
18. Miller HC, Brown DJ, Miller GA. Comparison of formulae used to estimate oxygen saturation of mixed venous blood from caval samples. *Brit Heart J* 1974;36:446–51.
19. Lindahl SG. Oxygen consumption and carbon dioxide elimination in infants and children during anaesthesia and surgery. *Brit J Anaesth* 1989;62:70–6.
20. Lundell BP, Casas ML, Wallgren CG. Oxygen consumption in infants and children during heart catheterization. *Pediatr Cardiol* 1996;17:207–13.
21. Kappagoda CT, Greenwood P, Macartney FJ, Linden RJ. Oxygen consumption in children with congenital diseases of the heart. *Clin Sci* 1973;45:107–14.
22. LaFarge CG, Miettinen OS. The estimation of oxygen consumption. *Cardiovasc Res* 1970;4:23–30.
23. Wilkinson JL. Haemodynamic calculations in the catheter laboratory. *Heart* 2001;85:113–20.
24. Bonow RO, Carabello BA, Chatterjee K et al. Focused update incorporated into the ACC/AHA 2006 guidelines for the management of patients with valvular heart disease: A report of the American College of Cardiology/American Heart Association Task Force on Practice Guidelines (Writing Committee to Revise the 1998 Guidelines for the Management of Patients with Valvular Heart Disease): Endorsed by the Society of Cardiovascular Anesthesiologists, Society for Cardiovascular Angiography and Interventions, and Society of Thoracic Surgeons. *Circulation* 2008;118:e523–661.
25. Patel MR, Bailey SR, Bonow RO et al. ACCF/SCAI/AATS/AHA/ASE/ASNC/HFSA/HRS/SCCM/SCCT/SCMR/STS 2012 appropriate use criteria for diagnostic catheterization: A report of the American College of Cardiology Foundation Appropriate Use Criteria Task Force, Society for Cardiovascular Angiography and Interventions, American Association for Thoracic Surgery, American Heart Association, American Society of Echocardiography, American Society of Nuclear Cardiology, Heart Failure Society of America, Heart Rhythm Society, Society of Critical Care Medicine, Society of Cardiovascular Computed Tomography, Society for Cardiovascular Magnetic Resonance, Society of Thoracic Surgeons. *J Thorac Cardiovasc Surg* 2012;144:39–71.
26. Cannon SR, Richards KL, Crawford M. Hydraulic estimation of stenotic orifice area: A correction of the Gorlin formula. *Circulation* 1985; 71:1170–8.
27. Gorlin R, Gorlin SG. Hydraulic formula for calculation of the area of the stenotic mitral valve, other cardiac valves, and central circulatory shunts. I. *Am Heart J* 1951;41:1–29.
28. Hakki AH, Iskandrian AS, Bemis CE et al. A simplified valve formula for the calculation of stenotic cardiac valve areas. *Circulation* 1981;63:1050–5.
29. Carabello BA. Advances in the hemodynamic assessment of stenotic cardiac valves. *J Am Coll Cardiol* 1987;10:912–9.
30. Cannon JD Jr., Zile MR, Crawford FA Jr., Carabello BA. Aortic valve resistance as an adjunct to the Gorlin formula in assessing the severity of aortic stenosis in symptomatic patients. *J Am Coll Cardiol* 1992;20:1517–23.
31. Cannon SR, Richards KL, Crawford MH et al. Inadequacy of the Gorlin formula for predicting prosthetic valve area. *Am J Cardiol* 1988;62:113–6.
32. deFilippi CR, Willett DL, Brickner ME et al. Usefulness of dobutamine echocardiography in distinguishing severe from nonsevere valvular aortic stenosis in patients with depressed left ventricular function and low transvalvular gradients. *Am J Cardiol* 1995;75:191–4.
33. Cui W, Dai R, Zhang G. A new simplified method for calculating mean mitral pressure gradient. *Catheter Cardiovasc Interv* 2007;70:754–7.
34. Freihage JH, Joyal D, Arab D et al. Invasive assessment of mitral regurgitation: Comparison of hemodynamic parameters. *Catheter Cardiovasc Interv* 2007;69:303–12.

5

Transesophageal 2D and 3D echocardiographic guidance

Joseph John Vettukattil

The technique of transcatheter intervention has evolved into highly complex and time-consuming mini-robotic device implantations that require careful preoperative assessment and intraprocedural guidance. Imaging techniques, too, have advanced to facilitate these procedures and assist the interventionist. Often, the echocardiologist and interventionist have developed an interdependency to achieve the best procedural outcome, reducing time, complication rate, and radiation dose. With the advance of real-time three-dimensional transesophageal imaging (3DTEE), 2DTEE has become almost redundant due to the limited spatial dimensions it can provide. Currently, TEE is used for most transcatheter interventions enhanced with 3D imaging. This includes accurate measurements of the aortic valve hinge points for valvoplasty and transcatheter valve implantation;[1] closure of aortic, mitral, and tricuspid paravalvar leaks (PVLs); transseptal puncture; left atrial appendage (LAA) closure; mitral valve annuloplasty; application of mitra-clip and similar devices; Fontan and Mustard baffle fenestrations; atrial septal defect (ASD) and patent foramen ovale (PFO) closure; and for congenital and acquired ventricular septal defect (VSD) closures. An extensive discussion of all these aspects is beyond the scope of this chapter, but some important aspects will be highlighted.

Preparation

The patient typically fasts for 6 hours before the introduction of the TEE probe. Under deep sedation with local anesthetic aerosol spray or preferably under general anesthetic, the probe is gently introduced while the patient does the swallowing movements lying in a lateral decubitus position. A mouth guard is applied to protect the patient as well as the probe. Ideally, the output from the echo monitor should be displayed by the side of the angiography display system with the operator positioned at the same side as the interventionist, allowing easy observation of the procedure and direct interactions.

Before imaging begins, all related information, including previous imaging and hemodynamics, must be reviewed to plan the procedure. Depending on the nature of the intervention, 2D and 3D data sets are collated and analyzed. Appropriate measurements are made and quantification of the severity of the lesion, nature, location, morphology, and the best approach for intervention are identified and discussed with the interventionist.

With the advances in miniaturization and computing technology, 2DTEE is possible almost at any age. 3D probes are currently available only for children weighing 28 kg or above. However, in critical lesions where the 3D information is likely to significantly change the management plan, patients as small as 18 kg have had 3DTEE performed safely.

Image acquisition, analysis, and display

Depending on the diagnostic system available, it is important to have presets to optimize the quality of images and to achieve the best frame rates possible. Focusing on the anatomy of interest, gain, depth, and number of cardiac cycles to be synchronized must be determined before starting the image acquisition.

Live 3D catheter guidance

Live 3D zoom is the best setting for continuous monitoring of the device and catheter position during an intervention. The probe is positioned perpendicular to the area of interest whenever possible, so that the best echo signals captured attain optimum resolution for immediate

display. Both lateral and vertical sector widths are set to include the whole of the structure of interest to be captured within the 3D frame. Details of the settings for individual lesions will be dealt with in the discussion of specific interventions.

Imaging for structural interventions

Mitral paravalvar leak

PVL is most commonly encountered with mitral prostheses. However, it is also seen with any prosthetic valve implantation. While assessing PVL in mitral prostheses, the actual area of dehiscence can be detected as an area of echo drop-out outside the sewing ring with appropriate adjustment of the gain settings. This must be confirmed by the presence of regurgitant jet on color-flow imaging.[3] In order to facilitate communication between the echocardiologist/cardiographer and the interventionist, the location of the dehiscence is best described in a standardized way, although it may be described in relation to internal landmarks such as the LAA, aortic valve, or the crux of the heart. The anatomic location of mitral PVL is best displayed in a clockface view with the aorta at the 12 o'clock position and the LAA between 9 and 10 o'clock positions (Figure 5.1). Various factors such as the anatomic location, size, shape, extent, course, severity, dimensions, proximity to the valve struts, nature of the adjoining tissue, mechanism of the lesion, exit and entrance points (especially in the paraaortic lesions), stability of the valve, the possible impact of device placement and suitability for interventions, and the best device for the specific intervention should be clearly defined before the intervention is attempted. Often, the PVL in the lateral aspect of the mechanical valve can be better accessed through the transseptal approach, whereas the transapical approach or a high septal puncture is necessary to gain access to the medially placed defects (Figure 5.2). A retrograde approach through the aortic valve may be suitable for some lesions in the anterolateral position (8–11 o'clock) and transseptal puncture from the superior vena cava (SVC) is favored by some for the more medially located lesions.

The echocardiologist should guide the interventionist throughout the procedure by describing the position of the tip of the sheath and the delivery system in relation to the anatomy of interest and neighboring structures, while carefully evaluating for any potential complication. It is preferable for the echocardiologist to interrupt the procedure to obtain accurate assessment when in doubt rather than provide inaccurate guidance.

Mitral PVLs may be multiple and the adjoining tissue is often friable. The suture lines may be tense, which has caused the lesion in the first instance; hence, further tension through the placement of an oversized device may increase the defect size. The medial defects are best approached through transapical or a hybrid approach (Figure 5.3). However, a high transseptal approach may also be appropriate to access a medial defect (between the 1 and 5 o'clock position).

Tricuspid PVL is less common, as the tricuspid valve is easily accessible and visible for the surgeon during the valve replacement. Even when present, the leaks are well tolerated except when there are associated lesions causing pulmonary or right ventricular hypertension. When present, it is best approached via the superior caval route. It is also possible to achieve a stable catheter and guide wire position by placing the guide wire in the branch pulmonary arteries (PAs).

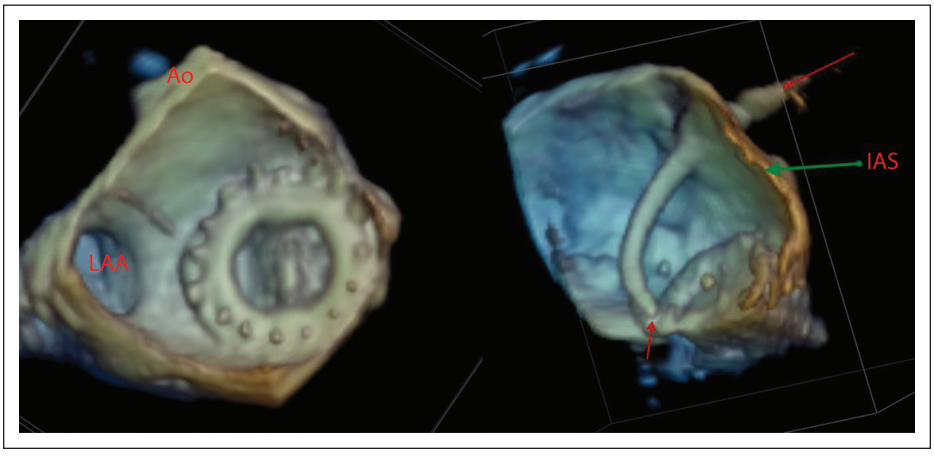

Figure 5.1 (**See color insert.**) The standard clockface display of a paravalvar leak with aorta at 12 o'clock position and LAA at 9 o'clock position (on the right). Here, the intervention is performed through the transseptal approach. The sheath comes out through the transseptal puncture being guided to the regurgitant orifice (arrow on the left).

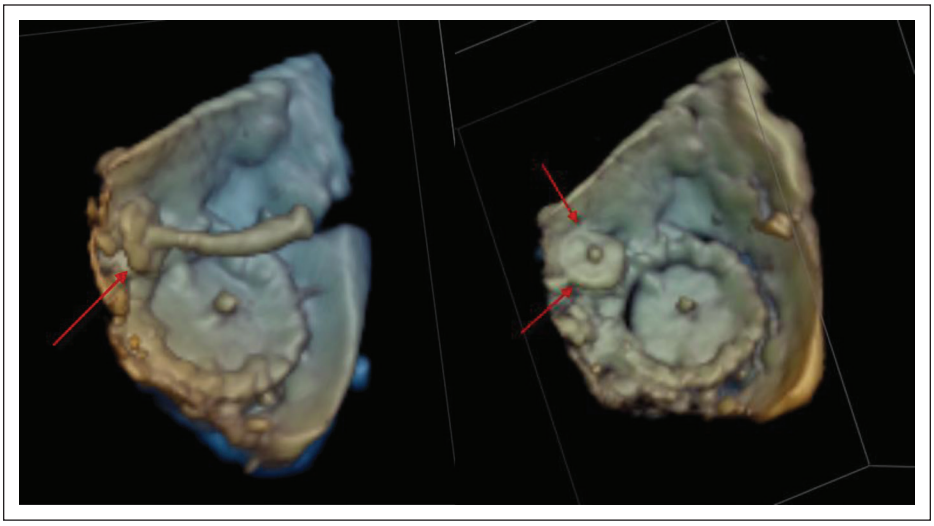

Figure 5.2 (**See color insert.**) The LA disk of the PVL device being positioned under 3D guidance (left arrow) and postdevice deployment on the right (red arrows).

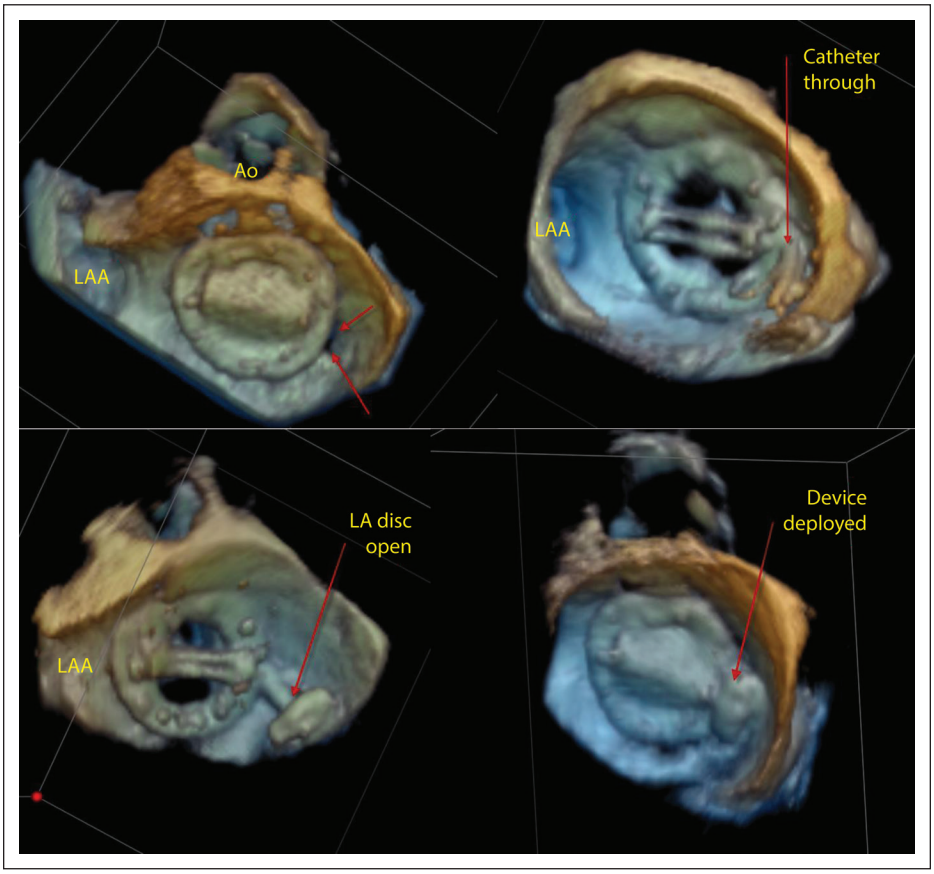

Figure 5.3 (**See color insert.**) Mitral PVL medial lesion at 3 o'clock position shown in these 3DTEE images. The approach here was through the transapical route. Catheter positioning and device manipulation is shown through serial images from left to right. Left upper image shows the defect. Upper right image shows the catheter passing through the defect. The lower two images illustrate the device placement and release in final position.

Aortic PVL

When aortic PVL is present, often 3D assessment can be best obtained preoperatively through trans thoracic echocardiography (TTE). The course and nature of the defect is easily demonstrable with TTE prior to TEE. Specific aspects to be considered when assessing the aortic PVL are the length and course of the tract, proximity to the coronaries, and relationship to the conduction system. It is also important to differentiate aortic PVLs from aorta to LV tunnels or fistulas.

Quantifying the severity of PVL is very similar to assessing mitral regurgitation. If 3DTEE is not available, multiplane 2D color-flow Doppler imaging is necessary to obtain a better understanding of the defect. On real time 3-Dimensional echocardiography (RT3DE), the flow through a significant lesion may be visible as an echogenic 3D shadow. When this is present, it always signifies a hemodynamically important lesion (Video 5.1) and live-color 3D images should always be obtained for assessing the dimensions and shape of the regurgitant orifice. Color 3D multiplanar reformatting or MPR is the best method for assessing these lesions. Ideally, the size of the defect should be expressed in relation to the circumference of the valve.

2DTEE is very sensitive in accurately identifying the leak (88%) and pointing out the exact location can be challenging, as the regurgitant jet may be overshadowed by the prosthetic valve. Transducer position behind the left atrium in TEE enables the visualization of mitral PVL unobscured by the prosthesis.

3DTEE

Mitral PVL is best visualized by the live zoom mode. To assess the position of the leak in relation to the rest of the cardiac structures, the display is standardized by positioning the anatomic structures in a clockface manner. Thus, the aorta is displayed anteriorly at 12 o'clock position and the LAA laterally at the 9 o'clock position, rendering the interatrial septum medially and the posterior wall of the left atrium at 6 o'clock position. Live-color 3D may be used to compare and visually quantify the leak. To derive the regurgitant orifice area, the most accurate method in experienced hands is the 3D MPR using color 3D full-volume loops. When aligned in anatomically appropriate planes, and frozen in peak systolic frame, vena contracta measured in three orthogonal planes gives the nearest possible data pertaining to the regurgitant orifice. A majority of the PVLs in mitral position are seen between 3 and 9 o'clock positions. For procedural guidance, 3D zoom function is most reliable and so is visualization of the catheter tip. The larger area of the cardiac anatomy is visible in this mode compared with live 3D. The echocardiologist/echocardiographer should be able to guide the interventionalist to the area of the leak with accurate visualization of the regurgitant orifice in relation to the catheter tip.

Trans catheter aortic valve implantation (TAVI)

The aortic valve does not have a true fibrous ring supporting the valve leaflets and, hence, it is not symmetric or circular (Figure 5.4). The geometry of the valve is further altered by the degree of thickening, calcification, and its morphology (number of leaflets and the degree and plane of fusion). The relative tension in neighboring chambers and the aortic wall itself also influences the morphology and shape of the "annulus," raising concerns about the accuracy of the measurement in one plane using 2DTEE. The assumed circularity of the aortic annulus leads to erroneous estimates resulting in discrepancy of measurements between different imaging techniques and modalities. TEE-measured aortic annular size is 1.36 mm more than the TTE. One cannot overemphasize the role of 3D MPR in accurately measuring the distances between the hinge points of the aortic valve leaflets in peak systole.

The 2DTEE-based measurements have been shown to be comparable to CT measurements. Using short-axis views, the opening of the aortic valve should be classified as central or eccentric and the severity, location, and symmetry of the aortic valve calcification accurately described.

During TAVI, the prosthesis anchors according to the resistance of the tissues behind the aortic leaflets. During implantation, the native aortic valve leaflets are crushed against the aortic wall and the differences in the tension across the valve may cause asymmetric deployment of the prosthesis and contribute to the risk of compression of the coronary arteries. In order to minimize the risk of coronary occlusion, it is advisable to measure the distance from the

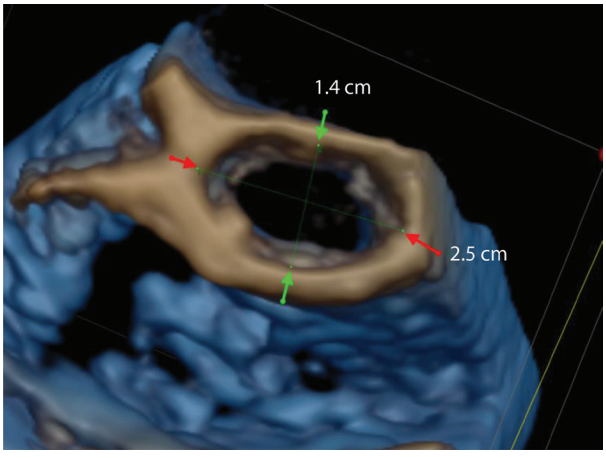

Figure 5.4 (**See color insert.**) Asymmetry of the aortic valve "annulus" seen on 3DTEE imaging.

aortic annulus to the ostia of the coronary arteries and to compare this with the length of the leaflets measured in a long-axis view. This measurement is best achieved with 3D MPR as the accurate visualization of the hinge points of the valve leaflets is possible, which may be in a different plane to that of the coronary ostia. Although the leaflets are typically shorter than the annular–ostial distances, those patients in whom the leaflet length exceeds the annular–ostial distances are at risk of ostial occlusion when the valve is deployed and the native leaflets are crushed to the side.

Although balloon inflation is normally performed during rapid right ventricular pacing to reduce stroke volume, the balloon may still migrate during inflation, particularly in those patients with severe septal hypertrophy or with a smaller sino-tubular junction. The loss of right ventricular capture or ventricular extra systole may also result in balloon migration. TEE may be used to confirm a stable position during inflation and to monitor the behavior of the calcified aortic leaflets during inflation.

During the deployment of the prosthesis, TEE is very helpful in confirming accurate positioning of the valve and is generally used in conjunction with fluoroscopy. The optimal position for the Edwards SAPIEN™ valve is with the ventricular side of the prosthesis positioned 2–4 mm below the annulus in the left ventricular outflow tract immediately following deployment; TEE is used to confirm satisfactory positioning and function of the prosthesis. When the prosthesis is positioned too low, it may impinge on the mitral valve apparatus or it may be difficult to stabilize in patients with marked septal hypertrophy. The native valve leaflets may also fold over the prosthesis and compromise the prosthetic valve function. If the prosthesis is implanted too high, it may migrate up the aorta and obstruct the coronary ostia, or cause significant PVL.[2]

It is important to confirm that all the prosthetic leaflets are moving well, that the valve stent has assumed a circular configuration (using 2D or 3D views), and that there is no significant valvar or PVL. Some regurgitation through the prosthesis will be common, while the delivery apparatus and/or guide wire remain across the valve and may persist, to a lesser degree, after their removal, as it may take a few minutes postimplant for the leaflets to completely recover from being crimped for deployment. Until this occurs, the leaflets may not coapt completely and mild transient regurgitation may be observed at the coaptation point. TEE views with continuous-wave, pulsed-wave, and color Doppler should be used to confirm satisfactory prosthetic valve position and function. To aid this, transgastric views may be obtained.

Aortic regurgitation has also been reported as a consequence of residual native aortic valve leaflet tissue prolapsing into the prosthesis, interfering with leaflet motion and coaptation. This may result from deficient containment of residual native aortic tissue by the prosthesis and/or positioning the valve too low. Monitoring complications such as perforation, clot formation, and tamponade is crucial during deployment. Device embolization and atrioventricular (AV) block are more common with Corevalve. Damage or distortion of the subvalvar mitral apparatus by the delivery system, although uncommon, is possible. Asymmetric left ventricular wall motion abnormalities may indicate acute coronary occlusion. Cardiac tamponade, or right ventricular or septal perforation are other complications that need to be watched for during the procedure. Rarely does dissection or rupture of the aortic root occur.

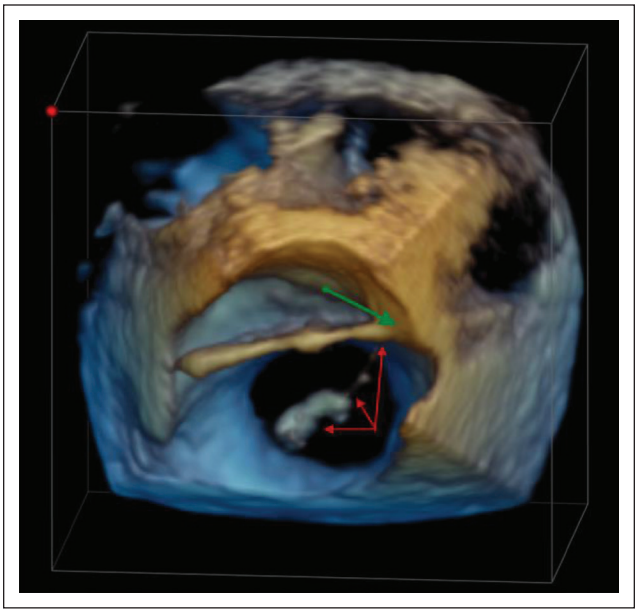

Figure 5.5 (**See color insert.**) 3D image of clot formation at the septal puncture site during LAA closure. Guide wire is through the transseptal puncture site (green arrow) and clot is attached to the interatrial septum (red arrow).

Left atrial appendage closure

Achieving a low septal puncture and accurate measurement of the landing zone for LAA closure devices are very important aspects for successful closure. With 3DTEE, better visualization of the morphology and dimensions of the landing zone can be made from a full-volume loop with MPR. It is equally important to watch for complications during the procedure, as thromboembolism or pericardial tamponade can be detrimental if not identified promptly (Figure 5.5).

Congenital interventions

ASD and PFO closure

Assessment of deficiency in the interatrial septum to determine the feasibility of device closure has been mostly performed using the multiplane 2DTEE imaging. More recently, 3DTEE has significantly improved the visualization of these defects, so that accurate sizing may be

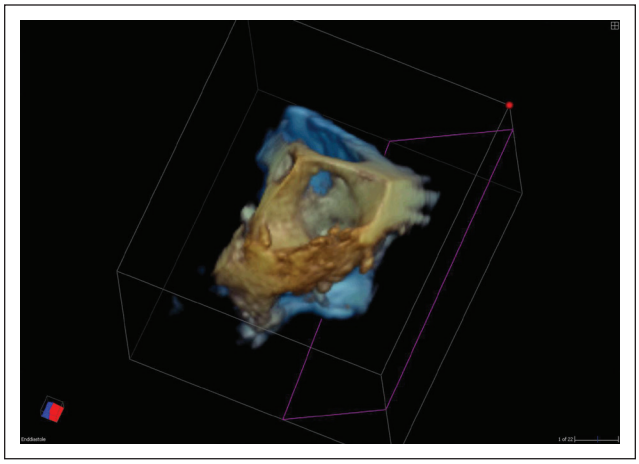

Figure 5.6 (**See color insert.**) Small secundum ASD at the region of the oval fossa viewed from the LA.

achieved, avoiding the need for balloon sizing. 2D imaging can often determine the hemodynamic significance and morphology of the defect. It also helps to identify the secundum defects from others, such as the sinus venosus or primum defects, which may be unsuitable for device closure. It is very important to ascertain the anatomic type of the defect, morphologic variations relating to size, shape, consistency, and adequacy of the margins, plane of the defects, and spatial orientation of the defect in 4D.[4]

During 2DTEE assessment, the viewing angle is rotated throughout the visible planes noting the relative position of the defect with regard to anatomic landmarks. It is important to identify the pulmonary veins as they open into the left atrium, the mouth of the coronary sinus, and opening of the systemic veins. At 0°, the crux of the heart with AV junction identifying the rim of the defect from the AV valves is made. Then the probe is rotated to visualize the coronary sinus at about 25–30 degrees with angulation. Following this, the aortic rim is best seen between 30 and 50 degrees, and at 90 degrees, the bicaval view is obtained. During device deployment, the best view is at 40–45 degrees, where the plane of the defect in relation to the aortic margin and the course of the delivery system is best visualized.

For 3D imaging, live 3D zoom is the most appropriate mode to visualize the plane and the morphologic characteristics of the defect, while adjusting the gain settings to define the margins well (Figures 5.6 through 5.9). 3D MPR must be used for accurate identification of the size of the defect(s) in atrial diastole. 3D assessment also helps to avoid oversizing and the need for balloon sizing. It reduces the potential for residual defects, and helps to detect and define associated malformations.

In addition to reducing the procedure time and radiation, in experienced hands, the information obtained by 3DTEE is superior to other imaging techniques, including intra cardiac echocardiography (ICE).

Transseptal puncture

TEE guidance is very helpful in transseptal procedures and baffle fenestrations. In this regard, left atrial appendage

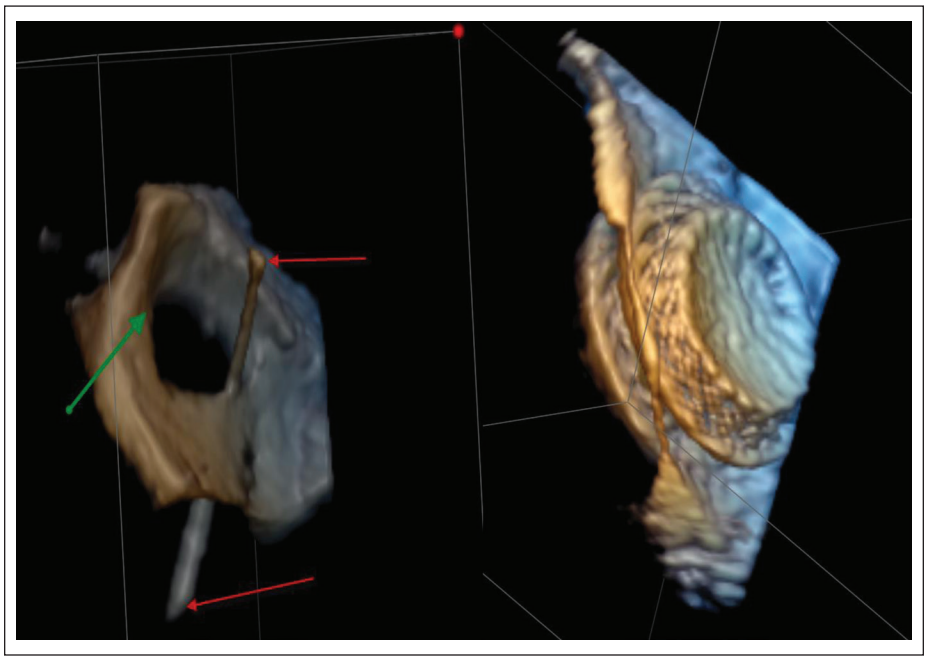

Figure 5.7 (**See color insert.**) A large ASD with adequate margins (except deficient aortic rim) closed with an Occlutech™ device. The defect with catheter passing from the IVC to the LA on the left and the device in position on the right.

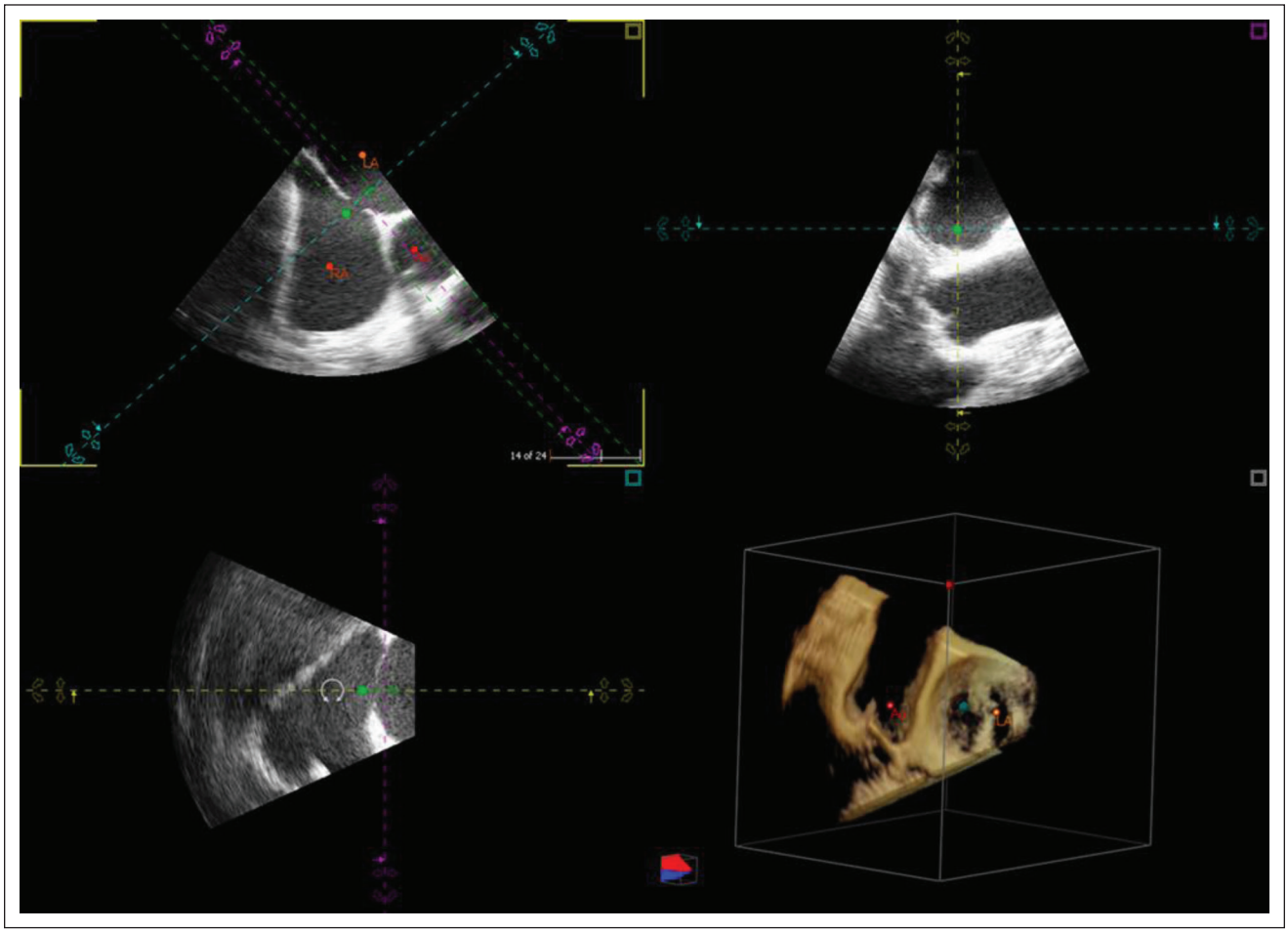

Figure 5.8 (**See color insert.**) Two ASDs in parallel identified as single defect on 2DTEE but visualized as two separate defects in 3DTEE.

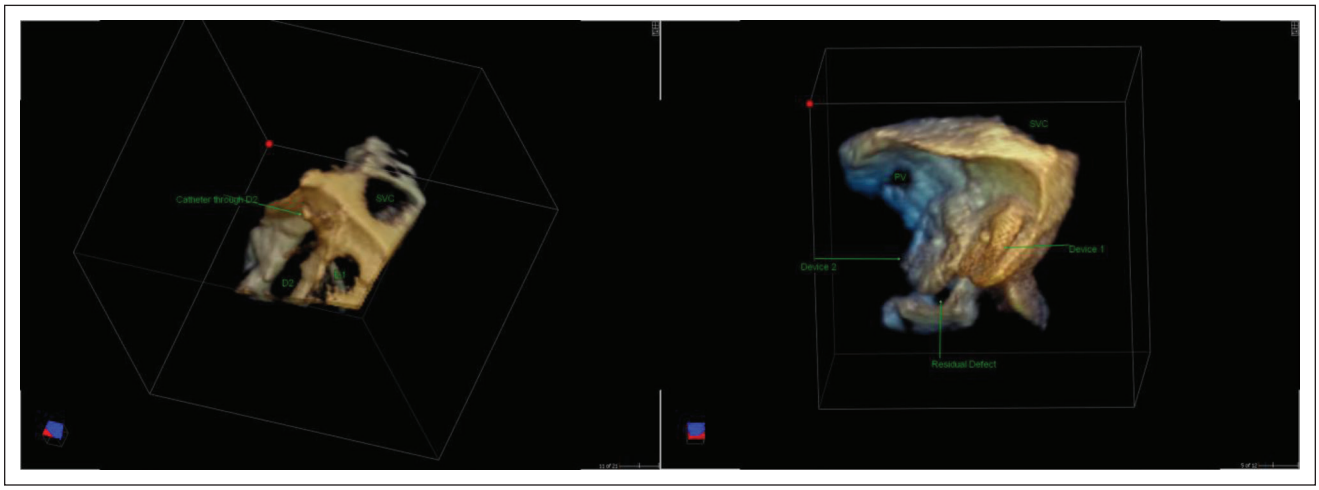

Figure 5.9 (**See color insert.**) 3DTEE showing two ASDs separated by a firm septum closed using two devices sitting comfortably, adjacent to each other with a small residual defect.

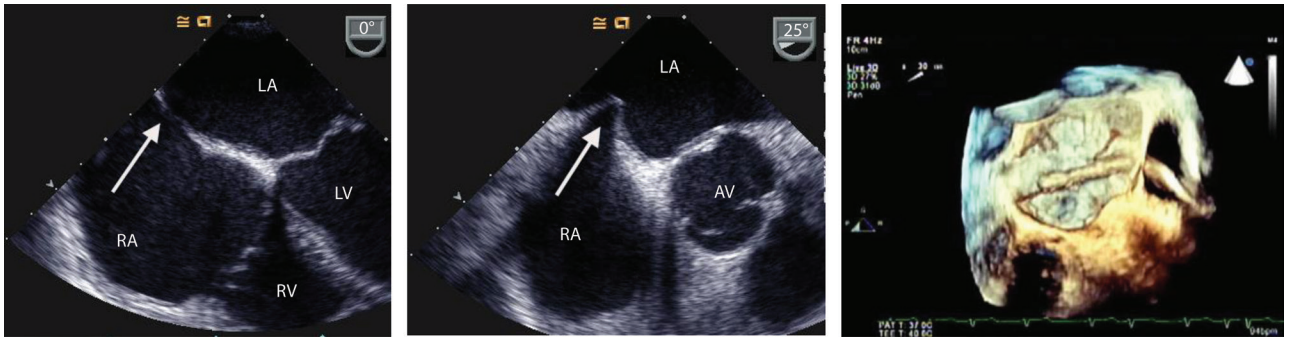

Figure 5.10 (**See color insert.**) Transseptal puncture under 2DTEE and 3DTEE guidance.

closure and relief of pulmonary vein stenosis and associated procedures benefit from TEE guidance (Figure 5.10).

Summary

Advanced cardiac imaging techniques through miniaturization and computing power have revolutionized visualization of the cardiac morphology and function leading to better bedside assessment and percutaneous catheter interventional therapy. Mastering these techniques provides new challenges. With the advent of high-speed Internet access, training and learning with collaborative research has become a reality. This is expected to further assist in the interactions and improved management of structural and congenital heart defects.[5]

References

1. Black D, Ahmad Z, Lim Z, Salmon A, Veltdman G, Vettukattil J. The accuracy of three-dimensional echocardiography with multiplanar reformatting in the assessment of the aortic valve annulus prior to percutaneous balloon aortic valvuloplasty in congenital heart disease. *J Invasive Cardiol* 2012;24(11):594–8.
2. Zamorano JL, Badano LP, Bruce C, Chan K-L, Gonçalves A, Hahn RT et al. EAE/ASE recommendations for the use of echocardiography in new transcatheter interventions for valvular heart disease. *Eur J Echocardiogr* 2011;12:557–84.
3. Wunderlich N, Franke J, Wilson N, Sievert H. 3D Echo guidance for structural heart interventions. *Interv Cardiol Rev* 2009;4(1):16–32.
4. Vettukattil JJ, Ahmed Z, Salmon AP, Mohun T, Anderson RH. Defects in the oval fossa: Morphologic variations and impact on transcatheter closure. *J Am Soc Echocardiogr* 2013;26(2):192–9.
5. www.3dechocardiography.com.

6

Intracardiac echocardiography (ICE)

Damien Kenny, Qi-Ling Cao, and Ziyad M. Hijazi

Introduction

The ideal multimodality intraprocedural imaging system to facilitate and guide the ever-increasingly complex array of congenital and structural heart interventions is one of the "holy grails" of interventional cardiology. The ideal system would provide detailed (real-time 3-D) near- and far-field images with minimal invasiveness, low cost, minimal interventional interference, and easy interface with the user, which ideally would be the interventionalist performing the procedure. Many of the intraprocedural imaging modalities available to the interventionalist (including CT, MRI, transthoracic echocardiography [TTE], and transesophageal echocardiography [TEE]) provide some of these functions but each has its own limitations. Intracardiac echocardiography [ICE] is attractive in that it provides excellent near-field and reasonable far-field imaging without the need for anesthesia and with minimal interference with the intervention, and it is manipulated entirely by the interventionalist performing the procedure. Radiation exposure through fluoroscopy may also be minimized. Consequently, it has become one of the most widely used ultrasound-based imaging adjuvants in the catheterization laboratory, obviating the need for support for anesthesiologists and echocardiographers, providing a potential procedural cost savings.[1] This chapter evaluates the historical development of ICE and the available systems, and provides examples of the congenital and structural interventions in which it has proved itself invaluable.

Historical perspectives and currently available systems

Ultrasound-tipped catheters were described in the 1970s, and later evolved into high-frequency intravascular ultrasound imaging probes to evaluate coronary artery disease in the 1980s.[2,3] It has only been over the past two decades that intracardiac transducers have been developed to evaluate intracardiac anatomy.[4,5] This has involved an evolution from high-frequency low-power catheters with 360° axial imaging capabilities for intravascular imaging to the development of lower-frequency transducers with greater depth penetration and more focused evaluation of segmental anatomical structures. Initial systems maintained radial imaging capabilities, and reports that assessed ventricular size and function soon followed.[6,7] However, it was with the realization of intracardiac imaging to guide interventional procedures, particularly initially in the field of electrophysiology, with need for access to the left atrium,[8,9] that significant developments were made in respect to maneuverability and advanced imaging support techniques.[10] Linear-array transducers gave way to phased-array catheters with lower frequencies and Doppler imaging capabilities.[11,12] Since this time and in line with the resurgence in transseptal puncture to access the left heart for structural interventions, ICE has evolved into one of the most widely used imaging modalities for noncoronary interventional cardiac procedures.[13] A list of cardiac interventional procedures for which ICE has been utilized is provided (Table 6.1).

Currently, there are five commercially available intracardiac imaging systems (Table 6.2).[14] The Ultra ICE™ system (Boston Scientific, San Jose, California) is a mechanical single-element system that is covered fully in another chapter and will not be discussed further here. The other systems are side-looking 64-element catheters without integrative functionality for 3-D electrophysiological mapping systems. The systems designed specifically for 3-D mapping integration are beyond the scope of this chapter and reference will be limited to Table 6.2. The AcuNav system (Biosense Webster, Diamond Bar, California) (Figure 6.1) is a side-looking 64-element phased-array transducer with four-way (anterior/posterior/left/right) handle steerability and a locking knob available as 8 and 10 F single-use catheters. The transducer has a frequency that varies from 5.5 to 10 MHz and scans in the longitudinal monoplane providing a 90° sector image with tissue penetration of 12 cm for the 10 F system and 16 cm for the 8 F system. The entire catheter system is freely torquable, providing the potential for imaging through multiple planes of the

Table 6.1 Interventions utilizing ICE imaging

Intervention	Advantages	Disadvantages
ASD closure	Good profiling of the entire interatrial septum, including the inferior portion Obviates the need for heavy sedation or general anesthesia	May be more difficult to interpret multiple or complex ASDs
PFO closure	As above with clear imaging of variants in PFO anatomy and tunnel morphology Limits the need for fluoroscopy	Catheter stability may be an issue during device deployment
VSD closure	Excellent profiling of the membranous septum in a number of different achievable views	May not be optimal for midmuscular or more apical defects
Aortic valvuloplasty/TAVR	Provides excellent accurate imaging of the aortic valve annulus May fit the workflow pattern of TAVR better than TEE as the procedure evolves	Limited experience to date, although this is likely to evolve
Pulmonary valvuloplasty/tPVR	Provides excellent imaging of the pulmonary valve, including assessment of residual stenosis or new regurgitation following intervention Limits the requirement for repeated angiography	May be perceived as expensive and unnecessary in this setting
Mitral valvuloplasty	Used to guide transseptal puncture and mitral interventions with full operator control	Left heart structures, particularly the left atrial appendage, may be a challenge to image from the right heart
Transseptal puncture	Provides detailed imaging of the atrial septum with its inherent anatomical variations No need to move the probe when using fluoroscopy	Lack of multiplanar imaging may limit the immediate view of the needle position following puncture
Left atrial appendage occlusion	Operator dependence	May require imaging from the left atrium to obtain detailed views, which may require a second transseptal access

Table 6.2 Commercially available ICE systems

Device name	Company	Features
UltraICE	Boston Scientific	9 F nonsteerable rotational motor-driven gray scale-only system (see Chapter 7)
AcuNav	Siemens, Biosense Webster	Side-looking 64-element phased-array four-way steerability, 8 F and 10 F; gray scale, color Doppler, tissue Doppler, 3-D localization with Cartosound
EP Med View Flex Catheter	St Jude Medical	Runs side-looking 64-element catheter on the Viewmate scanner, 10 F introducer, two-way flex color Doppler, gray scale, tissue Doppler 8–2 MHz
ClearICE	St Jude Medical	Derived from the hockey stick, 64-element side-looking highly steerable four-way side-looking array with two sets of electrodes for integration of 3-D localization with NavX; runs on the GE Vivid *i* scanner; gray scale, tissue Doppler, synchronization mapping, 2-D speckle tracking
SoundStar Catheter	Biosense Webster	This is a new catheter, just now marketed as a 10 F (3.33-mm) device with integrated ultrasound array (like AcuNav) but with the CARTO magnetic sensor in the tip.
AcuNav V	Siemens	Provides real-time volume imaging, but limited clinical experience to date

Source: Taken (with additions) from Hijazi ZM, Shivkumar K, Sahn DJ. *Circulation* 2009;119:587–96.

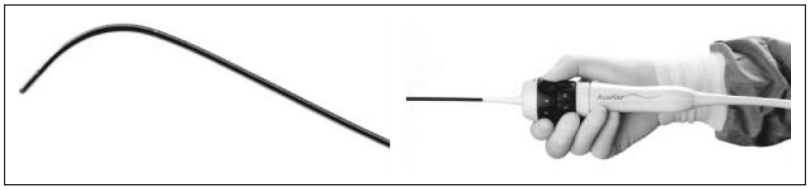

Figure 6.1 The AcuNav catheter. Left: The tip of the catheter can be manipulated in four different directions. Right: The control handle has three knobs: one to move the tip in posterior/anterior directions; one to move the tip right/left; and the last knob is a locking one that will fix the tip in the desired orientation.

heart, and with the locking system, allowing maintenance of a stable, fixed-tip orientation that gives the interventionalist freedom to provide "hands-free" imaging during the desired intervention. The system can provide full Doppler capabilities, including spectral, color, and tissue imaging.

Imaging protocols

The catheter is introduced through an appropriately sized sheath (8 or 10 F) in the femoral vein. The connection to the echocardiographic machine must be kept dry and a sterile cover is required for the cable. A longer 30 cm sheath may be used to ensure that the rigid ICE catheter clears some of the curves of the pelvis. Either way, fluoroscopic guidance should be used to screen catheter advancement into the mid-right atrium to ensure there is no trauma to the venous conduits to the heart. In adult patients, the AcuNav catheter can be introduced in the same (femoral) vein used for the septal device delivery. However, for patients weighing less than 35 kg (i.e., children), the contralateral femoral vein is used. When ICE is being used for mitral valve interventions requiring large venous sheaths, again the contralateral femoral vein is preferred.

Standard views

With the ICE catheter in the mid-right atrium aligned parallel to the spine, this is referred to as the neutral or "home" view. With the transducer rotated so that it is facing the tricuspid valve, the inflow, apical, and outflow portions of the right ventricle should be clearly seen. Further clockwise rotation will demonstrate the left ventricular outflow tract with the aortic valve and the ascending aorta with further rotation demonstrating the mitral valve and the left atrial appendage (LAA). Counterclockwise rotation is used to reestablish the home view and from here various maneuvers can be used to image the area of interest.

Atrial septum

The use of ICE during atrial septal defect (ASD) and patent foramen ovale (PFO) closure is well reported and has become the imaging modality of choice in adults,[15–17] often facilitating early hospital discharge.[18] At the start of the case, a complete evaluation of the defect(s) and surrounding anatomy is performed. The intensity of this interrogation will in part depend on the adequacy and completeness of imaging prior to the procedure. For patients with an ASD, the size of the defect via 2-D imaging (with and without being stretched by a balloon) as well as the measurement of surrounding rims is obtained. Contrast injection via agitated saline microbubbles is performed for patients with a PFO to confirm the presence of a right-to-left shunt.

Stepwise protocol for ICE imaging to guide ASD or PFO closure

Step 1: From the "home view," the ICE catheter is flexed posteriorly using the knob so that the transducer faces the interatrial septum. Fluoroscopy showing the position of the catheter as well as a corresponding anatomic diagram is shown in Figure 6.2. The ICE image obtained shows the interatrial septum as well as the coronary sinus and pulmonary veins, depending on the exact location of the transducer. This can be referred to as the "septal view" (Figure 6.2b). One can obtain further views by locking the tip in this position and rotating the entire handle or by fine adjustments of the posterior/anterior or right/left knobs.

Step 2: The ICE catheter itself is then advanced in a cephalad direction toward the superior vena cava (SVC). This can be referred to as the SVC or "long-axis view." A fluoroscopic image showing the position of the catheter, as well as a corresponding anatomic diagram, is shown in Figure 6.2c. The ICE image obtained is also shown. In this plane, the transducer faces the interatrial septum and the SVC can be seen as it relates to the right atrium. The interatrial septum is shown in a superior/inferior plane and corresponds to the TEE long-axis view. Greater portions of the SVC can be seen by continued advancement of the ICE catheter in this flexed position toward the SVC. Greater portions of the inferior septum can be similarly imaged by withdrawing the ICE catheter toward the inferior vena cava in the flexed position. A defect of the interatrial septum can be well profiled, and the superior and inferior rims as well

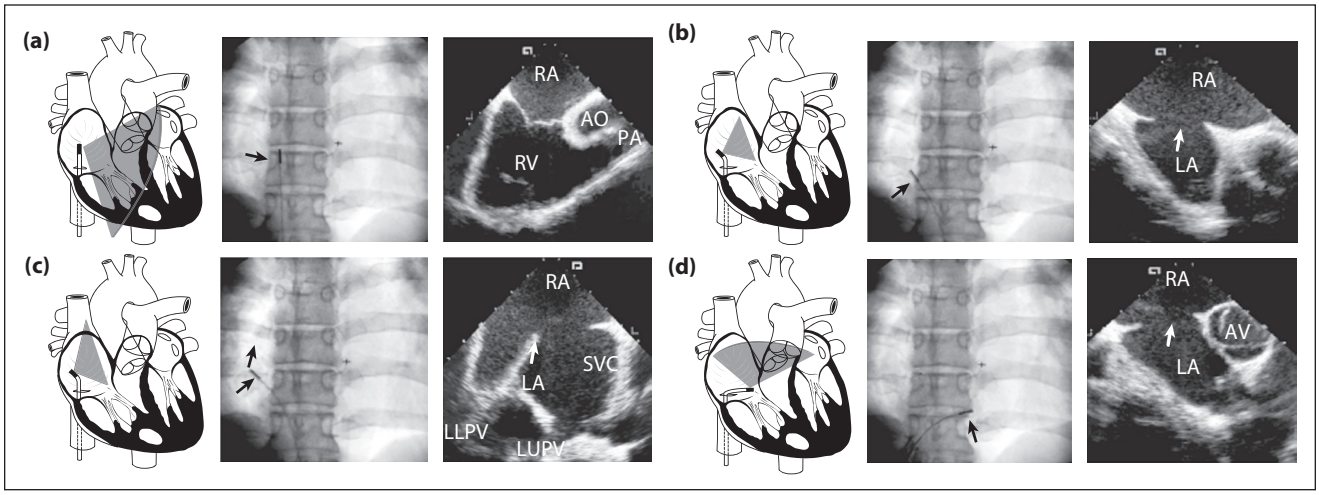

Figure 6.2 (a) Images in the home view. Left: Sketch representing the heart with the position of the intracardiac catheter inside the heart with the ultrasonic array box in the neutral "home view" position. The shaded area represents structures seen in this view. Middle: A cine fluoroscopy image showing the position of the ICE catheter (arrow) in the mid-right atrium with the transducer facing the tricuspid valve and parallel to the spine. Right: An actual intracardiac echocardiographic image with the ultrasonic box in the neutral home view position. The tricuspid valve and right ventricle outflow and inflow are well seen in this position. The aortic valve and pulmonic valve can also be seen. AO: aortic valve; RA: right atrium; PA: pulmonary artery; RV: right ventricle. (b) Images in the septal view. Left: Sketch representing the heart with the position of the intracardiac catheter inside the heart with the ultrasonic array box in the posterior flexed position looking at the atrial septum "septal view." The shaded area represents structures seen in this view. Middle: A cine fluoroscopy image showing the position of the ICE catheter (arrow) in the right atrium with the transducer flexed posterior looking at the septum. Right: An actual intracardiac echocardiographic image with the ultrasonic box in the septal view. The atrial septal defect (arrow) and the left and right atria are well seen. (c) Images in the long-axis "caval view." Left: Sketch representing the heart with the position of the intracardiac catheter inside the heart with the ultrasonic array box in the posterior flexed position with a cephalad advancement looking at the atrial septum and the superior vena cava caval view. The shaded area represents structures seen in this view. Middle: A cine fluoroscopy image showing the position of the ICE catheter (black arrow) in the right atrium with the transducer flexed posterior looking at the superior vena cava (white arrow). Right: An actual intracardiac echocardiographic image with the ultrasonic box in the caval view. The atrial septal defect (arrow), the left and right atria, the left pulmonary veins, and superior vena cava are all well seen. SVC: superior vena cava; LLPV: left lower pulmonary vein; LUPV: left upper pulmonary vein. (d) Images in the "short-axis view." Left: Sketch representing the heart with the position of the intracardiac catheter inside the heart with the ultrasonic array box in the flexed position and the entire handle rotated clockwise until the imaging transducer is above the tricuspid valve looking at the aorta from below. In this position, fine rotation of the knobs can demonstrate different parts of the atrial septum. The shaded area represents structures seen in this view. Middle: A cine fluoroscopy image showing the position of the ICE catheter (black arrow) in the right atrium with the transducer above the tricuspid valve. Right: An actual intracardiac echocardiographic image with the ultrasonic box in the short-axis view. The atrial septal defect (arrow), the left and right atria, and the aortic valve are all well seen. This view is similar to a TEE short-axis view with the left atrium in the far field (opposite to the TEE).

as the diameter of the defect can be measured. In this view, both the right and left pulmonary veins may also be imaged, depending on the exact angle of the imaging plane.

Step 3: The catheter (in its locked position) is then rotated clockwise until it sits in a position with the transducer near the tricuspid valve annulus, and inferior to the aorta. A fluoroscopic image showing the catheter position and a corresponding anatomic diagram is shown in Figure 6.2d. The ICE image obtained is also shown. In this view, the aortic valve can be seen in short axis as well as the interatrial septum. This corresponds to the basal short-axis view obtained with TEE and is known as the "short-axis view." However, the right atrium is in the near field and the left atrium is in the far field, which is opposite of what is seen with TEE.

Prior to the actual device-deployment procedure, the above views are obtained in order to image the ASD or PFO. Additional views can be obtained by advancing the catheter through the ASD or PFO into the left atrium (see below). From this position, an equivalent of the transthoracic four-chamber view can be obtained with views of the mitral valve, LV, and RV. The catheter can be further manipulated to view the LAA, which may be helpful in procedures to occlude the LAA. The catheter is then withdrawn back to the right atrium. During the exchange wire and delivery sheath positioning, the long-axis view is felt to best delineate

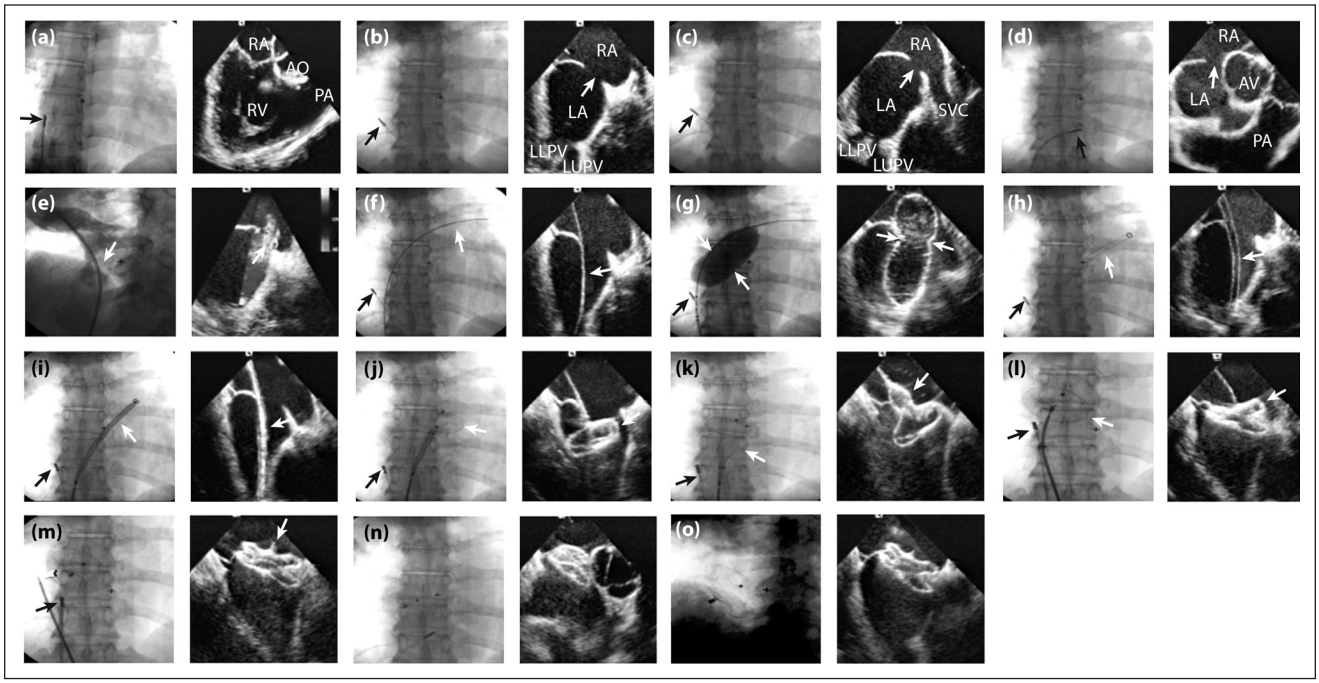

Figure 6.3 Cine fluoroscopic and ICE images in a 54-year-old female patient with a large secundum ASD who underwent closure using a 28 mm Amplatzer septal defect. (a) Left: Cine of the ICE catheter in the home view (arrow). Right: Image obtained showing the tricuspid valve, right ventricle, aorta, and pulmonary artery. (b) Septal view images. Left: ICE transducer (arrow) facing the septum. Right: ICE image obtained demonstrating the defect (arrow), pulmonary veins, and left and right atria. (c) Caval view images. Left: ICE transducer (arrow) facing the upper septum and looking at the superior vena cava. Right: ICE image obtained demonstrating the defect (arrow), SVC, pulmonary veins, and left and right atria. (d) Short-axis view images. Left: ICE transducer (arrow) above the tricuspid valve. Right: ICE image obtained demonstrating the defect (arrow), aortic valve, pulmonary artery, and left and right atria. (e) Left: Angiogram in the right upper pulmonary vein demonstrating the defect (arrow). Right: ICE image with color in septal view demonstrating the defect and shunt (arrow). (f) Left: Cine fluoroscopy image demonstrating the ICE catheter (black arrow) in the septal view position during passage of the exchange guide wire (white arrow) through the defect into the left upper pulmonary vein. Right: Corresponding ICE image showing the guide wire (arrow) through the defect. (g) Left: Cine fluoroscopy image demonstrating the ICE catheter (black arrow) in the septal view position during balloon sizing of the defect to obtain the stretched diameter (white arrows). Right: Corresponding ICE image showing the indentations on the balloon (arrows). (h) Left: Cine fluoroscopy image demonstrating the ICE catheter (black arrow) in the septal view position during passage of the delivery sheath (arrow) into the left atrium. Right: Corresponding ICE image showing the delivery sheath (arrow) inside the left atrium. (i) Left: Cine fluoroscopy image demonstrating the ICE catheter (black arrow) in the septal view position during passage of a 28-mm Amplatzer Septal Occluder within the sheath (arrow). Right: Corresponding ICE image showing the device inside the sheath (arrow). (j) Left: Cine fluoroscopy image demonstrating the ICE catheter (black arrow) in the septal view position during deployment of the left atrial disk (arrow) of a 28-mm Amplatzer Septal Occluder in the left atrium. Right: Corresponding ICE image showing the left disk in the left atrium (arrow). (k) Left: Cine fluoroscopy image demonstrating the ICE catheter (black arrow) in the septal view position during deployment of the connecting waist (arrow). Right: Corresponding ICE image showing the connecting waist (arrow). (l) Left: Cine fluoroscopy image demonstrating the ICE catheter (black arrow) in a modified septal short-axis view position during deployment of the right atrial disk (arrow). Right: Corresponding ICE image showing the right atrial disk (arrow). (m) Left: Cine fluoroscopy image demonstrating the ICE catheter (black arrow) in a modified septal short-axis view position after the device has been released from the cable (white arrow). Right: Corresponding ICE image showing the device after it has been released (arrow). (n) Left: Cine fluoroscopy image demonstrating the ICE catheter in a modified short-axis view position. Right: Corresponding ICE image showing the aortic valve and both disks of the device. (o) Left: Cine fluoroscopy image in the four-chamber view demonstrating the position of the device. Right: ICE image with color Doppler showing good device position and no residual shunt.

intracardiac relations. Device deployment is monitored in the long-axis view as well to demonstrate the relation of the disks to the interatrial septum. Figure 6.3a–o demonstrates a case of a patient with a large secundum ASD who underwent device closure. This figure demonstrates all the steps involved in device closure using the Amplatzer Septal Occluder. Color Doppler imaging as well as contrast echocardiography is used to assess for the presence or absence of any residual shunts. For assessment of residual right-to-left shunting following PFO closure, a Valsalva maneuver may be performed with greater efficacy than in patients who have undergone TEE-guided closure (Figure 6.4).

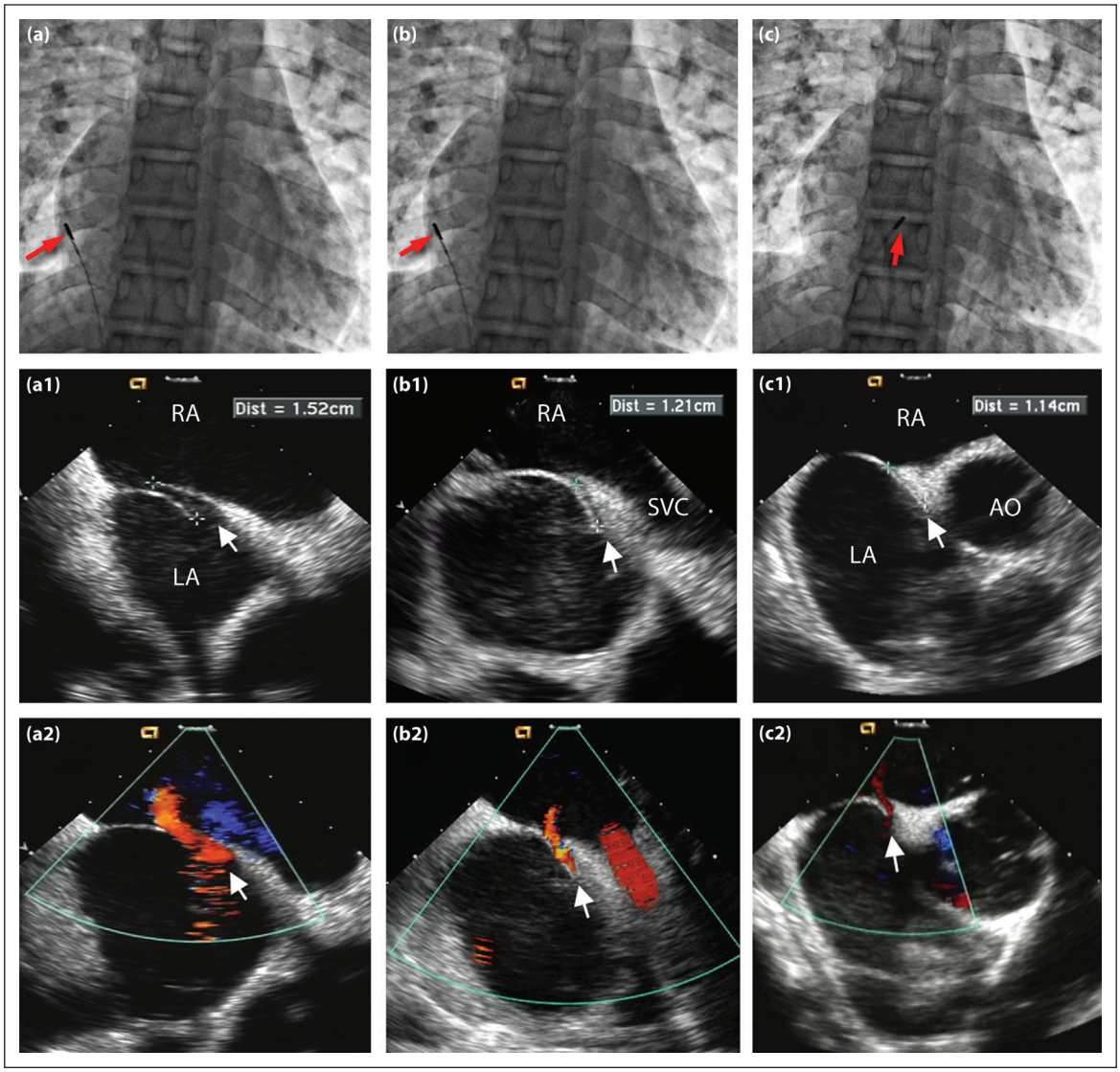

Figure 6.4 (**See color insert.**) A series of images outlining PFO closure with the Gore Septal Occluder. (a–c) Initial diagnostic assessment of the PFO. (a–a2) The septal view of the atrial septum with and without color Doppler (demonstrating L–R shunt) with corresponding position of the ICE catheter on fluoroscopy outlined by the red arrow. (b–b2) The long-axis view (c–c2) demonstrating the short-axis view with the tunnel length measuring between 11 and 15 mm (a1, b1, c1). (d–f) Fluoroscopy images with ICE catheter position (red arrow) with the corresponding ICE image below. (d) R–L shunt of bubble contrast across the PFO with (e) clearly showing the wire crossing the defect and (f) balloon sizing of the defect, which is optional outside of most clinical trails. (g–i) Delivery of the HELEX device with corresponding fluoroscopy and ICE images in various views. (i) The left atrial component of the device deployed with (j, k) demonstrating the device pulled back to the septum and further deployment of the right atrial component of the device with it fully deployed in the long-axis (k) and short-axis views (l). (m, n) Release of the device on fluoroscopy with corresponding postdeployment ICE assessment with short-axis views and long-axis views with and without color (o1, o2, p1, p2).

Stepwise protocol using ICE to guide VSD

The use of ICE to guide transcatheter ventricular septal defect (VSD) closure has been described.[19]

Step 1: ICE imaging is initiated in the RA with the "home-view" similar to ASD and PFO closure as described above. From this position, the RA, the RV inflow, and the membranous/perimembranous portion of the interventricular septum (IVS) are seen. The defect within the IVS is noted and its relationship to the tricuspid valve is shown in Figure 6.5a.

Step 2: The short-axis view is similar to that obtained during ASD and PFO closure. The catheter is flexed posteriorly and locked. The entire handle is rotated clockwise and advanced slightly just above the tricuspid valve until the short-axis view is achieved, with the transducer in

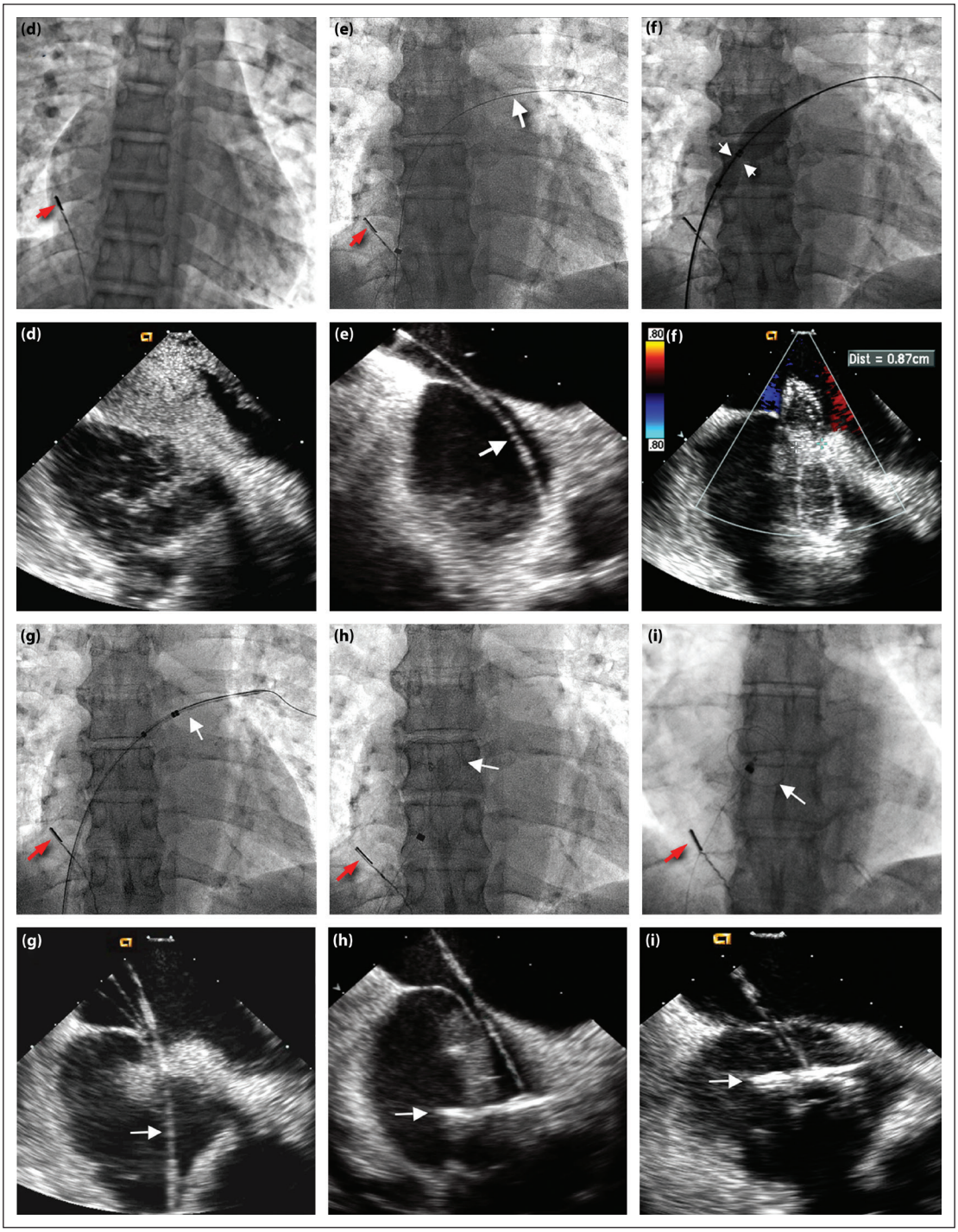

Figure 6.4 (continued) A series of images outlining PFO closure with the Gore Septal Occluder. (a–c) Initial diagnostic assessment of the PFO. (a–a2) The septal view of the atrial septum with and without color Doppler (demonstrating L–R shunt) with corresponding position of the ICE catheter on fluoroscopy outlined by the red arrow. (b–b2) The long-axis view (c–c2) demonstrating the short-axis view with the tunnel length measuring between 11 and 15 mm (a1, b1, c1). (d–f) Fluoroscopy images with ICE catheter position (red arrow) with the corresponding ICE image below. (d) R–L shunt of bubble contrast across the PFO with (e) clearly showing the wire crossing the defect and (f) balloon sizing of the defect, which is optional outside of most clinical trails. (g–i) Delivery of the HELEX device with corresponding fluoroscopy and ICE images in various views. (i) The left atrial component of the device deployed with (j, k) demonstrating the device pulled back to the septum and further deployment of the right atrial component of the device with it fully deployed in the long-axis (k) and short-axis views (l). (m, n) Release of the device on fluoroscopy with corresponding postdeployment ICE assessment with short-axis views and long-axis views with and without color (o1, o2, p1, p2).

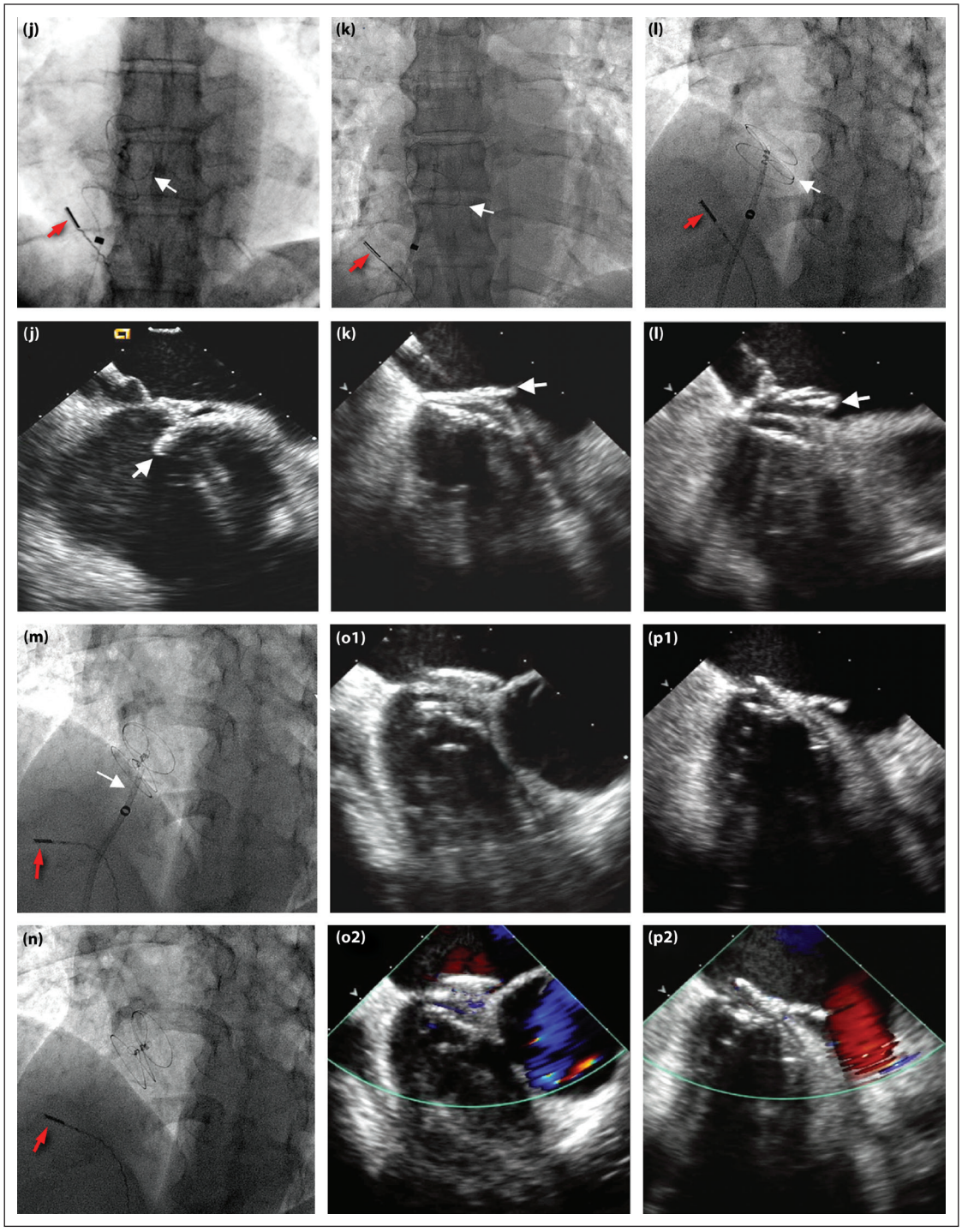

Figure 6.4 (continued) A series of images outlining PFO closure with the Gore Septal Occluder. (a–c) Initial diagnostic assessment of the PFO. (a–a2) The septal view of the atrial septum with and without color Doppler (demonstrating L–R shunt) with corresponding position of the ICE catheter on fluoroscopy outlined by the red arrow. (b–b2) The long-axis view (c–c2) demonstrating the short-axis view with the tunnel length measuring between 11 and 15 mm (a1, b1, c1). (d–f) Fluoroscopy images with ICE catheter position (red arrow) with the corresponding ICE image below. (d) R–L shunt of bubble contrast across the PFO with (e) clearly showing the wire crossing the defect and (f) balloon sizing of the defect, which is optional outside of most clinical trails. (g–i) Delivery of the HELEX device with corresponding fluoroscopy and ICE images in various views. (i) The left atrial component of the device deployed with (j, k) demonstrating the device pulled back to the septum and further deployment of the right atrial component of the device with it fully deployed in the long-axis (k) and short-axis views (l). (m, n) Release of the device on fluoroscopy with corresponding postdeployment ICE assessment with short-axis views and long-axis views with and without color (o1, o2, p1, p2).